Metabolic analysis of Developmental progression in *Drosophila*

Tharindu Fernando

University College London

and

The Francis Crick Institute

PhD Supervisor: Alex P. Gould

A thesis submitted for the degree of

Doctor of Philosophy

University College London

June 2017

Declaration

I, Tharindu Fernando confirm that the work presented in this thesis is my own. Where information has been derived from other sources, I confirm that this has been indicated in the thesis.

Abstract

The growth and development of all animals involves transitions between different physiological states. The key developmental transition of critical weight (CW) in the fruit fly *Drosophila melanogaster* dramatically changes the growing larva's response to nutrient restriction (NR). Developmental progression is arrested by NR before CW whereas it proceeds without delay when NR occurs after CW. It is known that the time of onset of CW and other developmental transitions are regulated by the steroid hormone ecdysone but questions remain concerning the nature of the physiological changes at CW and how they might confer NR-resistant developmental progression. To begin to answer these questions, I have analysed how the larval metabolome changes when nutrition is altered either side of the CW transition. The larval metabolome was recorded via nuclear magnetic resonance (NMR) spectroscopy and fitting reference spectra to recorded peaks enabled identification of the metabolites. Absolute metabolite concentrations could then be back-calculated from these spectra using the volume determination with two standards (VDTS) technique (Ragan, et al. 2013), which was further adapted to measure metabolite concentrations from the volume released from homogenisation of solid whole larval and adult samples. Through use of these techniques, I found that progression past CW correlates with the ability of fed and NR larvae to sustain a substantial increase in the concentration of tyrosine. An interesting interplay between tyrosine and a possible storage form of the metabolite: o-phosophotyrosine (OPT), suggests a process regulating the conversion between the two that may indirectly affect the biosynthesis of ecdysone. Dietary and genetic manipulations have been undertaken to draw a molecular mechanism for how varying tyrosine levels affected by CW attainment can effect time to pupariation (larval maturation). These results highlight how the field of NMR-metabolomics can be used to direct subsequent experiments to address biological questions.

Acknowledgement

I'd like to thank Alex for allowing me to apply my (at that time) limited skills with NMR to "the Ferrari of model organisms". Because of you, I've had a thrilling, exciting, stressful, entertaining, stressful and wonderful 4 years. From my original thesis title: "Carnosine functional metabolomics in *Drosophila"*, your guidance, encouragement and patience have made this thesis possible.

I'd also like to thank the past and present members of the Gould lab: Pata, Andrew, Rami, Vava, Fabrice, Annick, Bobby, Ola, Fumi, Ana, Eva, Clare, André, Pany and Irina, whose advice, discussions and humour, enabled me to get to the end. I have to give special thanks to: Irina, who gave a "structure kid" the confidence to work with larvae; Rami, who taught me "the results of an experiment can be confusing but the reason why you did that experiment should never"; Bobby, who lived, worked and drank with me (no easy task); and Ola, who forgave me for taking her on a scenic (3 hour) journey to Warwick.

I want to give massive thanks to my thesis committee: Luiz, JP and Cristina, the Vincent, Salecker, Tapon, Thompson labs and our fly techs for all their encouragement and support.

To my parents, brother and my favourite (Nina) you are the bedrock to all I achieve.

Finally I'd like to thank Paul Driscoll. You first gave me a chance. It hasn't all been plain sailing but I feel we weathered the storm quite well together and made it to calmer waters. Thanks for everything Drizzler.

For Amma and Thatthi

Table of Contents

Table of figures

List of tables

Abbreviations

$[D]_0$	Initial concentration of DSS
$[S]_0$	Initial concentration of (4-Cl-DNBA/^{13}C-formate) standard
$[X]_h$	Hemolymph concentration of metabolite X
$[X]_{WA}$	Whole adult concentration of metabolite
$[X]_{WL}$	Whole larval concentration of metabolite
17-βHSD	17β-Hydroxysteroid dehydrogenase
1D	one dimensional
20E	20-hydroxyecdysone
2x	Standard feed
2x+Tyr	Standard medium + with 1.5 g/L tyrosine
4-Cl-DNBA	4-Chloro-3,5-dinitrobenzoic acid
Akt	Protein kinase B.
Alp	Alkaline phosphatase
Alp1i	Alp1 knock down
Alp4i	Alp4 knock down
Alp4i;;Alp1i eL3	Early L3 Alp double knock down larvae
Alp4i;;Alp1i wL3	Wandering L3 Alp double knock down larvae
ANOVA	Analysis of variance
Arg	Arginine,
ASL	Human arginosuccinate lyase
BMRB	BioMagResBank
CA	Corpora allata
CC	Corpora cadiaca
CDD22	Chemically defined diet 22 (1 g/L histidine)
CDD22–His	CDD22 with 0 g/L histidine
CDD22+His	CDD22 with 2 g/L histidine
CSI	Chemical shape indictor
Ctrl wL3	Wandering L3 tub>w^{1118} larvae
CW	Critical body weight
CW	Critical weight
CW(F)	Critical weight/fatness
D_2O	Deuterium oxide

Ddc	Dopa decarboxylase
dfYFP	Deformed fused to YFP
DHR4	*Drosophila* hormone receptor 4
dIlps	*Drosophila* insulin like peptides
DSS	4,4-dimethyl-4-silapentane-1-sulfonate
EcR	Ecdysone receptor
E_{lower}	Lower energy state
ER	Endoplasmic reticulum
ERK	Extracellular signal-regulated kinase
E_{upper}	Upper energy state
FoxO	Forkhead Box class O transcription factor
FSH	Follicle-stimulating hormone
GC	Gas chromatography
GD	Gut depletion
GnRH	Gonadotropin-releasing hormone
Got2	Glutamate oxaloacetate transaminase 2
GPCR	G protein coupled receptor
GPI anchor	glycosylphosphatidylinositol anchor
h	Planck's constant
HCl	Hydrochloric acid
HFD	High fat diet
HMDB	Human Metabolome Database
Hn	Henna
hr ALH	hours after larval hatching
HSD	Honestly significant difference
I'^{S}	Concentration of the (4-Cl-DNBA/^{13}C-formate) standard in the "opened" sample
$I_C'^{S}$	Concentration of the (4-Cl-DNBA/^{13}C-formate) standard in the "blank" sample
IIS	Signalling through the Insulin-like receptor
InR	Insulin-like receptor
JH	Juvenile hormone
KD	Knock down
L1, L2, and L3	Larval instar 1, 2 and 3

LH	Luteinizing hormone
Lsps	Larval serum proteins
MS	Mass spectrometry
MT	Mitochondria
MVA	Multivariate analysis
MVDTS	Matched VDTS
MVW	Minimal viable weight
NADA	N-acetyldopamine
NBAD	N-β-alanyldopamine
NMR	Nuclear magnetic resonance
NR	Nutrient restricted
NR+Tyr (at sat. sol.)	NR + tyrosine at saturated solubility
ob	obese gene
Octβ3R	β3-octopamine receptor
OPC	O-phosphocholine
OPE	O-phosphoethanolamine,
OPT	O-phosphotyrosine
OPT:Tyr	Ratio of whole larval OPT to tyrosine concentration
PBS	Phosphate buffered saline
PC	Principal components
PC1	Principal component 1
PC2	Principal component 2
PCA	Principal component analysis
PG	Prothothatic gland
PI3K	Phosphatidylinositide 3-kinase.
ppm	parts per million
PPO1	Prophenoloxidase 1
PQN	Probabilistic quotient normalisation
PTTH	Prothoracicotropic hormone
qRT PCR	quantitative reverse transcriptase polymerase chain reaction
Raf	Rapidly accelerated fibrosarcoma.
Ras	Rat sarcoma.
RNAi	Ribonuclei acid interference

Smad	Mothers against decapentaplegic homolog 1.
Tdc	Tyrosine decarboxylase
Tdc2	Tyrosine decarboxylase 2
TGFβ	Tissue growth factor beta
TGP	Terminal growth phase
TRiP	Transgenic RNAi Project
TTP	Time to pupariation
tub	tubulin 1α promoter
USP	Ultraspiracle
v	Nuclear larmor frequency
V_D	Volume of DSS
VDRC	Vienne *Drosophila* RNAi Centre
VDTS	Volume determination with two standards
V_h	Volume of hemolymph recovered
v_{ref}	frequency of the standard's NMR peak
V_S	Volume of (4-Cl-DNBA/^{13}C-formate) standard
V_t	Transfer volume
V_{WA}	Volume recovered after whole adult homogenisation
V_{WL}	Volume recovered after whole larval homogenisation
wL3	Wandering L3 larvae
WPP	White prepupa
δ	Chemical shift

Chapter 1. Introduction

The development of animals from embryo to adult is accompanied by a series of temporal transitions that can radically alter aspects of morphology, growth, metabolism, and physiology. These transitions are regulated by genetic networks that, in several species, are now well defined. For example, in both mammals and insects, steroid hormones are known to play a key role in the transition from juvenile to adult stages. It is also clear that this transition is sensitive to environmental factors such as diet. However, much remains to be discovered about the mechanisms by which the inputs from nutrition, hormones and genes are integrated to trigger the onset of developmental transitions. In this chapter, I compare and contrast what is known about the factors that regulate the juvenile-to-adult transition in humans and also in the genetic model used in this thesis: the fruit fly *Drosophila melanogaster*. I also introduce metabolomics, a key method that was used to identify new factors regulating the timing of the juvenile-to-adult transition in *Drosophila*.

1.1 Onset of sexual maturation in humans

In humans, sexual maturation provides a reliable marker of the juvenile-adult transition at the end of development. The timing of sexual maturation is controlled by steroid hormones, which in turn, are regulated by genetic factors as well as environmental influences such as nutrition (Parent et al., 2003; Roa et al., 2010). In humans, the onset of puberty is regulated by the hypothalamic-pituitary-gonadal (HPG) axis (Grumbach et al., 1974) (Figure 1-1). Neurons within the hypothalamus, secrete Gonadotropin-releasing hormone (GnRH) in pulses that are regulated by monoamines such as norepinephrine, dopamine and serotonin (see Appendix for chemical structures; Swerdloff and Odell, 1975). GnRH secretion can be suppressed by food restriction and excessive exercise (Hill et al., 2008). GnRH released into the local portal system travels from the hypothalamus to the anterior pituitary gland (adenohypophysis) to stimulate the release of the gonadotropins luteinizing hormone (LH) and follicle-stimulating hormone (FSH) into the peripheral blood (Plant, 2015). These two hormones target cells in the testes and ovaries to produce sex-specific blends of gonadal steroid hormones. These hormones change

in plasma concentration during development, with dramatic increases at puberty in the concentrations of testosterone in males and oestradiol in females (Figure 1-2). These steroid hormones have two primary roles that are spatially separated. Within the gonads, the steroid hormones enable reproductive capacity and, within the brain, they specify aspects of sexual behaviour (Plant, 2015; Sisk and Foster, 2004). In males, the steroid hormones testosterone, dihydrotestosterone and oestradiol direct spermatogenesis in the testes and, via a negative feedback loop involving Kisspeptin neurons, they tonically downregulate secretion of GnRH and consequently LH and FSH (Sisk and Foster, 2004; Smith, 2013; Swerdloff and Odell, 1975). In females, steroidal oestrogens such as oestradiol and progesterone direct follicle maturation in the ovaries and, via Kisspeptin negative feedback, they also tonically downregulate GnRH, LH and FSH secretion (Sisk and Foster, 2004; Smith, 2013; Swerdloff and Odell, 1975). In both sexes, puberty triggers a significant increase in the frequency of GnRH secretion pulses, which boosts steroid hormones to the level required to trigger gonad maturation and reproductive behaviour. It is thought that the pubertal GnRH increase is triggered by the integration of multiple signals from an innate developmental clock and other internal and external cues including nutrition (Sisk and Foster, 2004). However, the molecular nature of the developmental clock and other mechanistic details are not yet clear in mammals.

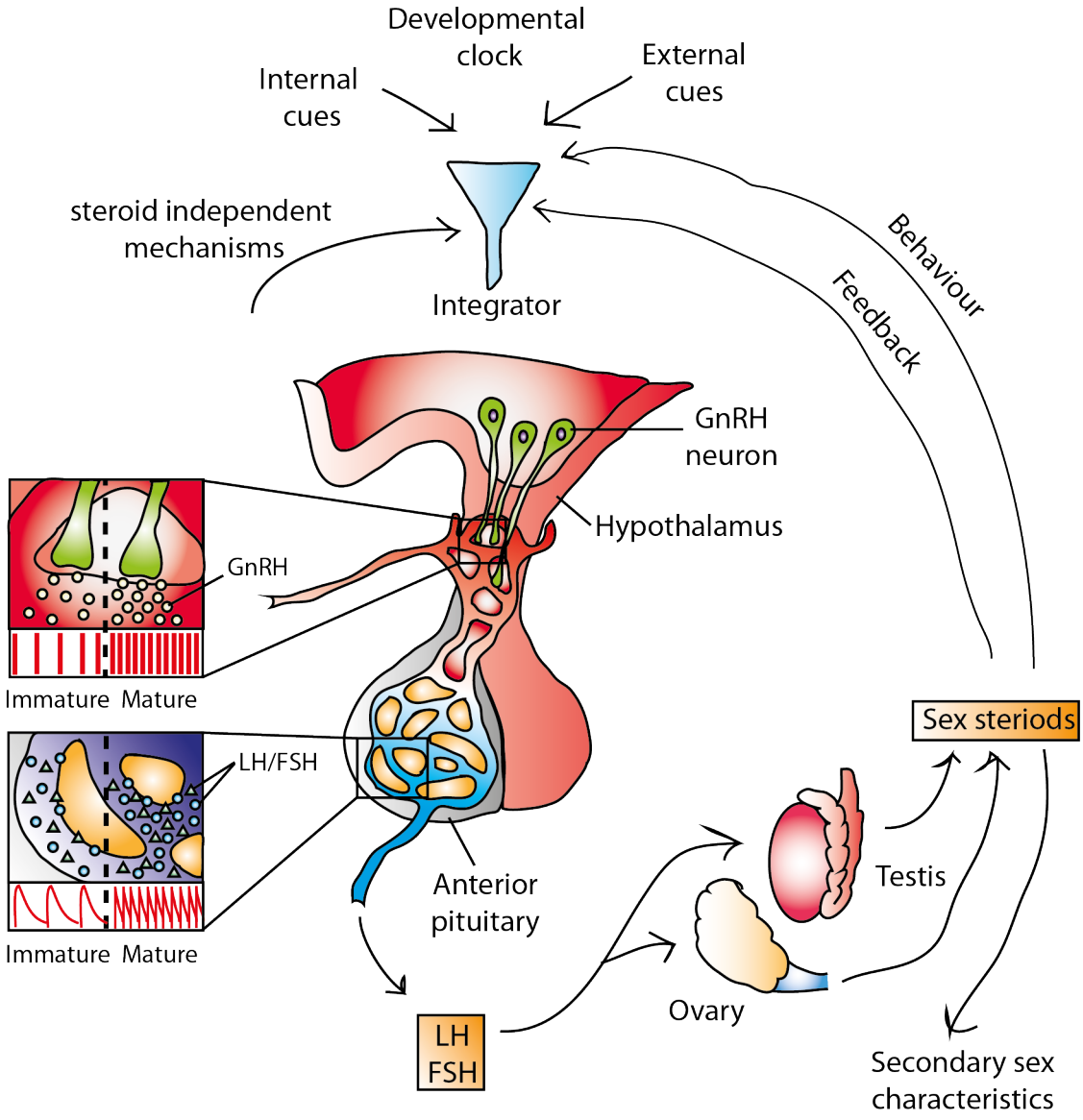

Figure 1-1: The hypothalamic-pituitary gonadal axis.

Multiple integrated signals determine firing of GnRH neurons in the hypothalamus, which directs the secretion of gonadotropins (LH and FSH) from the anterior pituitary gland and sex-specific steroid hormones from the gonads. Sex steroids then orchestrate secondary sex characteristics in peripheral tissues and, via neuroendocrine feedback, regulate GnRH secretion and social behaviours. At puberty, multiple steroid and non-steroidal mechanisms are integrated to increase GnRH and gonadotropin secretion within the "mature" HPG-axis, thus elevating sex steroids to a level necessary to support reproductive behaviour. Permission to adapt this figure has been granted by Nature neuroscience (adapted Sisk and Foster, 2004).

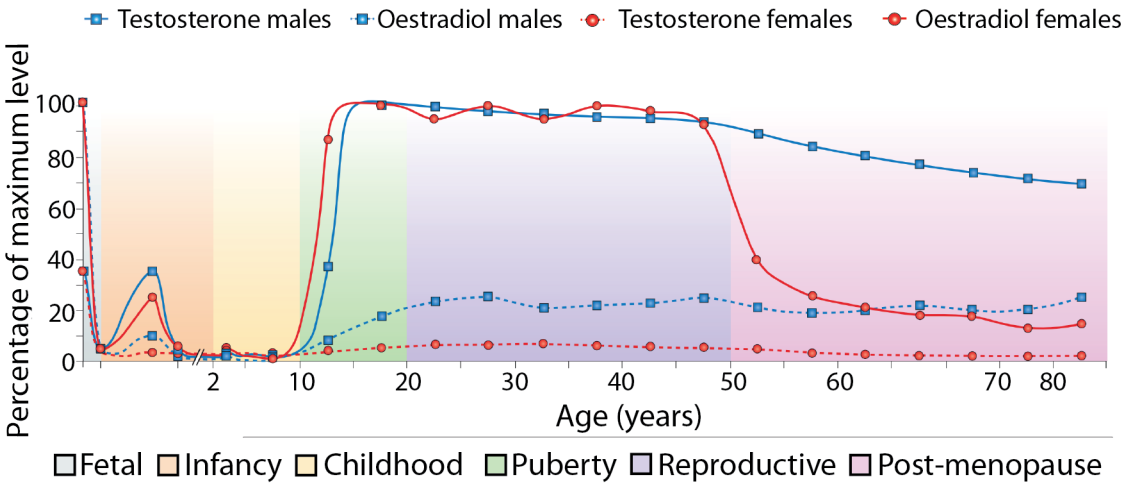

Figure 1-2: Time course of sex-steroid levels in males and females.

Testosterone and oestradiol levels in blood plasma are displayed as a percentage of the maximum mean levels from fetal to post-menopausal stages. Permission to adapt this figure has been granted by Nature Neuroscience (adapted from Ober et al., 2008).

Kelch et al., (1973) reported that an immature, pre-pubertal hypothalamus is more sensitive to the suppressive effects of gonadal steroids in comparison to an adult hypothalamus. Based on this, a hypothesis was proposed whereby the hypothalamus progressively loses sensitivity to negative feedback from steroids, thus increasing GnRH secretion and, in turn, achieving sexual maturity (Grumbach et al., 1974; Grumbach, 1978). The argument that nutrition and consequently the attainment of sufficient energy reserves triggers the onset of sexual maturation was made more than half a century ago. Thus, Kennedy and Mitra, (1963) reported that menarche (the first occurrence of menstruation, a marker of female sexual maturation) in the rat was influenced by both body size and food intake. In humans, regardless of whether the age of menarche is early or late, mean body weight is roughly invariant (48 kg in American, Dutch, Finnish and English girls), leading Frisch and Revelle, (1971) to propose a causal relationship between a critical body weight (CW) and menarche. The CW proposal was later redefined as a measure of body composition, specifically percentage body fat, directly effecting menarche (Frisch and McArthur, 1974). Observations from Nimrod and Ryan, (1975) suggest that human adipose tissue can provide a significant extra-gonadal source of sex steroids. For example, adipose tissue expresses aromatase and 17β-Hydroxysteroid dehydrogenase (17-βHSD), two enzymes involved in sex steroid

biosynthesis and modification (Kershaw and Flier, 2004). It has therefore been proposed that puberty would only become triggered upon attainment of a critical weight/fatness (CW(F)), when there is sufficient adipose tissue to sustain peak oestrogen levels (Frisch, 1981; Scott and Johnston, 1982). This would then trigger desensitisation of the hypothalamus to oestrogen, as proposed by Grumbach (1978). The negative feedback system of the HPG-axis would then be "reset" at puberty to a higher GnRH level, therefore producing the elevated levels of gonadal steroids needed to induce menarche and sexual maturation (Frisch et al., 1973; Frisch, 1981; Frisch and McArthur, 1974; Frisch and Revelle, 1971, 1970).

1.1.1 Permissive hormonal factors for sexual maturation

Leptin, encoded by the obese (*ob*) gene in the mouse, is a secreted protein hormone that is expressed primarily in white adipose tissue and informs the brain about the "size" of fat stores (Casanueva and Dieguez, 1999; Zhang et al., 1994). With concentrations proportional to fat mass, this adipokine circulates in the plasma at levels that are low in anorexics, high in obese individuals, and that decrease upon weight loss (Casanueva and Dieguez, 1999). In human patients with mutation(s) in the leptin gene or the leptin receptor, puberty is often absent and this correlates with hypogonadotrophic hypogonadism (Froguel et al., 1998; Strobel et al., 1998). In mice and rats, experimentally boosting leptin levels does not result in precocious puberty but leptin is required to provide a metabolic gate for the onset of puberty (Ahima et al., 1996; Cheung et al., 1997). Based on these findings, leptin has been regarded as a permissive rather than an instructive factor for the onset of puberty (Casanueva and Dieguez, 1999).

Ghrelin is a peptide hormone produced primarily from the gastrointestinal tract that serves to signal energy insufficiency and can delay the onset of puberty (Roa et al., 2010; Tena-Sempere, 2007). Ghrelin has been observed to increase after food deprivation and plasma levels correlate negatively with body mass index (Tena-Sempere, 2007). Low doses of ghrelin administration in male rats suppress LH secretion and testosterone levels, delaying balanopreputial separation - a marker of male rat pubertal onset (Fernández-Fernández et al., 2005). Although, a similar effect on pubertal timing was not observed with low doses of ghrelin in female rats,

higher and more frequent doses are sufficient to delay vaginal opening and ovulation in pubertal females (Fernández-Fernández et al., 2005; Roa et al., 2010; Tena-Sempere, 2007). Ghrelin levels have been observed to decline steadily during puberty in humans (Soriano-Guillén et al., 2004). If ghrelin's actions in humans are similar to its action in rats, it has been suggested that this orexigenic (appetite inducing) hormone may play a permissive negative role in the timing of puberty. In summary, high leptin and low ghrelin concentrations may be required in order to provide a permissive window for the onset of puberty.

1.1.2 CW(F) as a trigger for sexual maturation

The Frisch and colleagues CW(F) hypothesis that nutrition regulates the timing of puberty accommodates the general idea that a female becomes fertile only when she has sufficient body reserves to sustain pregnancy (Frisch et al., 1973; Frisch, 1981; Frisch and McArthur, 1974; Frisch and Revelle, 1971, 1970). The CW(F) hypothesis is consistent with the observed trend of a declining age of menarche in western countries, as the height and weight of girls have increased (Parent et al., 2003). It is also consistent with the observed advancement of menarche in obese girls, delayed menarche in slower growing girls at high altitude, and delayed menarche in undernourished girls (Currie et al., 2009; Frisch, 1972; Kapoor and Kapoor, 1986). The CW(F) hypothesis can also account for oligomenorrhea and amenorrhea (irregular or absent menstrual cycles, respectively) in high performance athletes, ballet dancers or women suffering from anorexia nervosa (Scott and Johnston, 1982). According to the hypothesis, women facing any of the circumstances above would have low body fat and therefore would not produce the level of steroid hormones necessary to "reset" the HPG feedback loop. Refining the CW(F) hypothesis further, it can also be suggested that females with the conditions mentioned above have insufficient leptin and excessive ghrelin levels, both leading to a failure to upregulate the HPG-axis. In addition, it has been recognised that psychological stress can also delay or block menarche (Frisch and McArthur, 1974).

In spite of the convenience proposed by the CW(F) model, scrutiny of the hypothesis has resulted in several criticisms (Cameron, 1976; Scott and Johnston, 1982; Trussell, 1980). These include observations that individuals that do not meet

the strict CW(F) definition are nevertheless able to menstruate and that amenorrhea can linger even after anorexics regain weight on a nutritious diet (Osler and Crawford, 1973; Rakoff, 1967). Also, the CW(F) hypothesis of Frisch and colleagues only accommodates female puberty (the onset of menarche): no mechanism is provided for how the onset of puberty in males is timed. More generally in both humans and model organisms, greater attention has been paid into the onset of sexual maturation in females than in males, probably because menarche is such a convenient marker of this developmental transition.

1.2 *Drosophila* as a model to study the juvenile-adult transition

The holometabolous (undergoing complete metamorphosis) fruit fly *Drosophila melanogaster* has a long and distinguished track record as a genetic model organism (Ashburner and Bergman, 2005). More recent utility of *Drosophila* as a physiological model has been possible due to a fully sequenced genome (Zhao et al., 2000) and sophisticated genetic manipulation techniques, enabling up- or down-regulation of virtually every gene in the genome, in almost any cell type, at any developmental stage (St Johnston, 2002). *Drosophila* now provides a powerful model for studies into metabolism, growth control, behaviour and ageing (Edgar, 1999; Padmanabha and Baker, 2014; Partridge et al., 2011). In *Drosophila*, a ~10-day life cycle at 25 ^{o}C (~20 days at 18 ^{o}C, all further timings used in this thesis will be stated for development at 25ºC unless otherwise stated) is punctuated by transitions that separate four distinct morphological phases: the embryo, the larva encompassing three instars (the time between each moult; numbered L1-L3), the pupa and the adult (Figure 1-3). As with humans, the majority of *Drosophila* growth occurs during the juvenile stage (the larva) and sexual maturity is not attained until adulthood (Tennessen and Thummel, 2011). A net growth (mass gain) of ~ 200 fold occurs during larval development: from hatching at L1 until the end of L3, when pupal development and the process of metamorphosis occurs. Larval growth is made possible by moults at the L1/L2 and L2/L3 transitions, when the larva's rigid chitinous exoskeleton, the cuticle, is replaced to accommodate a larger body size (Church and Robertson, 1966). The moults at the larval transitions involve the synthesis of a new cuticle by epidermal cells and shedding of the old cuticle as a

remnant. The steroid hormone ecdysone is a key developmental timer in *Drosophila*, orchestrating larval moulting and the onset of metamorphosis - the process that transforms the juvenile larva into a sexually mature adult. A loose analogy can be drawn between sexual maturation in humans (puberty) and in *Drosophila* (metamorphosis). In both cases, steroid hormones shut down most body growth and trigger a series of major physiological and morphological changes enabling reproductive capacity to be attained (Gilbert et al., 2002; Sisk and Foster, 2004). In fact, puberty and subsequent adolescence can be regarded as marking the “metamorphosis” of a child into an adult (Sisk and Foster, 2004).

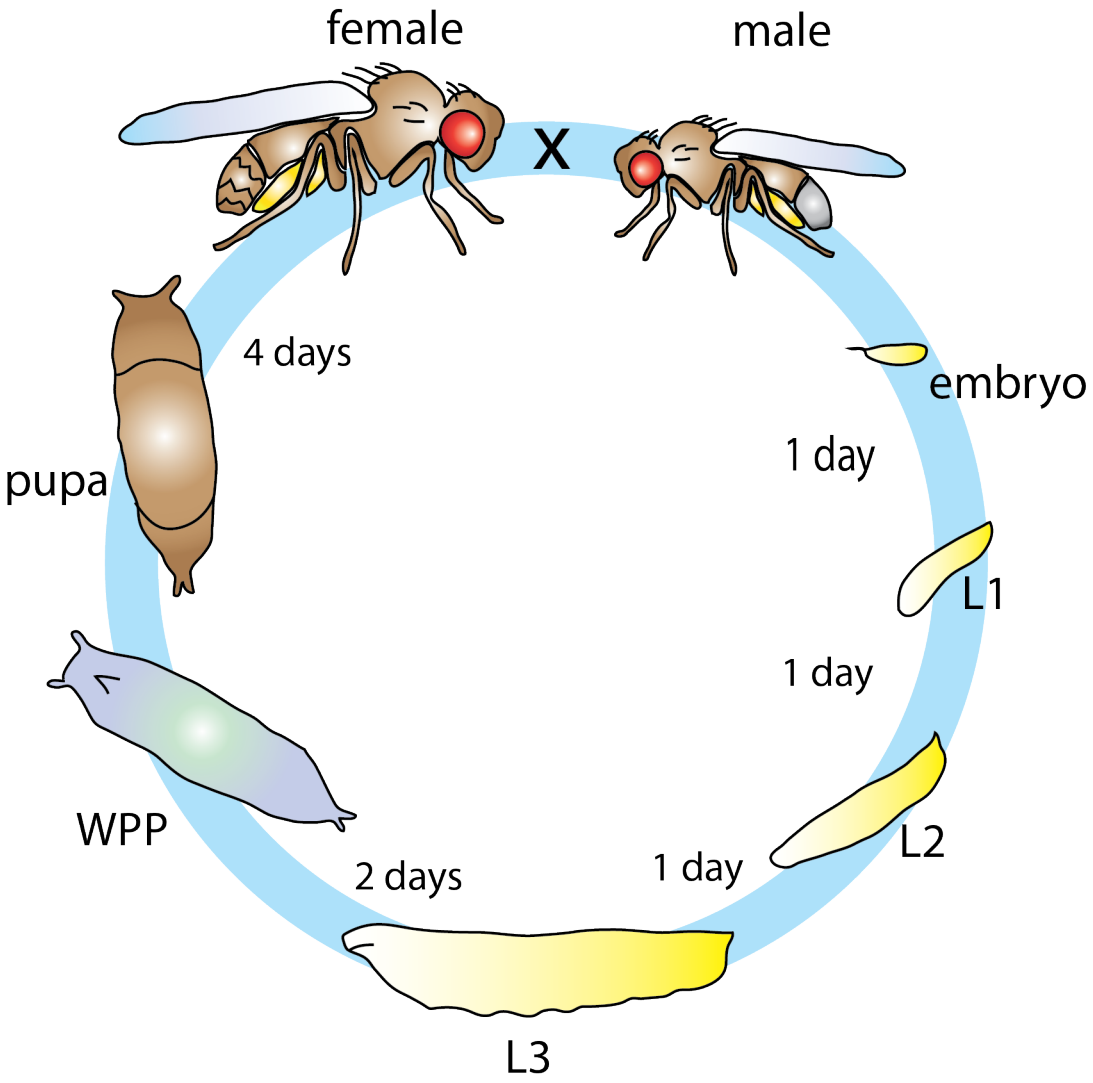

Figure 1-3: The life cycle of *Drosophila.*

The life of *Drosophila* encompasses a ~10 day developmental cycle, including (clockwise) embryonic, larval (including three larval instars: L1, L2 and L3) and pupal phases before reaching adulthood. Larvae in the third instar (L3) pupariate into a white prepupa (WPP) ~24 hr before the pupal membrane is synthesized, a process that defines pupation proper.

1.2.1 Ecdysone signalling

Three classes of hormones primarily regulate developmental timing in insects (Di Cara and King-Jones, 2013). The ecdysteroids include the moulting prohormone ecdysone and its biologically active metabolite 20-hydroxyecdysone (20E). In addition, there is the neuropeptide prothoracicotropic hormone (PTTH) and the sesquiterpenoid juvenile hormone (JH). JH is a negative regulator of PTTH release in many insects and its suppression results in a precocious transition from the larva into a pupa (Daimon et al., 2012; Nijhout and Williams, 1974). In contrast, in *Drosophila,* JH is not required to sustain larval development but, instead, plays key roles during pupal development and adulthood (Baumann et al., 2010). Hence, in *Drosophila*, ecdysone and PTTH are the major hormones controlling the timing of the larval-larval and the larval-pupal developmental transitions.

Pulses of ecdysone dictate progression through the distinct morphological stages of *Drosophila* development (Figure 1-4). Each pulse is precisely timed, has a particular amplitude and duration and triggers a different set of biological responses (Ou and King-Jones, 2013). For example, the ecdysone pulse during late embryogenesis regulates cell movement and future cuticle deposition (Chávez et al., 2000). The pulses during L1 and L2 trigger larval moults leading to the synthesis of new cuticles with a unique morphology for each instar (Riddiford and Truman, 1993). A pulse at the end of L3 arrests growth, initiates wandering behaviour, signals pupariation and the onset of adult maturation, which is then followed by a high titre pulse ~24 hours later that subsequently triggers pupation (De Reggi et al., 1975; Karim and Thummel, 1991; Tennessen and Thummel, 2011).

Figure 1-4: Ecdysone pulses trigger developmental transitions in *Drosophila.*
Schematic representation of 20E concentration during *Drosophila* development. Large bursts in the 20E titre coincide with hatching, larval moults, pupariation and pupation. Three minor peaks are also observed during L3 that prepare the larvae for metamorphosis; these peaks include the commitment to metamorphosis upon attainment of a CW: the “CW peak”. PP: prepupa. Permission to adapt this figure has been granted by Current Topics in Developmental Biology (adapted from Ou and King-Jones, 2013).

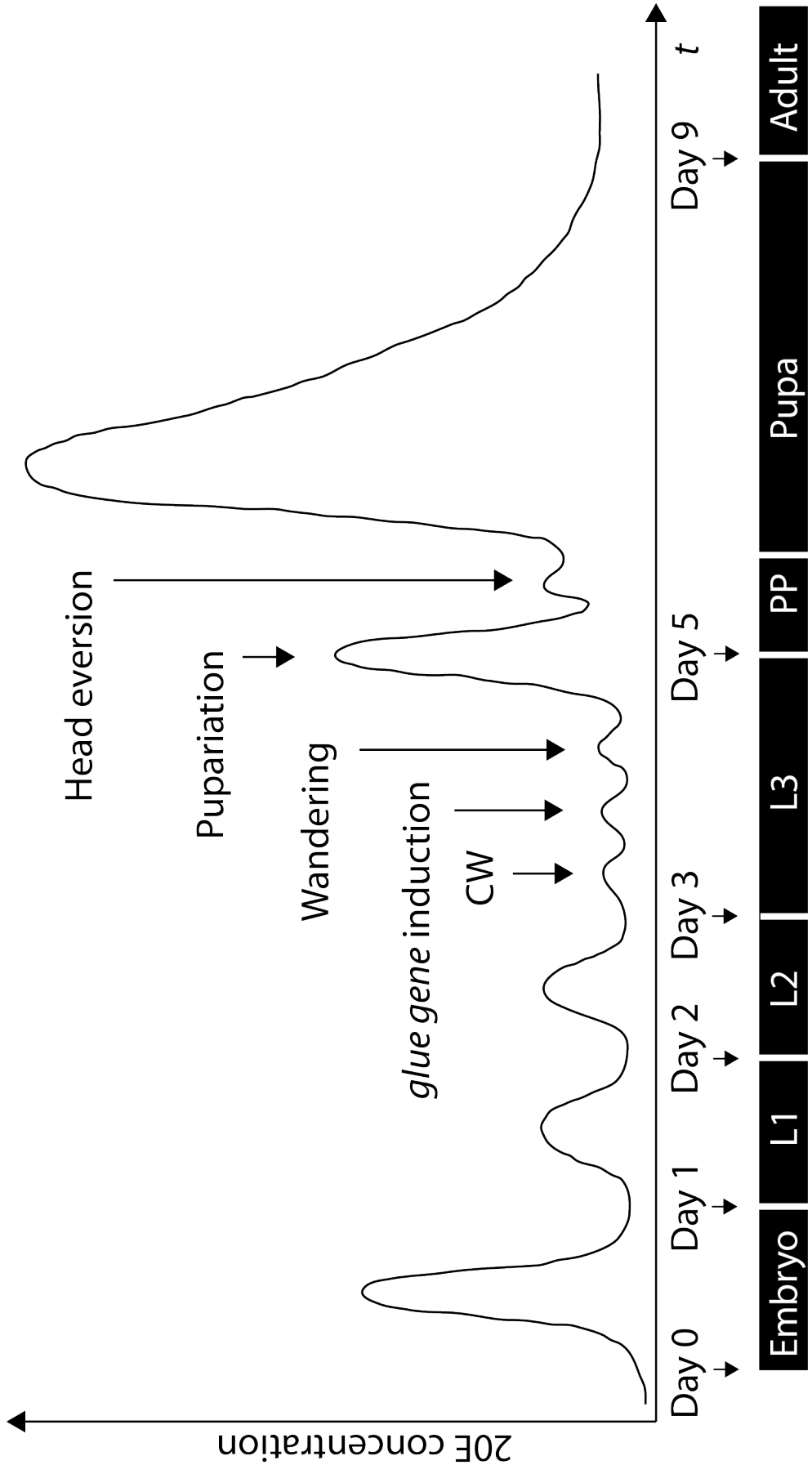
20E concentration
Day 0
Day 1
Day 2
Day 3
Day 5
Day 9
t
Embryo
L1
L2
L3
PP
Pupa
Adult
Head eversion
Pupariation
Wandering
glue gene induction
CW

Ecdysone is synthesised in the prothoracic gland (PG) cells of the ring gland, from cholesterol after a series of reactions (Figure 1-5) involving: Neverland (an electron oxygenase), Shroud (a short-chain dehydrogenase) and the "Halloween" family of cytochrome P450 enzymes: Spookier, Cyt6t3, Phantom, Disembodied and Shadow (Chávez et al., 2000; Gilbert, 2004; Niwa et al., 2010; Nüsslein-Volhard and Wieschaus, 1980; Warren et al., 2004, 2002; Yoshiyama et al., 2006). The ring gland of *Drosophila* is a composite endocrine organ made up of the corpora allata (CA), corpora cadiaca (CC) and the PG. Although the synthesis of ecdysone is known from 5β-Ketodiol and the synthesis of 7-dehydrocholesterol from cholesterol, the exact pathway of conversion from 7-dehydrocholesterol to 5β-Ketodiol (which is known to include shroud, spookier and Cyt6t3), remains elusive and is termed the "Black Box" (Ou and King-Jones, 2013). Following synthesis, ecdysone is subsequently secreted from PG cells and converted into the biologically active form of 20E in peripheral tissues by the action of Shade – the final P450 enzyme of the Halloween family (Petryk et al., 2003).

Figure 1-5: Ecdysone biosynthesis in prothoracic gland cells.

Cholesterol is converted by at least 4 enzymes (Neverland, Shroud, Spookier and Cyp6t3) to 5β-Ketodiol in the endoplasmic reticulum (ER) of PG cells. 5β-Ketodiol is subsequently converted into ecdysone via Phantom, Disembodied and Shadow in the mitochondria (MT). Ecdysone is then secreted from the PG cells into the hemolymph and converted to 20E via Shade in the ER of peripheral tissues. Stars represent enzyme actions involved in ecdysone biosynthesis. Permission to adapt this figure has been granted by Current Topics in Developmental Biology (adapted Ou and King-Jones, 2013).

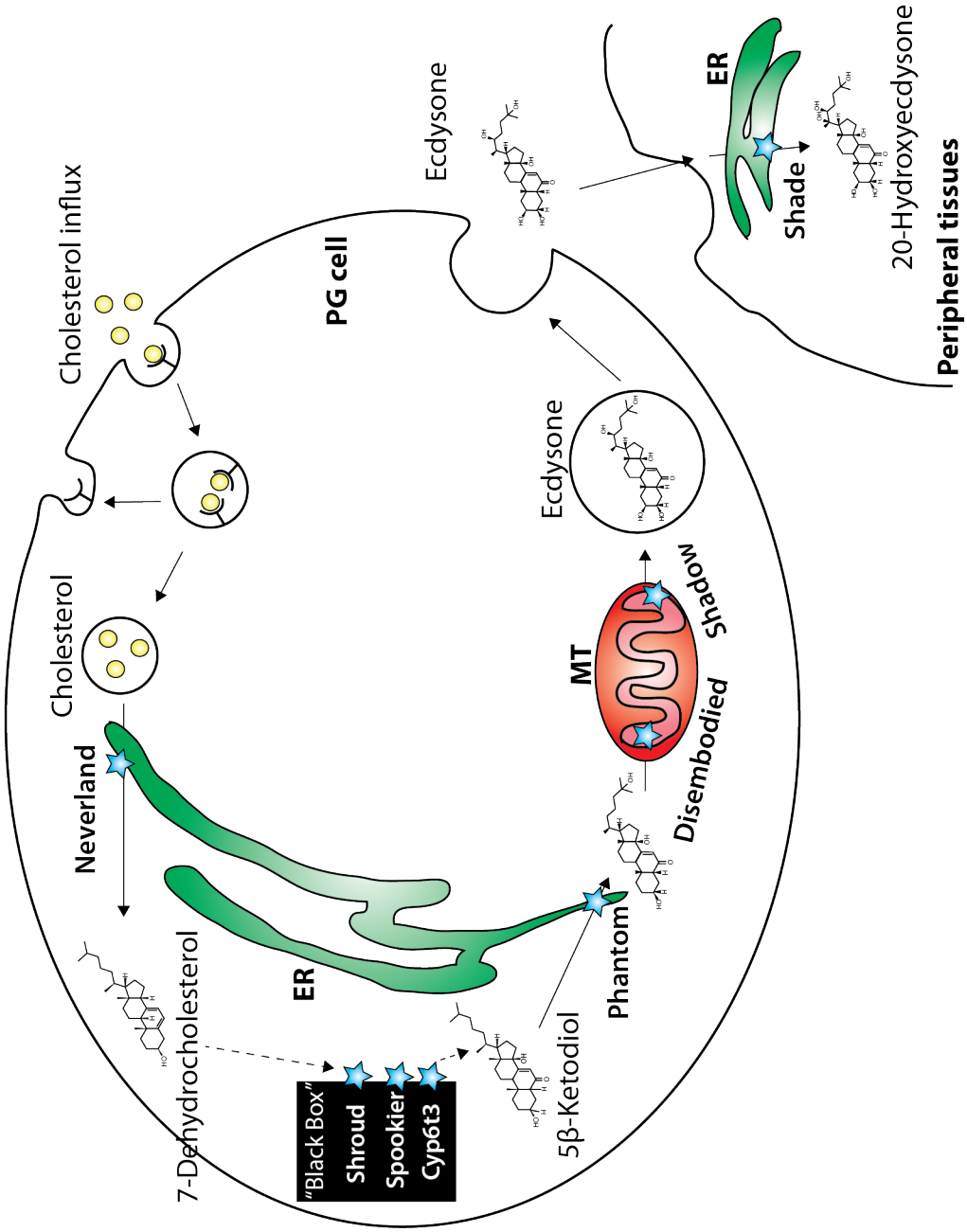
Cholesterol influx
PG cell
Ecdysone
ER
Shade
20-Hydroxyecdysone
Peripheral tissues
Cholesterol
Neverland
Ecdysone
MT
Shadow
Disembodied
ER
7-Dehydrocholesterol
"Black Box"
Shroud
Spookier
Cyp6t3
5β-Ketodiol
Phantom

PTTH is released in an ultradian manner from two pairs of lateral neurosecretory cells in the brain that terminate onto the PG cells of the ring gland (McBrayer et al., 2007; Mizoguchi et al., 1990; Ou and King-Jones, 2013). PTTH binds to its receptor, Torso, on PG cells and activates the extracellular signal-regulated kinase (ERK) pathway. PTTH/ERK signalling, together with insulin and tissue growth factor beta (TGFβ)/activin signalling, stimulates ecdysone synthesis in cells of the PG (Figure 1-6) (Chen et al., 1996; Gibbens et al., 2011; Rewitz et al., 2009). PTTH stimulates ecdysone production via a pathway involving two sequential repressions. First, PTTH/ERK signalling represses nuclear localisation of *Drosophila* hormone receptor 4 (DHR4). In turn, nuclear DHR4 negatively regulates an ecdysone biosynthetic gene, *Cyp6t3* (Ou et al., 2011). Cell-to-cell co-ordinated expression of ecdysone biosynthetic genes among PG cells is achieved by monoaminergic signalling (Ohhara et al., 2015). The monoamine tyramine is secreted from PG cells and it activates, in an autocrine manner, a G-protein coupled receptor (GPCR): β3-octopamine receptor (Octβ3R). Activation of Octβ3R then increases responsiveness to *Drosophila* insulin like peptides (dIlps) and also to PTTH (Ohhara et al., 2015). Knock down of *Octβ3R* via RNAi, significantly decreases expression of the Halloween genes: *neverland, spookier, shroud, Cypt6t3, phantom, disembodies* and *shadow* in the PG and results in developmental arrest, due to ecdysone insufficiency (Ohhara et al., 2015).

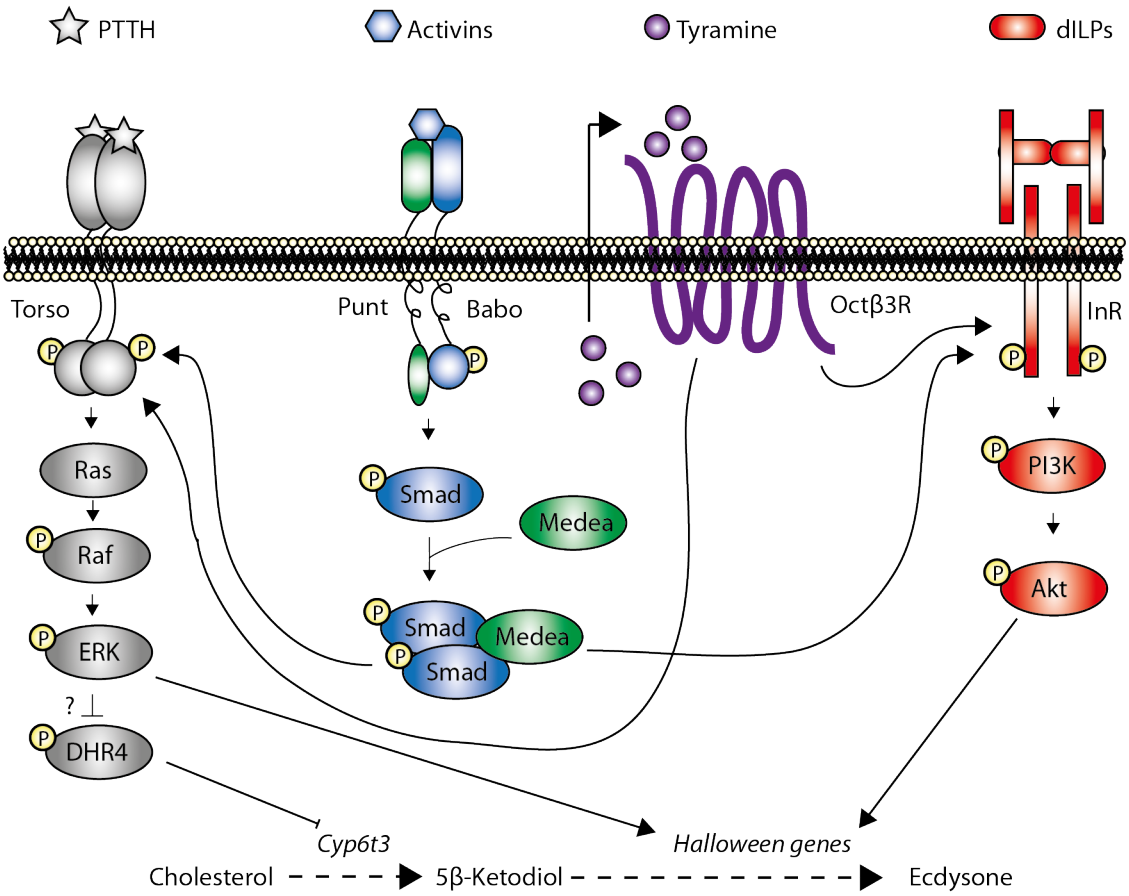

Figure 1-6: Regulation of ecdysone biosynthesis.

PTTH, Activin, Octβ3R and insulin signalling cascades regulate ecdysone synthesis. PTTH and insulin signalling regulate expression of the P450 ecdysone biosynthetic genes of the Halloween group, whereas activin and Octβ3R signalling mediate responsiveness of the PG cell to PTTH and insulin signalling. In addition, the ERK pathway is thought to regulate DHR4 nuclear localisation, in turn, nuclear DHR4 supresses' expression of the Halloween gene *Cyp6t3*. Ras: rat sarcoma. Raf: rapidly accelerated fibrosarcoma. Smad: mothers against decapentaplegic homolog 1. PI3K: phosphatidylinositide 3-kinase. Akt: protein kinase B. P: phosphorylated residue. Permission to adapt this figure has been granted by Current Topics in Developmental Biology (adapted from Ou and King-Jones, 2013).

Surprisingly, genetic ablation of PTTH producing neurons does not result in a lethal phenotype. Instead, developmentally delayed, larger animals with prolonged larval instars are observed (McBrayer et al., 2007). In the ablated animals, the first and second larval instars were ~8 hr delayed and the time to pupariation (TTP) after the L2/L3 moult, was 5 instead of 2 days. As Halloween gene expression was reduced in the ablated animals, it was suggested that the developmental delays result from insufficient ecdysone biosynthesis (McBrayer et al., 2007).

The gene expression cascade triggered by a single ecdysone pulse, elegantly explained in the Ashburner model (Ashburner et al., 1974; Ashburner and Richards, 1976), is initiated through 20E binding to a heterodimer of two nuclear receptors: the Ecdysone receptor (EcR) and Ultraspiracle (USP) (Hu et al., 2003; Koelle et al., 1991; Yao et al., 1993, 1992). However, the Ashburner model does not fully explain how individual tissues respond differently to the same ecdysone pulse or how the same tissue responds differently to temporally different ecdysone pulses (Andres and Thummel, 1995; Mou et al., 2012). A complex system of feed-forward and feed-back loops regulate ecdysteroidogenesis and impinge on EcR expression (reviewed in Rewitz et al., 2013). For example, EcR expression in PG cells is promoted by low levels of 20E, which stimulates further ecdysone biosynthesis, however, high levels of 20E decrease ecdysone biosynthesis via inhibition of EcR expression (Koelle et al., 1991). The diverse cellular responses that are observed in reaction to different ecdysone pulses in different tissues may, in part, be explained by differential expression pattern of EcR isoforms (Bender et al., 1997). The three EcR isoforms (EcR-A, EcR-B1 and EcR-B2) differ in N-terminal regions but share a common DNA-binding domain. EcR-B1 is predominantly expressed in larval tissues, which are targeted for apoptosis after pupariation, whereas EcR-A is predominantly expressed in imaginal discs that will form the integument of the adult (Talbot et al., 1993).

Three low-titre peaks of ecdysone occur during the third larval instar and have been assigned roles in preparing the animal for pupariation (Figure 1-4) (Warren et al., 2006). In temporal order, they have been assigned to the attainment of a CW (defined in 1.2.2), the induction of salivary *gland glue* genes and the switch from

feeding to wandering behaviour (Lehmann, 1996; Mirth et al., 2005; Sokolowski, 2001; Warren et al., 2006).

1.2.2 Critical Weight in *Drosophila*

CW in *Drosophila* is defined as the weight at which starvation will no longer delay the TTP (Mirth and Riddiford, 2007; Stieper et al., 2008). CW corresponds to the "seventy-hour" (after egg laying) change documented in experiments by Beadle et al., (1938) and Bakker (1959). In these classic experiments, it was observed that larvae starved at or after CW produce undersized yet viable individuals without a developmental delay, whilst larvae starved prior to this point arrest development and often die if not ultimately returned to food (Figure 1-7). In *Drosophila*, although not in other insects, starvation applied after CW shortens TTP by several hours, compared to fully fed controls. As the TTP for L3 larvae starved pre-CW is longer than that of larvae starved post-CW, a break point method can be used to estimate CW from plots of TTP *versus* larval weight at the onset of starvation (Stieper et al., 2008). Minimal viable weight (MVW) is another closely related nutritional checkpoint that is attained at almost the same time as CW in *Drosophila*, although in many other insects MVW is attained much earlier than CW. This is defined as the weight necessary to survive until metamorphosis, regardless of whether or not there is a developmental delay (Mirth et al., 2005; Nijhout, 1975).

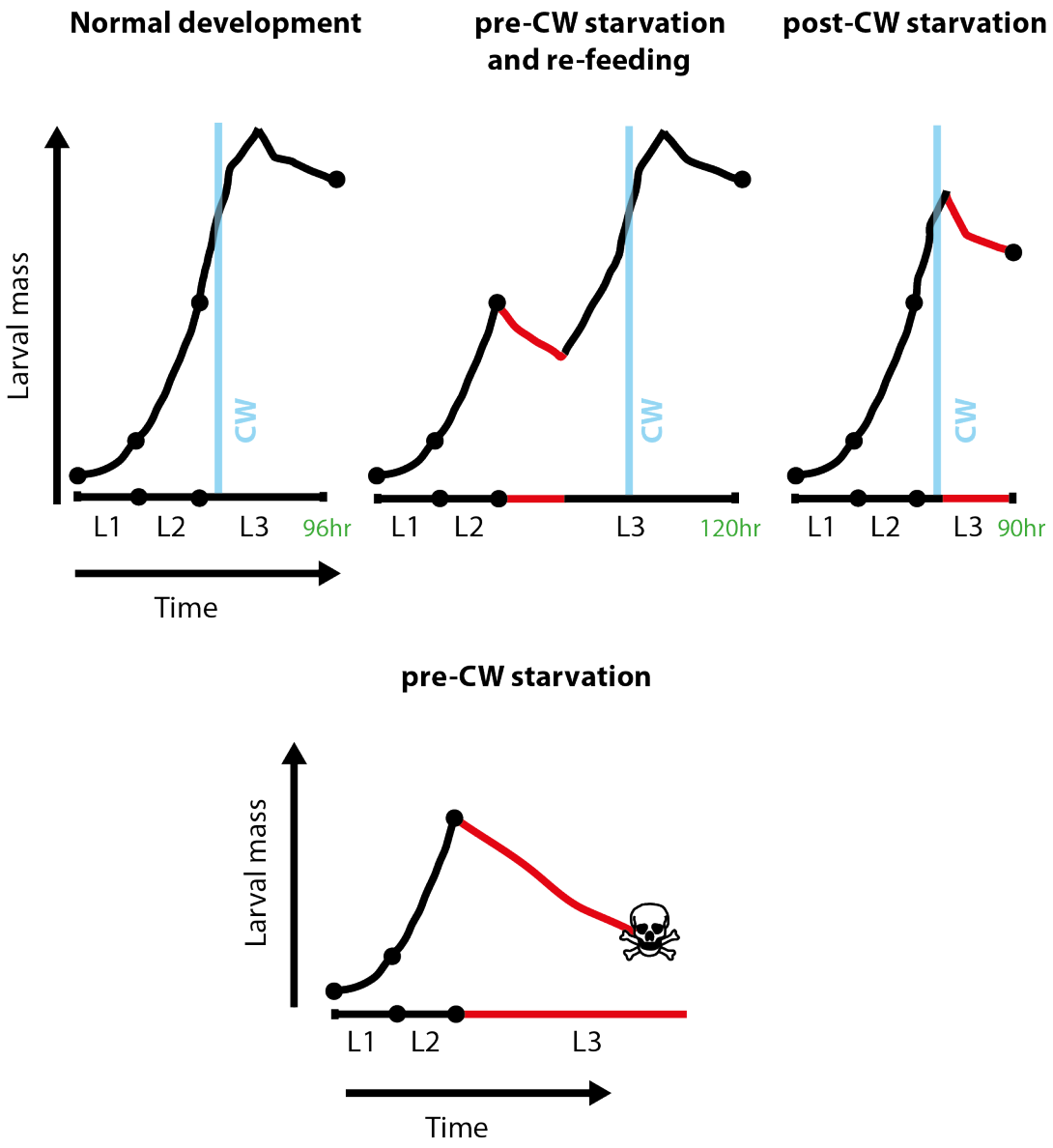

Figure 1-7: Effects of starvation before or after CW in *Drosophila*.

Schematic representation of *Drosophila* larval development and the response to starvation. Larvae experience exponential growth (black line) throughout the larval instars (L1-L3) and, if fed on an optimal diet, pupariate at ~96 hr after larval hatching. Starvation pre-CW and subsequent re-feeding delays TTP by a margin larger than the period of starvation but does not affect final body size. Starvation post-CW does not delay TTP but decreases final body size. Continuous starvation administered pre-CW, results in developmental arrest and eventually death. Period of feeding: black trace. Period of starvation: red trace. CW attained: blue line. Permission to adapt this figure has been granted by Current Biology (adapted from Tennessen and Thummel, 2011).

The feeding period of larval development after attainment of CW is referred to as the terminal growth phase (TGP), during which time the larva can quadruple its size depending upon nutrient availability (Beadle et al., 1938; Edgar, 2006). Signalling via the Insulin-like receptor (InR) produces different outcomes either side of CW. Pre-CW, the decrease in insulin signalling through the InR (IIS), triggered by moving larvae to a nutrient restricted (NR) medium, reduces the growth rate and delays TTP (Prabhu and Robertson, 1963). However, post-CW, alteration of IIS during the TGP does not alter TTP but does regulate final body size (Prabhu and Robertson, 1963). Furthermore, experimentally manipulating IIS in the PG can alter ecdysone biosynthesis. For example, increasing IIS in the PG boosts ecdysone levels, leading to precocious CW attainment and even pupariation at a smaller-than-normal size during the L2 stage (Mirth et al., 2005).

1.2.3 Molecular mechanisms underlying CW

Larvae commit to metamorphosis at CW and this is thought to be mediated by a small ecdysone pulse at ~60 hours after larval hatching (hr ALH, all times of development will be reported as hr ALH unless explicitly stated otherwise) (Koyama et al., 2014; Mirth and Riddiford, 2007; Mirth and Shingleton, 2012). Koyama et al. (2014), proposed a model to account for the developmental arrest of pre-CW starved larvae. Larval moults involve a short period of non-feeding and, in their model, starvation at the L2/L3 moult reduces IIS and so increases nuclear localisation of Forkhead Box class O transcription factor (FoxO), which then binds to USP in the PG. The formation of FoxO-USP then inhibits EcR-USP signalling in the PG, thus decreasing Halloween gene expression and ecdysone biosynthesis. After the L2/L3 moult, feeding gradually increases IIS in the PG during the third instar, leading to FoxO phosphorylation and nuclear exclusion, thus decreasing FoxO complexed to USP and enabling EcR-USP signalling to stimulate ecdysone biosynthesis. During L3, ecdysone levels eventually reach a threshold at CW and initiate the processes that commit to the onset of pupariation. In the Koyama model, starvation pre-CW results in nuclear FoxO remaining bound to USP, thus repressing ecdysone biosynthesis and resulting in developmental arrest (Koyama et al., 2014).

Ohhara et al. (2015) subsequently proposed a model accounting for how the large

titre ecdysone peak is generated downstream of the CW larval-size checkpoint. Ohhara et al. (2015), observed a progressive decrease in tyramine levels in PG cells after 60 hr, which they concluded is due to increased tyramine secretion from the PG and thus increased autocrine Octβ3R signalling. The depletion of intracellular tyramine stores after 60 hr could be abrogated by starvation before but not after CW. Furthermore, they found that experimentally decreasing tyramine signalling in the PG (via tissue-specific Octβ3R knockdown) abrogated the increase in IIS and PTTH/ERK signalling normally observed in PG cells between 48 hr to 60 hr (Ohhara et al., 2015). Octβ3R knockdown caused larval developmental arrest unless this knockdown was triggered after 72 hr, strongly suggesting that autocrine regulation of Octβ3R by tyramine acts to increase PG responsiveness to dIlps and PTTH, elevating Halloween gene expression and therefore boosting ecdysone biosynthesis to levels high enough to trigger the larval to pupal transition.

1.3 Metabolic profiling and metabolomics

Several *Drosophila* studies have shown how nutrition, temperature and oxygen levels can influence when CW is attained (Callier et al., 2013; Colombani et al., 2005; De Moed et al., 1999; Ghosh et al., 2013). It nevertheless remains unclear how CW and ecdysone signalling are linked to downstream metabolic changes that drive the process of pupariation. It is also unclear whether or not any of these downstream metabolic changes might feed back upon the timing of the peaks in ecdysone signalling. These are questions that I address in this thesis by using metabolomics to identify small molecules that change during larval development in a CW attainment-dependent manner.

Metabolites are the end products of all cellular processes and thus could be said to be more proximal to the phenotype of the organism than are mRNA transcripts or proteins (Camacho et al., 2005; Worley et al., 2013). Therefore, sampling the metabolome at different points in the developmental progression of an organism could show how developmental transitions and dietary/genetic manipulations alter the metabolism of an organism. Metabolic profiling typically describes the analysis of a whole (homogenised) organism or an organism-derived bodily fluid (e.g. hemolymph, serum or plasma) through high-resolution nuclear magnetic resonance (NMR) spectroscopy and/or mass spectrometry (MS) (Camacho et al., 2005).

These techniques provide, essentially, an instantaneous global snapshot of the small molecule complement of an organism (or tissue) at a post-transcriptional and post-translational level. In comparison to MS, NMR spectroscopy suffers from low sensitivity. However, NMR requires little-to-no sample purification or chemical derivatisation and so can deliver reliable and reproducible estimates of absolute metabolite concentrations (when internal standards are used). NMR is arguably unmatched at solving the chemical structures of "unknowns" and, in combination with isotopic labelling, also provides a powerful method for pinpointing key changes in metabolism between different biological samples (Fan and Lane, 2016; Markley et al., 2017; Nagana Gowda and Raftery, 2015). In this thesis, NMR spectroscopy is used to record and analyse *Drosophila*-derived metabolomes; therefore, an introduction into the basic physics of the NMR phenomena will follow.

1.3.1 NMR spectroscopy

The basis of ^{1}H NMR spectroscopy involves recording NMR signals arising from excitation of hydrogen nuclei (protons) by radiofrequency radiation. The generation of a NMR signal is possible due a quantum mechanical property of the proton called spin, which can be thought of as a magnetic moment vector and results (in a semi-classical picture) in the proton behaving like a small magnet (Rattle, 1995). When a nucleus is placed into an applied magnetic field, the spin vector can be thought of as aligning with the applied field, following a processional motion with angular frequency proportional to the field strength – the Larmor or resonance frequency (Balcı, 2005; Keeler, 2010; Rattle, 1995). As a proton has a spin quantum number of ½, protons in an applied magnetic field can exist in one of two energy (spin) states – a lower and higher energy configuration (Balcı, 2005). A nucleus in the lower energy state can absorb a photon to transition to the higher energy state. The energy of the photon needed for this level transition is proportional to its frequency and this frequency is equal to the Larmor frequency of the nucleus (Rattle, 1995). In simple terms, the peaks on a NMR spectrum are the result of the transitions between energy levels of nuclei, achieved via application of a short intense pulse of radio frequency radiation at the appropriate frequency (Rattle, 1995)(Figure 1-8).

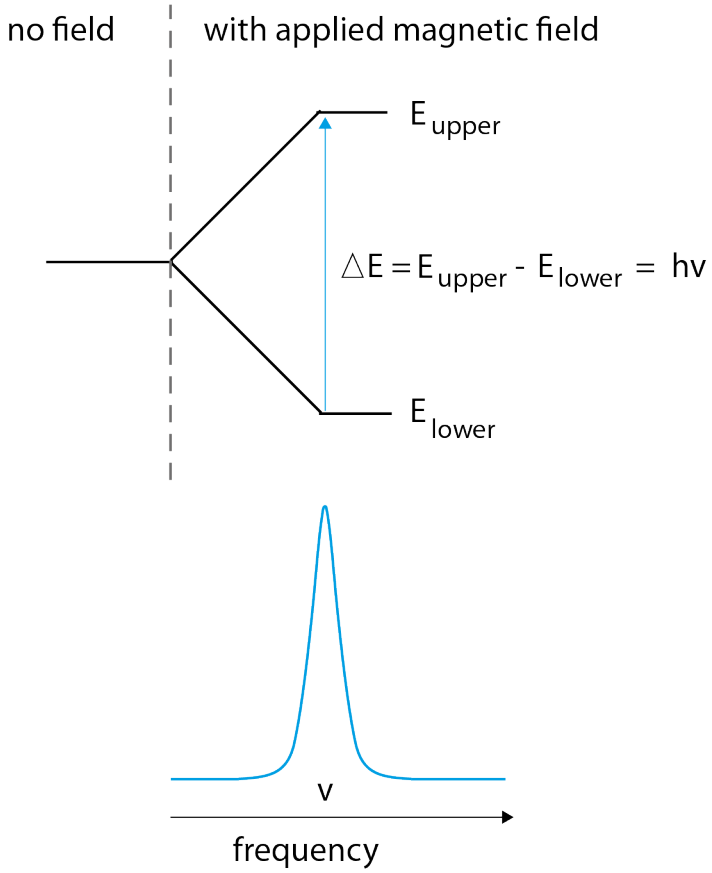

Figure 1-8: Nuclei transition to a higher energy configuration upon absorption of a photon.

The application of an applied magnetic field results in splitting of a hydrogen nucleus into two energy states: an upper (E_{upper}) and lower (E_{lower}) energy state. A nuclei can transition to the E_{upper} if it absorbs a photon with energy equal to $E_{upper} - E_{lower}$, which is also equal to Planck's constant (h: 6.626 x 10^{-34} J s) multiplied by the Larmor frequency of the chosen nucleus (v). The result is an absorption line in the spectrum, at frequency v.

The Larmor frequency of a nucleus is proportional to the "total magnetic field" at the nucleus; this total field differs from an applied field as the applied field induces an opposing magnetic field in the surrounding electrons (Keeler, 2010). The nucleus is said to be "shielded" to various degrees depending on the density of the electron cloud at the nucleus, itself dependent on the local chemical environment (i.e. bonding). The different effective magnetic fields "felt" by the nucleus allow distinction between different chemical environments within the same molecule. Therefore, the different nuclei of the same element (e.g. the proton) in the molecule will have different resonant frequencies; this effect is termed the chemical shift

phenomenon (Keeler, 2010; Rattle, 1995). The chemical shift is a precise metric of the chemical environment around a nucleus and is reported as the difference between the Larmor frequency of the nucleus in question and a standard, normalised to the frequency exhibited by that standard and is expressed mathematically by:

$$\delta\ (ppm) = 10^6 \times \frac{\nu - \nu_{ref}}{\nu_{ref}}$$

where the chemical shift (δ) is expressed in parts per million (ppm), v is the frequency of the NMR peak in question and v_{ref} is the frequency of the standard's NMR peak (Keeler, 2010).

As the lines on an ^{1}H NMR spectrum denote protons in different chemical environments (at different chemical shifts), the area under a given resonance, the peak integral, is proportional to the number of protons in equivalent chemical environments giving rise to that feature – i.e. the number of equivalent protons present (Keeler, 2010). Nuclei experiencing different chemical environments from each other are termed non-equivalent nuclei. Non-equivalent nuclei exert an effect on each other if the distance between these nuclei is less than or equal to three bond lengths, this effect is termed spin-spin or J coupling and results in peak splitting and the appearance of multiplets (Keeler, 2010; Rattle, 1995). In simple terms, the position of NMR peaks (/NMR peak clusters) on a spectrum defines a metabolite's identity (set of chemical environments), peak heights (area under the curve) correspond to equivalent protons and the collective peak heights (the height of all the peak clusters of the same metabolite) informs on the concentration of the metabolite. Figure 1-9 displays ^{1}H NMR spectra for ethanol at two concentrations. As can be observed in the spectra, different chemical environments in the molecule result in two peak clusters or multiplets; the height (or signal intensity) of the peaks in spectrum A is twice that of the peaks in spectrum B, due to the higher concentration of ethanol in spectrum A.

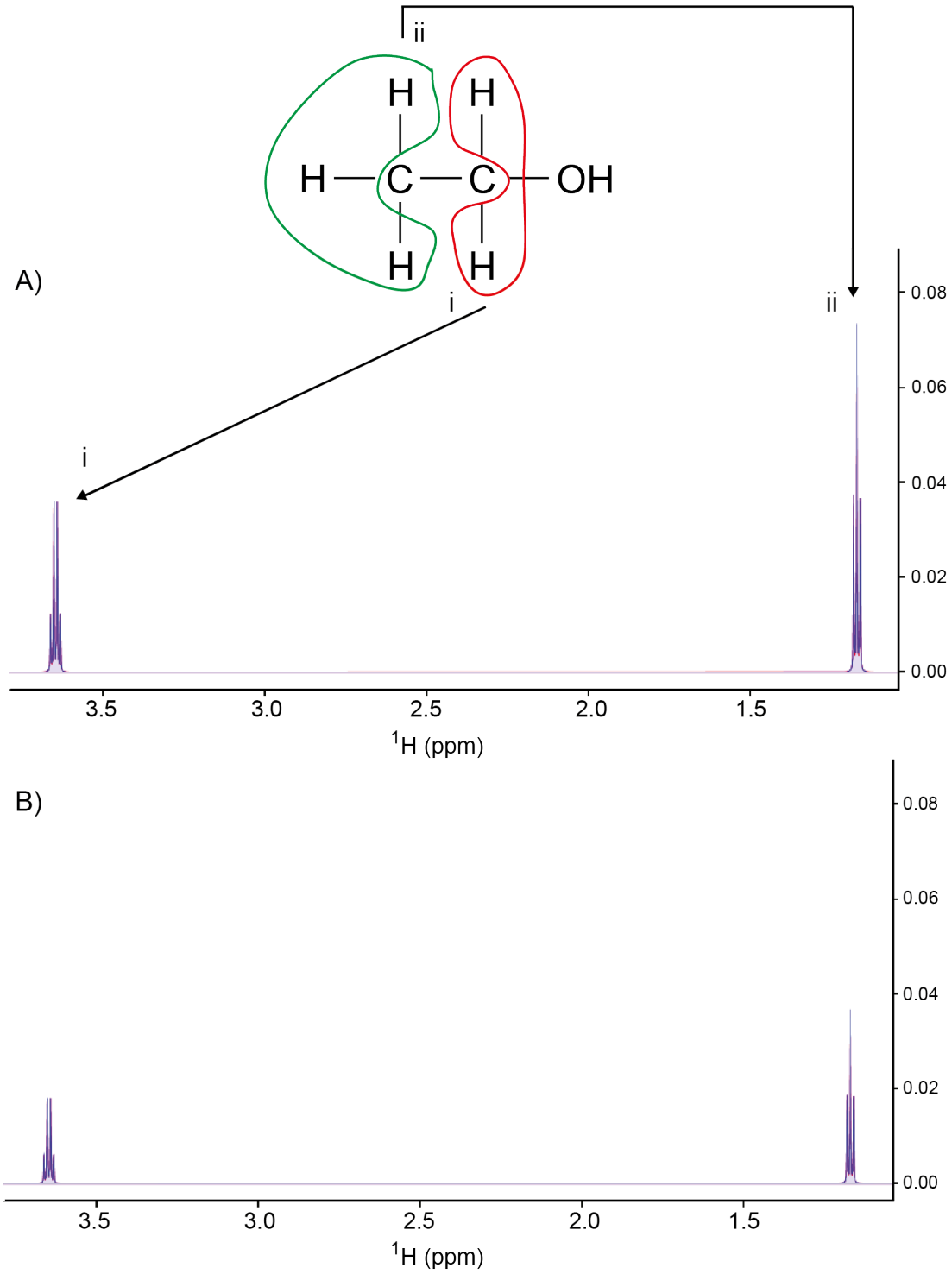
ii
H
H
H
C
C
OH
H
H
A)
i
ii
i
ii
0.08
0.06
0.04
0.02
0.00
3.5
3.0
2.5
2.0
1.5
1H (ppm)
B)
0.08
0.06
0.04
0.02
0.00
3.5
3.0
2.5
2.0
1.5
1H (ppm)

Figure 1-9: NMR peak positions and collective peak heights define metabolite identity and concentration.

Synthetic 700 MHz ^{1}H NMR reference spectra for A) 0.3 mM ethanol; B) 0.15 mM ethanol. Equivalent methylene protons i (enclosed in red trace) correspond to the NMR peak cluster i in both spectra. Equivalent methyl group protons ii (enclosed in green trace) correspond to the NMR peak cluster ii in both spectra. A peak for the hydroxyl proton is absent from the spectra as it exchanges with the solvent, deuterium oxide (D_2O).

1.3.2 Targeted profiling

The primary aim of metabolic profiling studies is to identify from the recorded spectra the individual metabolites that vary between two or more biological conditions. Identification of the peaks that correspond to metabolites in recorded NMR spectra of unknown metabolite mixtures can be achieved using targeted profiling. Here, spectra are characterised by "fitting" reference metabolite spectra to the experimental spectrum, which upon cumulatively fitting of reference spectra can eventually model the experimentally recorded spectrum (Weljie et al., 2006). These reference spectra are stored in databases such as the Human Metabolome Database (HMDB), the BioMagResBank (BMRB) and the *Chenomx* software library (Chenomx Inc.) (Ulrich et al., 2008; Weljie et al., 2006; Wishart et al., 2007). In particular, use of the *Chenomx NMR Suite* software enables not only identification of a large number of metabolite resonances but also enables quantification of metabolite concentrations in the NMR sample, when related to the known concentration of a NMR standard. Once the quantified concentrations of metabolites between samples is collected into a data matrix, statistical methods such as analysis of variance (ANOVA) followed by post-hoc tests such as Tukey's "honestly significant difference" (HSD) (Abdi and Williams, 2010) can determine if significant differences exist in a metabolites concentrations between the groups and between which groups this significance exists respectively.

Targeted profiling excels at assigning metabolite identity to individual peak clusters in areas where the peaks for multiple metabolites overlap (Weljie et al., 2006) (Figure 1-10). However, the use of targeted profiling in identifying "significant" metabolites becomes a major challenge as the number of biological conditions to

be analysed increases. For example, targeted profiling can become especially labour intensive when replicate NMR spectra are analysed from males *versus* females, different developmental stages, and genetic/dietary manipulated samples.

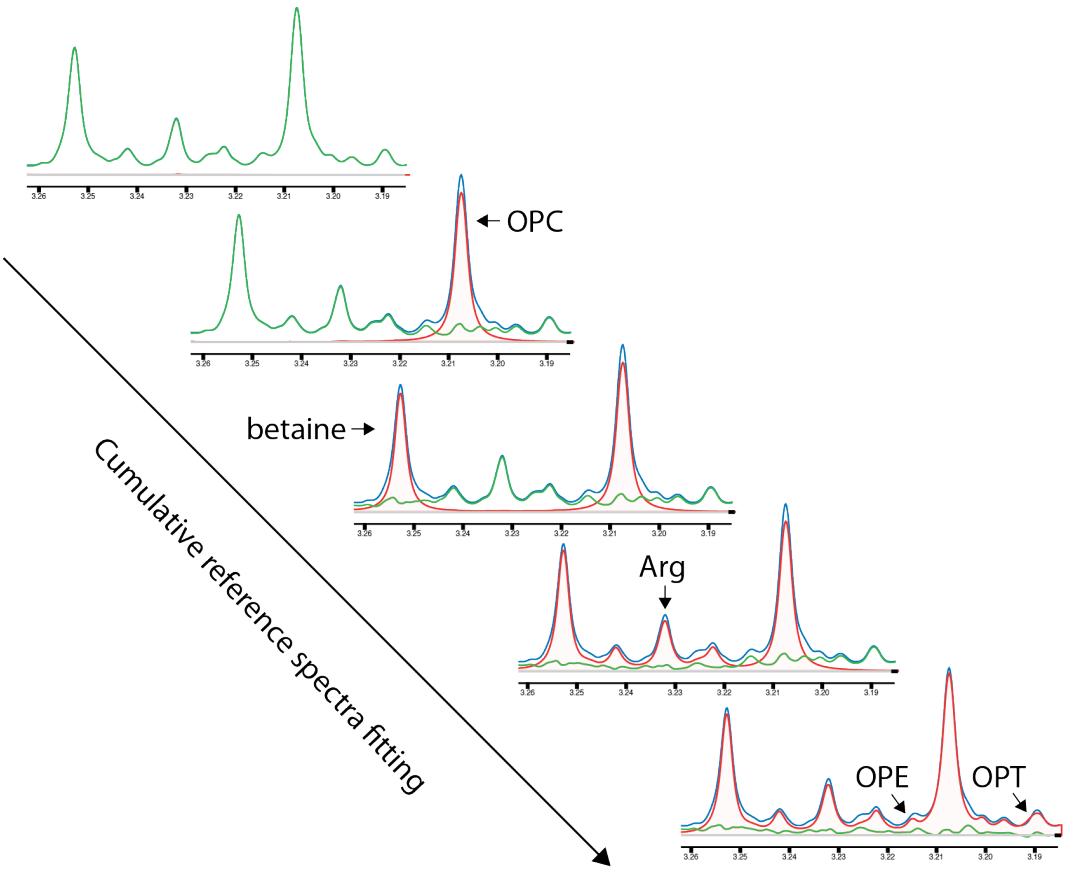

Figure 1-10: Targeted profiling enables identification of peaks corresponding to metabolites.

Fitting of reference spectra (red traces) to recorded spectra (blue trace) in a cumulative manner enables identification of peaks corresponding to metabolites, even in areas of metabolite peak overlap. The green trace is the difference between the recorded spectrum and the "fitted" spectrum. OPC: O-phosphocholine, Arg: arginine, OPE: O-phosphoethanolamine, OPT: O-phosphotyrosine.

1.3.3 Multivariate analysis of large metabolomic datasets.

The challenge posed by large metabolomic datasets can be addressed through the use of multivariate analysis (MVA) methods (Gowda and Raftery, 2017). In principle, MVA methods can be used to effectively reduce the size of the dataset from a large number of recorded variables, many of which are inter-correlated, to a manageable form from which it is possible to extract deterministic properties (Worley and Powers, 2013).

A first port of call when applying MVA to a large collection of NMR spectra is principal component analysis (PCA) (Mercier et al., 2011). In essence, PCA can be used in an unbiased, unsupervised manner to find an approximation reduced form of the original data matrix (i.e. the collected spectra) with a much smaller number of variables than were originally measured (Kemsley, 1996). PCA thus achieves "dimensionality reduction" and facilitates the identification of patterns and trends in the data (Wold et al., 1987). The new uncorrelated variables, cast in terms of principal components (PCs), are linear combinations of the original inter-correlated variables (Kemsley, 1996). PCs are ranked by the proportion of the variance of the original data that they each capture (usually expressed as a percentage). It is assumed that the magnitude of the variance correlates with importance, e.g. large variance in the signal intensities between two samples means that those two samples are different in some way. Each sample is scored according to the summed contributions of the PCs that best approximate the corresponding spectrum. Thus samples that display similar spectral features (similar metabolites at similar concentrations) will cluster together when their scores are visualised in a PCA scores plot (Wold et al., 1987) (Figure 1-11). Each point on the scores plot represents a single spectrum; for a set of spectra the positions on the scores plot shows how sample spectra relate to one another (Smolinska et al., 2012). This means that the PCA scores plot effectively reports on the group structure in the original data, i.e. one expects to see clustering between similar sample classes and separation between different sample classes, at least when variation between groups is greater than that within a group (Worley and Powers, 2013). Therefore, PCA can provide a relatively straightforward means to check the integrity of the data and/or the presence of interesting "structure". For example, biological

replicates are expected to provide similar spectra and so should cluster together on the PCA scores plot. Outliers, samples that fail to cluster with their fellow replicates, represent samples for which there is variation that requires explanation.

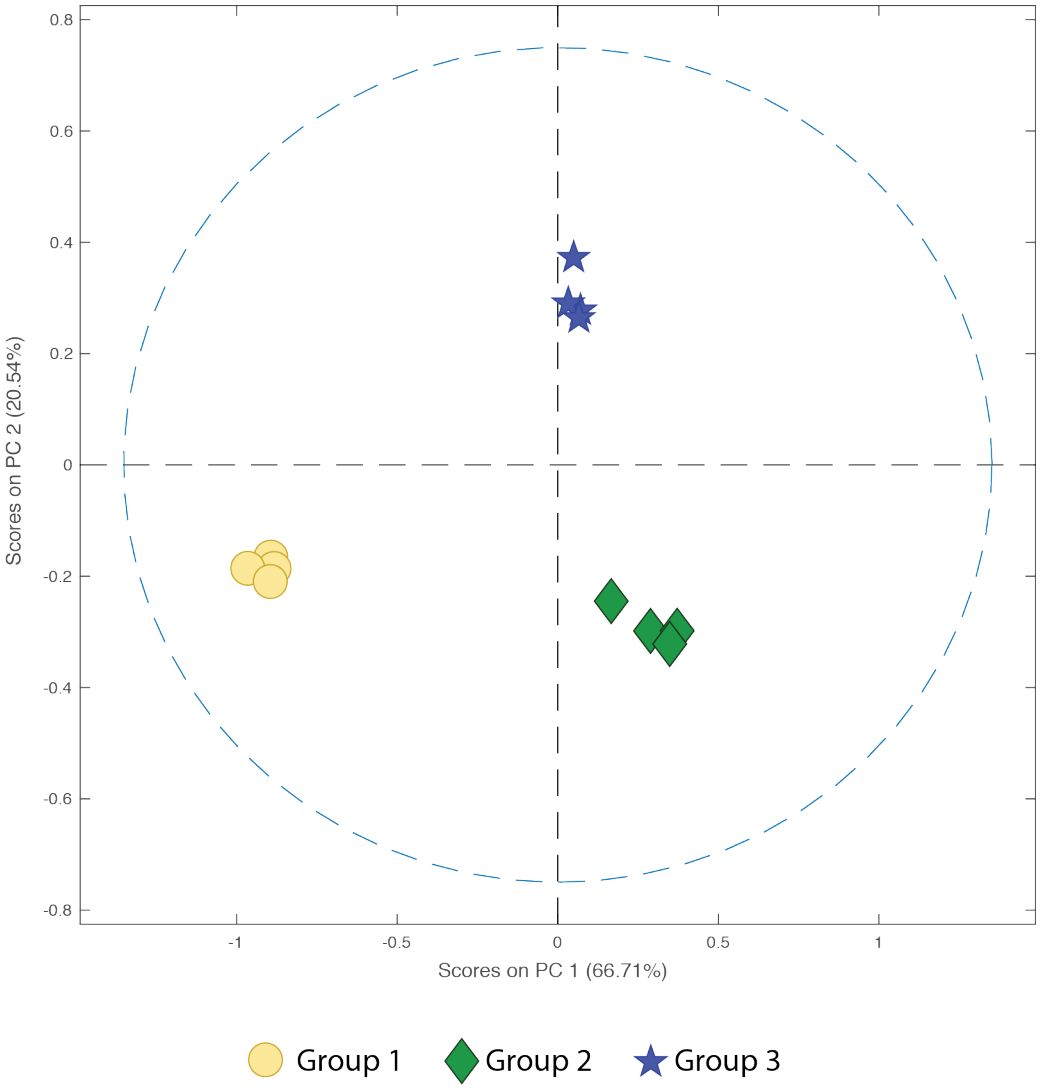

Figure 1-11: Similar spectral groups cluster together in a PCA scores plot.
The standard two-dimensional PCA scores plot summarises the scores assigned to the spectral groups along the first and second principal components (PC1 and PC2). The example provided here is a PCA scores plot for 12 one-dimensional NMR spectra from three distinct sample groups (each represented by a different symbol). In total, for this example, this plot captures ~87% of the variance in the whole dataset.

Another set of outputs generated in PCA are the loadings. The loadings encode the variables within the spectra responsible for the sample separation in scores space. The loadings can be interrogated to identify the metabolites that differ in concentration between sample classes and thus are the basis of separation (Smolinska et al., 2012). Each PC has a corresponding loading. Ideally class separation corresponds to features that emerge in the first PC (PC1), and be directly "read-off" from the corresponding loadings plot. In the case of PCA applied to the samples presented in Figure 1-11, the loadings from PC1 would highlight the features (metabolites) that distinguish Group 1 from the other two groups, whilst the loadings for PC2 would highlight the differing features between Group 3 and the other two groups.

1.3.4 *Drosophila* studies using metabolomics

Proton NMR spectroscopy followed by MVA has been widely implemented to identify "biomarker" metabolites in humans, or model organisms that distinguish sample classes in cancer, diabetes, infection, longevity and nutrition (Adamko et al., 2016; Shen et al., 2016; Wei et al., 2014; Wijeyesekera et al., 2012; Zhang et al., 2016). However, a major challenge for metabolomic studies involving flies, rather than mammals, is their small size and the consequent difficulties in producing tissue samples of sufficient volume for analysis. Dilution of these small volume samples is required for further NMR analysis. However, differing dilutions resulting from a lack of an *a priori* knowledge of the exact volume recovered from the specimen can mask subtle specific (possibly significant) variation in features (metabolites) between the samples. Appropriate normalisation can be used to account for non-specific overall dilution effects, enabling visualisation of any specific variation present (Figure 1-12). Probabilistic quotient normalisation (PQN) has proven to be a robust method to account for dilution of complex biological mixtures (e.g. urine samples), outperforming other commonly used means of statistical normalisation, such as integral normalisation (Dieterle et al., 2006). PQN has been shown to be effective in handling non-specific variation (dilution) in a set of spectra, as this variation is assumed to apply to the majority of features in the spectrum. After PQN, specific variation observed for a minority of features between sample groups becomes apparent. However, successful application of PQN is

limited by a requirement for the “spectral mass difference” between the spectra to be lower than ~50% (Dieterle et al., 2006). In other words, if experimental manipulations significantly alter the number of features (concentrations of metabolites) that differ between groups of recorded spectra by more than 50%, normalisation via PQN might fail to highlight that specific variation.

Figure 1-12: Normalisation uncovers specific variation.

Schematic representation of the NMR spectra of two independent samples pre- (A) and post- (B) PQN normalisation. The blue sample is diluted by a factor of three in comparison to the red. After normalisation, specific variation in a few features (signified by *) becomes apparent. Figure adapted from Dieterle et al., (2006).

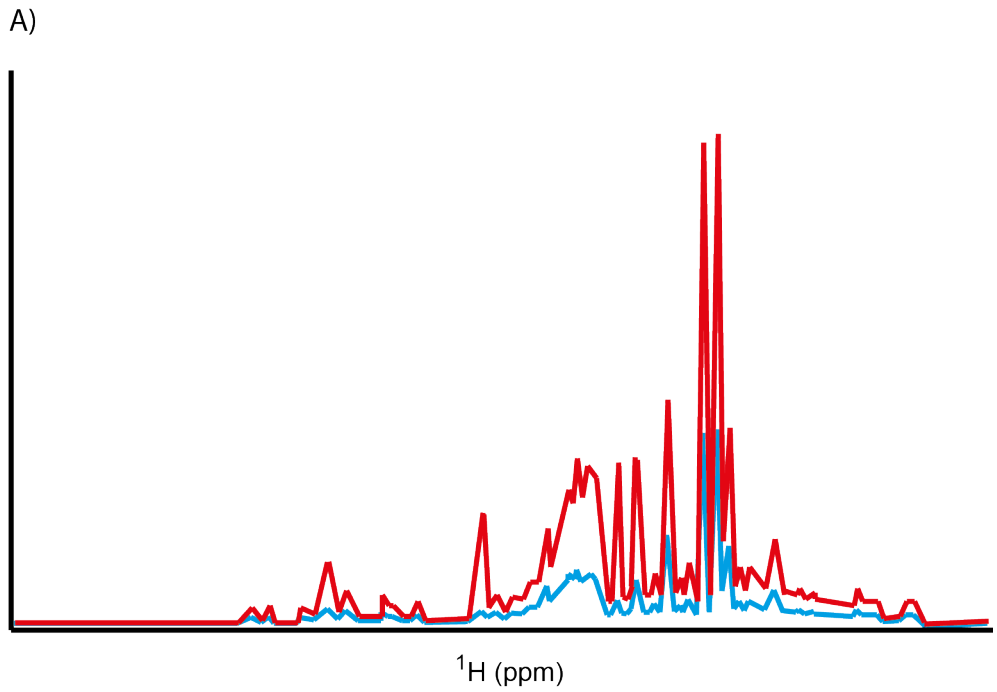
A)
^{1}H (ppm)
normalisation
B)
*
*
*
^{1}H (ppm)

Relatively recent work in the Gould lab has developed a technique for obtaining absolute metabolite concentrations from sub-microlitre *Drosophila* samples (Cheng et al., 2011; Ragan et al., 2013). The methodology, known as volume determination with two standards (VDTS), facilitates the determination of absolute metabolite concentrations from small amounts of *Drosophila* hemolymph (blood) of unknown volume using a back-calculation method (Ragan et al., 2013) (see Materials and Methods 2.4). The measurement of absolute rather than relative concentrations of metabolites is particularly important when studying the effects of starvation, as in this thesis. This is because starvation decreases the concentration of the vast majority of features in the spectrum, in comparison to fed samples, resulting in unsuccessful normalisation via PQN (Ragan et al., 2013). Successful normalisation of fed and starved sample-derived spectra can instead be achieved via normalisation using the determined recovered volumes of hemolymph.

Many metabolomic studies of *Drosophila* have now been published. Gas chromatography (GC) MS-based metabolome analysis have demonstrated, for example: the similarities between tumour metabolism and metabolism during *Drosophila* embryogenesis; how the collection of metabolite profiles can enable the development of models to predict embryonic stage; and how the diet of *Drosophila* larvae can alter the lipid composition of their membranes (An et al., 2014; Carvalho et al., 2012; Tennessen et al., 2014). Interestingly, investigations into age-related metabolome changes have associated the vitamin-like metabolite choline with longevity in *Drosophila* as well as in *Caenorhabditis elegans* and in the mouse (Fuchs et al., 2010; Sarup et al., 2012; Wijeyesekera et al., 2012). Silimarily, Gogna et al., (2015) employed a NMR-MVA metabolomics approach to demonstrate that several metabolites, observed to oscillate during the *Drosophila* daily cycle, are also conserved in a silimar cycle in mice and humans (Ang et al., 2012; Minami et al., 2009). These studies, that demonstrate a conserved association between metabolites and a biochemical mechanism, provide a justification for using organisms like *Drosophila* to model aspects of mammalian biology.

Heinrichsen et al., (2014), employed both transcriptomic and metabolomic analyses to flies fed a high fat diet (HFD) and observed that the flies displayed an altered

amino acid, fatty acid and carbohydrate metabolism. In particular, lactic and uric acid were significantly increased relative to controls, suggesting that genes involved in carbon and nitrogen metabolism may be affected. Interestingly, CG9510, which shares sequence similarity to human arginosuccinate lyase (ASL), an enzyme involved in carbon and nitrogen metabolism, was found to be downregulated in flies on a HFD. Flies with RNAi-mediated knock down of CG9510 were observed to share a similar metabolite profile and phenocopy (in terms of reduced cold tolerance) flies fed a HFD, whilst overexpression of CG9510 ameliorated some of the negative consequences of a HFD (Heinrichsen et al., 2014). In line with the abovementioned utility for *Drosophila* as a metabolic model for mammalian systems, it would be interesting to determine how manipulation of ASL in mammalian systems will affect animals fed a HFD.

Unlike the study conducted by Heinrichsen et al., the majority of *Drosophila* metabolomics studies reported are descriptive and little has been done thus far to follow up candidate metabolites at the functional level using the power of fly genetics. In contrast, this thesis starts with a descriptive metabolomic analysis of the *Drosophila* larval-to-pupal transition but then follows up selected metabolites at the functional level using *Drosophila* genetics.

Chapter 2. Materials & Methods

2.1 *Drosophila* stocks

All stocks were maintained on our standard (2x) growth medium (58.5 g/L glucose, 6.63 g/L cornmeal, 23.4 g/L dried yeast, 7.02 g/L agar, 1.95 g/L Nipagen, 7.8 mg/L Bavistan). The inbred, "isogenic" *Drosophila* strain: w^{1118}; 2_{iso}; 3_{iso} (*iso 31*) was kindly provided to us by John Roote from the University of Cambridge (Ryder et al., 2004). GAL4 drivers used in this study were: ;;*tubulin 1α promoter* (*tub*)-GAL4/*TM6,Sb,Hu,Deformed::YFP* (*dfYFP*) (Lee and Luo, 1999) and ;;*A58*-GAL4/*TM6,Sb,Hu,dfYFP* (self made by crossing ;;*A58*-GAL4/*TM6b,Tb,Hu* (a gift from Michael J. Galko (Galko and Krasnow, 2004)) to *tub*-GAL4/*TM6,Sb,Hu,dYFP*). *Tub*-GAL4 expresses GAL4 ubiquitously throughout development whilst *A58*-GAL4 expresses GAL4 in an epidermal specific manner throughout larval development. The following RNAi lines were used from the Vienna Drosophila RNAi Centre (VDRC) (Dietzl et al., 2007): VDRC ID #60000 (w^{1118} , the host strain for the RNAi library); prophenoloxidase 1 (CG42639) RNAi^{KK107599}; dopa decarboxylase (CG10697) RNAi^{KK109881}; glutamate oxaloacetate transaminase 2 (CG4233) RNAi^{KK106120}; and alkaline phosphatase (Alp) 4 (CG1461) RNAi^{GD6864}. The following RNAi lines were used from the Transgenic RNAi Project (TRiP) (Flockhart et al., 2006): y^1, v^1;P{CaryP}attP4 (used as a control TRiP RNAi line, hereafter called *TRiP Ctrl*); tyrosine decarboxylase 2 (CG30446) RNAi^{25871} ; Alp1 (CG5656) RNAi^{28564} ; Alp4 (CG1461) RNAi^{28740}. The double Alp4 and Alp1 KD (*Alp4i;;Alp1i*) was self made by crossing CG1461 RNAi^{GD6864} and CG5656 RNAi^{28564} (UAS-CG1461 RNAi^{GD6864};; UAS-CG5656 RNAi^{28564}).

2.2 Larval staging and collection

Polar metabolites were extracted from larvae of a *Drosophila melanogaster* isogenic strain (w^{1118} *iso 31*) (Ryder et al., 2004). Six different dietary regimes were applied to the larvae, exposing them to

either fed or NR conditions: 51 hr fed, 60 hr fed, 84 hr fed, 51 hr fed + 24 hr NR and 60 hr fed + 24 hr NR. To collect larvae from these regimes, L1 larvae were transferred to a 2x medium within 1 hour of hatching and raised at 25°C for either 51 or 60 hours. Larvae were then floated from the medium using a 30% glycerol/PBS, rinsed with PBS and either prepared for polar metabolite extraction, moved to a NR medium (1% agarose in PBS) for a further 24 hours at 25°C (51 hr fed + NR and 60 hr fed + NR samples) or moved to the 2x medium for a further 24 hours at 25°C (84 hr fed samples).

Larval samples were collected in single sex groups of 10 for the fed samples (51 hr fed, 60 hr fed and 84 hr fed); and 15 for the NR samples (51 hr fed + 24 hr NR and 60 hr fed + 24 hr NR). Each condition was collected in (at least) triplicate. Larvae were blotted dry on tissue paper, had their group weight measured and were then transferred to either a 45 mm culture dish for hemolymph extraction or a micro-centrifuge tube for whole larval homogenisation.

2.2.1 Dietary manipulations

For the “fed” dietary manipulation experiments, L1 *tub>TRiP Ctrl* and *tub>Alp4* RNAi^{28740} larvae were transferred to 2x supplemented with 1.5 g/L L-tyrosine (Sigma-Aldrich, T8566) within 1 hour of hatching, 4 replicate vials were collected for each condition with 15 larvae per vial. For the “NR” dietary manipulation experiments, L1 tub>TRiP Ctrl and tub>Alp1 RNAi^{28564} larvae were transferred from 2x after 60 hr to NR medium supplemented with tyrosine. NR medium was supplemented with tyrosine via two methods: acidifying a solution of NR supplemented with 1.5 g/L L-tyrosine with 1 M hydrochloric acid (HCl), until the solution becomes clear or collecting the supernatant of the NR solution supplemented with 1.5 g/L L-tyrosine after overnight mixing (generating a NR solution saturated with tyrosine). The pH of each solution was confirmed using pH Indicator and Test Paper Reels (Camlab, 1153787). From these NR supplemented with tyrosine solutions, 15 mixed sex larvae were collected per condition and each condition was collected in triplicate.

2.3 Measuring time to pupariation

TTP was determined for synchronised (at hatching) larval cultures in vials at 25 °C. 4 vials were set up in parallel for each condition and 15 larvae were cultured in each vial. New pupae were counted every two hours from emergence of the first, until all larvae that had been transferred to the vials had pupariated or no new pupae appeared for 36 hours. For data visualisation, the number of larvae that had reached pupariation was set as 100% and the number of larvae that had pupariated by a certain time was plotted as a percentage of the final number of pupae.

2.4 Non-matched VDTS

2.4.1 Hemolymph extraction

An optimised version of the VDTS technique (Ragan et al., 2013) was followed for the analysis of polar metabolites from hemolymph samples. This method involved using a Hamilton syringe (to ensure accuracy) to transfer either 10 µL of ice-cold saline with 25 mM sodium ^{13}C-formate (Sigma, 279412) or 10 µL of ice-cold saline with 4 mM sodium 4-Chloro-3,5-dinitrobenzoic acid (4-Cl-DNBA, Sigma, C38907) to each group of sorted larvae. Sharp forceps were used to tear the cuticle of each larva, releasing hemolymph into the transferred droplet, without damaging any internal organs. All larvae in the droplet were “opened” within 2 minutes and 7.5 µL of the saline/standard (either ^{13}C-formate or 4-Cl-DNBA)/hemolymph solution was then removed with a Hamilton syringe and added to 100 µL reverse-osmosis deionised water in microcentrifuge tube containing a 0.22 µm filter unit (Millipore, UFC30GV0S). Any cells present, such as hemocytes were cleared from the solution by centrifugation (1 minute at 13 krpm). 100 µL of the cleared solution was then transferred to 200 µL reverse-osmosis deionised water containing 90 µM sodium 4,4-dimethyl-4-silapentane-1-sulfonate (DSS), this would be the experimental, “opened” sample. To control for non-specific interaction

of the sodium formate or 4-Cl-DNBA with the larval cuticle and to determine volume of hemolymph released, another group of larvae were treated as described above but did not have their cuticles “opened” in the droplet and, therefore did not release hemolymph; this would act as the control “blank” sample.

2.4.2 Whole larval homogenisation

Determination of the volume released after whole larval homogenisation involved using a Hamilton syringe to transfer 10 µL of ice-cold saline with 25 mM sodium ^{13}C-formate to each group of sorted larvae within their microcentrifuge tubes. A homogeneous mixture of the whole larval (and formate solution) samples was then achieved using a motorised hand-held (Kontes) pellet pestle (Sigma-Aldrich, Z359947) with the microcentrifuge tube acting as a mortar. Larvae were homogenised for 30 seconds and the resulting suspension was pelleted by centrifugation (2 min at 13 krpm). 7.5 µL of the homogenised solution was then removed (again using a Hamilton syringe) and transferred to 200 µL reverse-osmosis deionized water containing 90 µM sodium-DSS, generating the “opened” sample. The “blank” sample was generated by treating another group of larvae as described above but without homogenisation.

2.4.3 Whole adult homogenisation

The optimised version of the whole larval VDTS technique, mentioned above, was further optimised to extract polar metabolites from whole adults. Adults were anesthetised on a CO_2 pad and then kept sedated by transference onto a chilled (with ice) glass plate, where the adults are washed thrice with 70 % ethanol. Washed adults blotted dry on tissue paper and subsequently transferred in groups of 10 to microcentrifuge tubes. Using a Hamilton syringe, 10 µL of ice-cold saline with 4 mM sodium 4-Cl-DNBA, was transferred to each group and a homogeneous mixture was again achieved using a motorised hand-held pellet pestle with the microcentrifuge tube acting as a mortar. The remainder of the technique follows 2.4.2.

2.4.4 Polar metabolite extraction

Polar metabolites were extracted from the homogenised/cleared hemolymph solution using the method of Bligh and Dyer (Bligh and Dyer, 1959). Briefly, the solution was mixed with 750 μL 2:1 methanol-chloroform solution by vortexing. Phase separation of polar metabolites and apolar lipids/amphipathic peptides was achieved by the addition of 250 μL chloroform followed by 250 μL of water. The upper, aqueous layer was then aspirated and evaporated to dryness (Savant DNA centrifugal evaporator), before re-suspension in 160 μL 99.9% D_2O (Millpore, 7789-20-0) and transfer to a 3 mm NMR tube (Bruker Biospin).

2.5 Matched VDTS

2.5.1 Matched hemolymph extraction

Matched hemolymph extraction follows the optimised version of the hemolymph VDTS technique detailed in 2.4.1, with the exception that 20 μL of ice-cold saline with 25 mM sodium ^{13}C-formate was transferred to each group of sorted larvae. After 1 min, 7.5 μL of this sodium-formate solution in contact with larvae was then transferred using a Hamilton syringe to 100 μL reverse-osmosis deionised water in microcentrifuge tube containing a 0.22 μm filter unit, this would act as the “blank” sample. Larval cuticles were then torn in the remaining sodium-formate droplet, thus releasing hemolymph. 7.5 μL of this sodium-formate-hemolymph solution was then transferred to another 100 μL reverse-osmosis deionised water in microcentrifuge tube containing a 0.22 μm filter unit; this would be the “opened” sample. Both microcentrifuge tubes were centrifuged (for 1 min at 13krpm) and 100 μL of the flow through was transferred to different aliquots of 200 μL reverse-osmosis deionized water containing 90 μM sodium-DSS.

2.5.2 Matched whole larval homogenisation

Matched whole larval homogenisation follows the optimised version of the whole larval VDTS technique detailed in 2.4.2, with the exception that 20 µL of ice-cold saline with 25 mM sodium ^{13}C-formate was transferred to each group of sorted larvae. 7.5 µL of this sodium-formate solution in contact with larvae was transferred using a Hamilton syringe to 200 µL reverse-osmosis deionized water containing 90 µM sodium-DSS; this would act as the "blank" sample. Larvae were then homogenised, in the same manner as in 2.4.2 and 7.5 µL of this homogenate solution was transferred to another aliquot of 200 µL reverse-osmosis deionized water containing 90 µM sodium-DSS; this would act as the "opened" sample.

2.6 Acquisition and processing of NMR spectra

One-dimensional (1D) ^{1}H NMR spectra of the metabolites extracted from the larval samples were acquired using the procedures as described in Ragan et al. (2013). This entailed spectral acquisition of each sample for ~30 min, with a Bruker Avance III instrument with a nominal ^{1}H frequency of 700 MHz. The standard Bruker pulse sequence noesypr1d was employed with the following parameters consistent with the recommendations provided for use of the *Chenomx NMR Suite* software package: sweep width 20 ppm, acquisition time 4 s, relaxation delay 1 s, mixing period 10 ms, with solvent presaturation power of 0.02 mW (B_1 field ~50 Hz) applied to the residual HOD signal at 4.7 ppm. Typically 300-500 transients were acquired per measurement. Free induction decays were then zero-filled, apodized with exponential multiplication (line broadening factor LB = 1 Hz), Fourier-transformed and the resulting spectra were phase corrected in *NMRLab* (Gunther et al., 2000), before transfer to *Metabolab* (Ludwig and Günther, 2011), where baseline correction and spectral binning (with a fixed bin width of 0.08 ppm) was applied. Finally, NMR peaks in the different spectra were aligned using *Icoshift* (Savorani et al., 2010).

2.7 Chemometeric analysis

Chemometric analysis was also carried out as in Ragan et al. (2013). This entailed transferring the baseline-corrected, peak-aligned NMR spectra from *Metabolab* to *MATLAB* (The MathWorks, Inc.). In *MATLAB*, spectra were normalised using volumes recovered from hemolymph release or whole larval homogenisation, depending on the source of the spectra. Normalised spectra were subsequently transferred to *PLS Toolbox* (Eigenvector Research Inc.). In *PLS Toolbox*, the region from 8.65 to 12.75 ppm was removed alongside 4.7 to 4.9 ppm and -3.2 to 0.72 ppm. Spectra were further mean-centred and variance-stabilised using Pareto scaling in *PLS Toolbox* (van den Berg et al., 2006) prior to PCA, which was also carried out using the *PLS Toolbox* software. A contiguous block validation method was applied during the PCA to ensure the stability of the model.

Metabolite concentrations were measured using the *Chenomx NMR Suite* programme. Here, after processing of the spectra (zero-filling, Fourier transformation, phase and baseline-correction) in *Chenomx NMR Processor*, a chemical shape indicator (CSI) is fitted to the DSS trimethylsilyl resonance. This fitting calibrates the *Chenomx* reference library of metabolite spectra. In *Chenomx NMR Profiler,* manually guided fitting of these reference spectra to the NMR peaks in the recorded spectra yielded a readout of metabolite concentrations relative to that of the DSS standard.

The derived metabolite concentrations were collected in a matrix, with each row corresponding to a particular spectrum (sample) and each column corresponding to a particular metabolite's concentration. Absolute metabolite concentrations were then calculated from these derived metabolite concentrations after determination of recovered hemolymph/whole larval volumes, using the formulae associated with VDTS (Ragan et al., 2013). The differences in metabolite levels between classes were tested by a two-way ANOVA test and significance was determined using Tukey's HSD test (Abdi, 2010), using *StatPlus:mac Pro* (AnalystSoft Inc.).

The volume of hemolymph recovered after cuticular tearing within the 4-Cl-DNBA solution (V_h), was achieved using the formula defined in Ragan et al. (2013). This formula is written as:

$$V_h = \left(\frac{I_c'^S}{I'^S} - 1\right) V_S$$

where $I_c{}'^S/I'^S$ is the ratio of the concentrations of the standard (which in the case of hemolymph VDTS is 4-Cl-DNBA) in the "blank" (control: $_c$) sample and the "opened" (hemolymph released) sample, respectively. These concentrations are obtained by the fitting of corresponding NMR resonance peak intensities in *Chenomx NMR Profiler* and the primes indicate that each of the two spectra have been normalised to the DSS trimethylsilyl resonance, which is assumed to have the same concentration in the two samples. In non-matched VDTS, $I_c{}'^S$ is the average concentration of the standard from all "blank" spectra. In matched VDTS, $I_c{}'^S$ is a single standard concentration from the appropriate "blank" sample each matched to "opened" sample (i.e each $I_c{}'^S$ is unique). This difference between non-matched and matched VDTS $I_c{}'^S$ values follows for matched and non-matched whole larval and whole adult VDTS. V_S is the volume of standard solution into which the hemolymph was initially released. Taking the ratio of V_S to V_h (the dilution factor), allows for determination of the absolute concentration of metabolite X in the hemolymph ($[X]_h$), according to:

$$[X]_h = \frac{I^X}{I^S}\frac{V_S}{V_h}[S]_0$$

where $[S]_0$ is the concentration of the standard transferred to the larval samples and I_X/I_S is the ratio of the concentration of metabolite X and the 4-Cl-DNBA standard obtained by fitting of the corresponding NMR resonance peak intensities in *Chenomx NMR Profiler.*

The volume recovered after whole larval homogenisation within the ^{13}C-formate solution (V_{WL}), was determined in much the same way, with the formula written as:

$$V_{WL} = \left(\frac{I_c'^S}{I'^S} - 1\right) V_S$$

here, V_S is the volume of the standard solution in which larvae are homogenised. Taking the ratio of V_S to V_{WL}, allows for determination of the absolute concentration of metabolite X in the homogenate from the whole larvae ($[X]_{WL}$), according to:

$$[X]_{WL} = \frac{I^X}{I^S}\frac{V_S}{V_{WL}}[S]_0$$

where $[S]_0$ is the concentration of the standard transferred to the larval samples and I_X/I_S is the ratio of the concentration of metabolite X and the ^{13}C-formate standard obtained by fitting of the corresponding NMR resonance peak intensities in *Chenomx NMR Profiler.*

Volumes recovered after whole adult homogenisation (V_{WA}), are determined using the same formula for the determination of volume of hemolymph recovered, replacing V_h with V_{WA}. Taking the ratio of V_S to V_{WA}, allows for determination of the absolute concentration of metabolite X in the homogenate from the whole adult ($[X]_{WA}$), according to:

$$[X]_{WA} = \frac{I^X}{I^S}\frac{V_S}{V_{WA}}[S]_0$$

Chapter 3. Optimisation and adaption of VDTS metabolomics

The original VDTS technique was developed by Dr Timothy J. Ragan and Dr Andrew P. Bailey, to determine absolute metabolite concentrations in the liquid hemolymph of post-CW *Drosophila* larvae (Ragan et al., 2013). In this chapter, I describe the optimisation of the VDTS technique for hemolymph extraction from pre-CW larvae, which are much smaller than their post CW counterparts. I also show how VDTS can be adapted to measure metabolite concentrations from solid tissue samples of whole larvae and adult flies.

3.1 Optimisation of the second standard for hemolymph VDTS

A typical 1D ^{1}H NMR spectrum is recorded from a 160-200 µL sample within a 3 mm NMR tube, the volume of hemolymph released from a late L3 fed female (~ 90 hr, 1.7 mg) larvae is ~700 nL (Ragan et al., 2013). Therefore hemolymph samples require dilution to evaluate the metabolite concentrations within the sample. However, without knowing the precise starting volume of the analyte solution, accurate back calculation of metabolite concentrations is not possible. As documented in Ragan et al., (2013), the volume of hemolymph released into a droplet can be determined by VDTS through the use of two NMR standards: DSS and ^{13}C-formate (Figure 3-1). One important factor for robust VDTS is the extent to which the ^{13}C-formate standard in the starting droplet is diluted by the hemolymph released from the ruptured larvae. If this dilution is too small to be accurately measured, as a difference in NMR peak heights, then VDTS will be compromised. It is therefore important to optimise both the concentration of ^{13}C-formate and the droplet size when only ~200-300 nL of hemolymph may be released from each ruptured larva, of a set of typically 15-20 animals. Ragan et al., (2013), used a ^{13}C-formate concentration of 100 µM and a droplet volume of 20 µL. I found that increasing the ^{13}C-formate concentration to 25 mM and decreasing the droplet volume to 10 µL gave a greater relative difference in the ^{13}C-formate H-1 signal between the undiluted “blank” (control) and the diluted “opened” (experimental) mimic (Figure 3-2) (6 µL water represented released hemolymph from 10 late L3 larvae). Therefore, hemolymph VDTS is improved by opening larvae in a 10 µL

drop of 25 mM ^{13}C-formate.

Figure 3-1: Outline of the *Drosophila* hemolymph extraction and measurement strategy.

An accurately measured volume (V_S) of saline containing ^{13}C-formate at a known concentration ($[S]_0$) is transferred to a number of larvae (n), with a collective hemolymph volume, V_h that can be released into the ^{13}C-formate droplet after larval cuticle rupture (a). An accurately measured volume (V_t) of the hemolymph/^{13}C-formate droplet is then transferred to a microcentrifuge tube with a filter (b) to remove hemocytes via centrifugation (c). The cleared filtrate is then transferred to a known volume (V_D) of chloroform/methanol/water (green) containing a fixed concentration, $[D]_0$ of DSS (d). After further separation of polar and non-polar components via the Bligh-Dyer method (e), the upper aqueous phase of polar metabolites is aspirated to a second microcentrifuge tube (f). The solution is evaporated to dryness (g) and the residue suspended in D_2O (h) prior to transfer to an NMR tube (i). $I_c'^S$: H-1 signal of ^{13}C-formate when no hemolymph is released into the ^{13}C-formate droplet. I'^S: H-1 signal of ^{13}C-formate when hemolymph is released into the droplet. $[X]_h$: Concentration of metabolite X in neat hemolymph. See Materials and Methods: 2.4.1 for details.

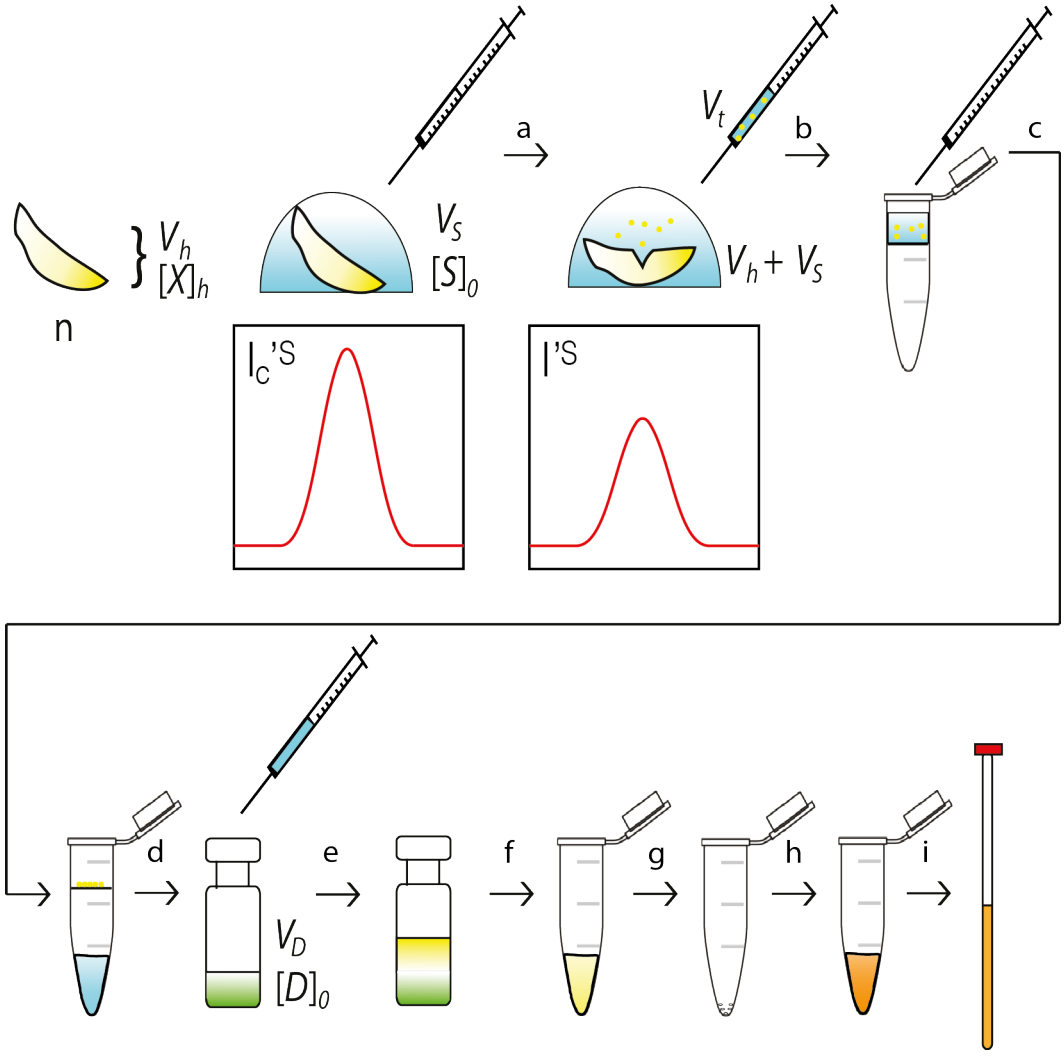
n
V_h
$[X]_h$
a
V_S
$[S]_0$
V_t
b
$V_h + V_S$
c
I_C'S
I'S
d
e
V_D
$[D]_0$
f
g
h
i

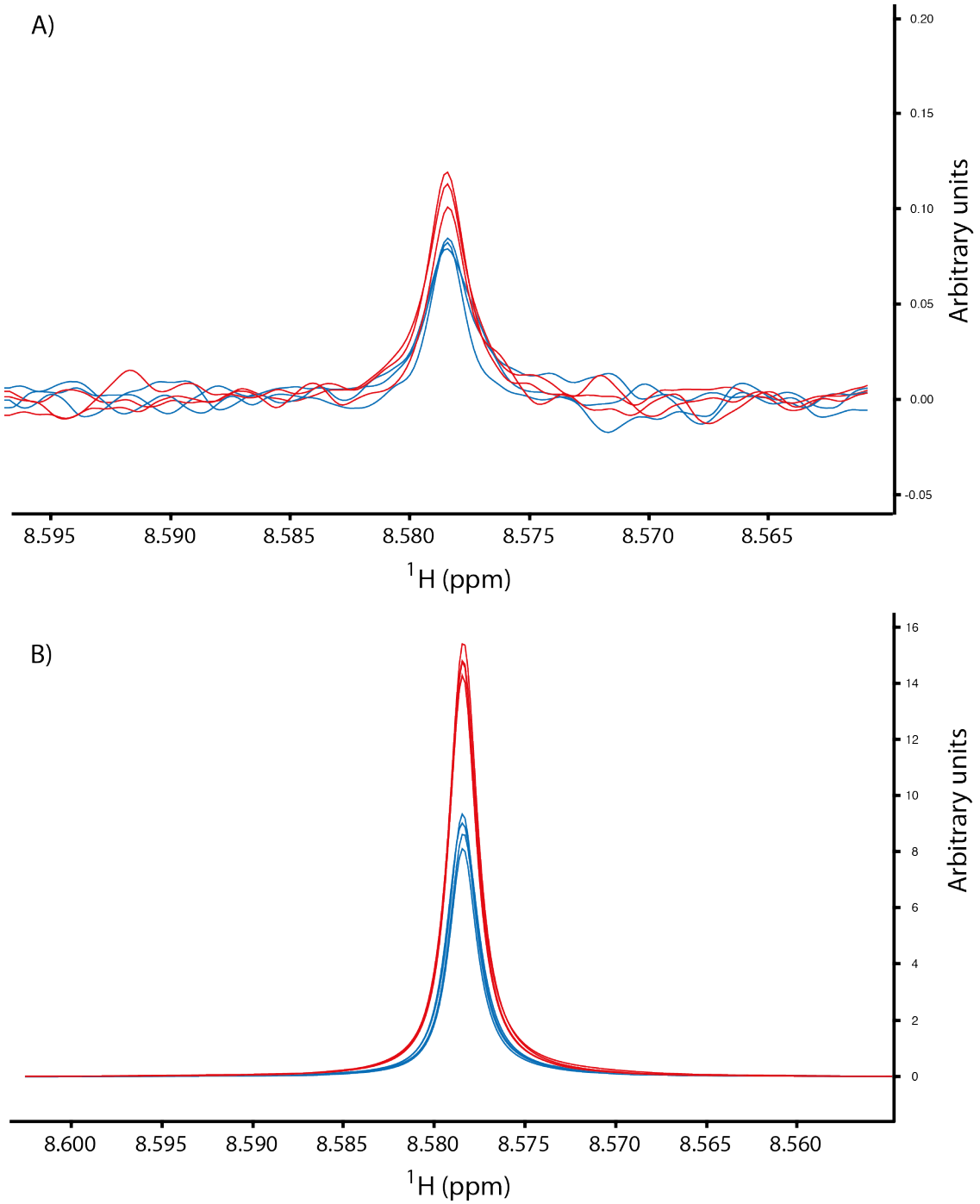

Figure 3-2: A smaller droplet volume and higher ^{13}C-formate concentration yield a greater signal difference between undiluted and diluted samples.

A) 700 MHz ^{1}H NMR spectra of 20 μL 100 μM ^{13}C formate droplets undiluted (red; n=3) or diluted with 6 μL of water (blue; n=3). B) 700 MHz ^{1}H NMR spectra of 10 μL 25 mM ^{13}C formate droplets undiluted (red; n=4) or diluted with 6 μL of water (blue; n=4). In both panels, the region of the spectrum between 8.56 and 8.60 ppm is expanded to show the upfield (leftmost) ^{13}C-formate H-1 signal.

Another source of error in VDTS arises from the contribution of formate (98.9 % ^{12}C-formate and 1.1% natural abundance ^{13}C-formate) endogenous from the larvae and exogenous from contaminated materials. If either of these formate sources are large enough, then there may arise a significant contribution to the ^{13}C-formate signal in the NMR spectrum. In spectra where the opened larval sample has a higher ^{13}C-formate H-1 signal than the “blank” sample, the volume of hemolymph released into the droplet cannot be reliably determined (Figure 3-3).

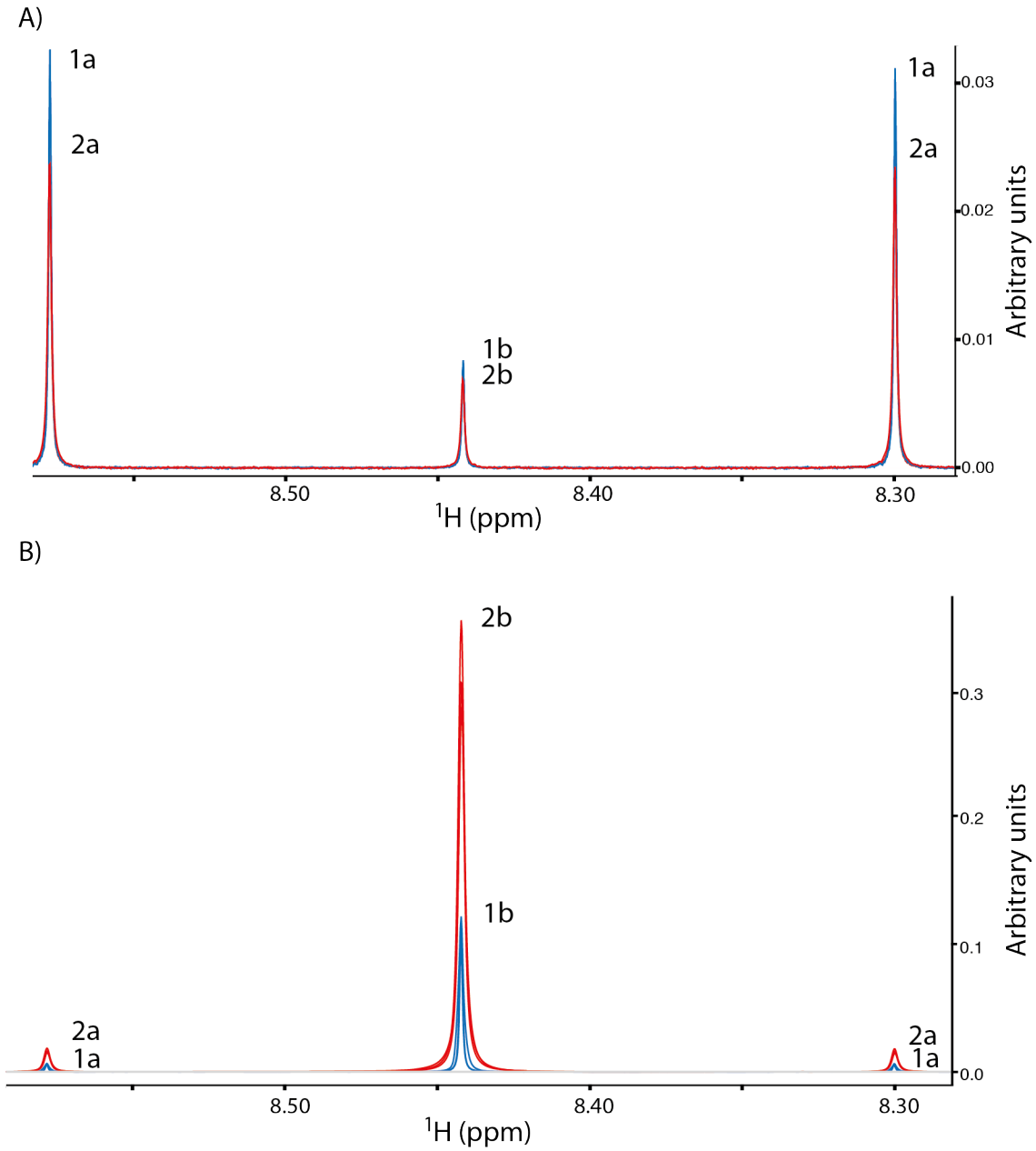

Figure 3-3: Formate contamination contributes to the ^{13}C formate H-1 signal.

A) 700 MHz ^{1}H NMR spectra of the extracted hemolymph polar metabolome for batches of "blank" (1; n=3) and "opened" fed larvae (2; n=3). B) 700 MHz ^{1}H NMR spectra of the "blank" (1') and "opened" hemolymph metabolome for batches of fed larvae, "contaminated" with a large amount of formate from sources other than the VDTS starting droplet (2'). In both panels, the region between ~8.25 and 8.60 ppm is expanded. Within this region, the H-1 doublet resonance of ^{13}C-formate in the "blank" (1a/1'a) and in the "opened" fed larvae (2a/2'a) can be visualised alongside the H-1 singlet resonance of ^{12}C-formate in the "blank" (1b/1'b) and "opened" fed larvae (2b/2'b).

To sidestep formate “contamination”, I trialled two other potential standards: 3,5-DNBA and 4-Cl-DNBA. Candidates were sought that had simple NMR spectra, polarity and pKa similar to formate, and with ^{1}H NMR signals that might be well resolved in typical metabolite profiling spectra (Weber et al., 2014). I observed 4-Cl-DNBA has fewer signals than 3,5-DNBA in its NMR spectrum (Figure 3-4); therefore, there is a smaller chance of signal overlap between the peak of the standard and signals from extracted hemolymph metabolites. As a result, 4-Cl-DNBA was tested as a potential replacement for ^{13}C-formate, for use as a standard in hemolymph VDTS.

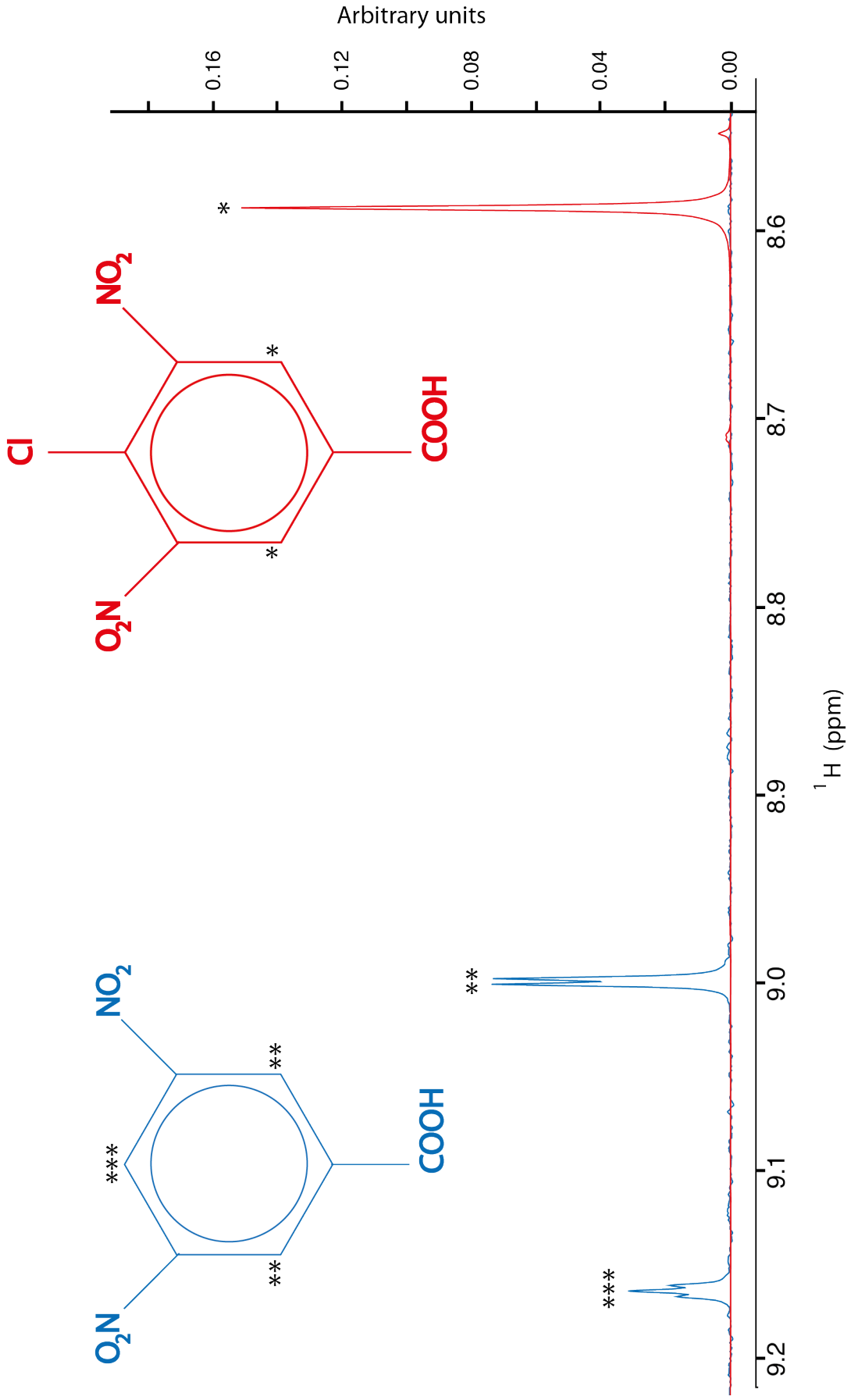
Arbitrary units
0.16
0.12
0.08
0.04
0.00
8.6
8.7
8.8
8.9
9.0
9.1
9.2
^{1}H (ppm)
NO2
Cl
COOH
O2N
NO2
COOH
O2N

Figure 3-4: Comparison of recorded NMR spectra for 3,5-DNBA and 4-Cl-DNBA.

The region between ~8.5 and 9.2 ppm is expanded in the 700 MHz ^{1}H NMR spectra of 20 µL droplets of 4 mM 4-Cl-DNBA (red) and 3,5-DNBA (blue). The chemical structure for 4-Cl-DNBA and 3,5-DNBA is depicted in red and blue respectively. NMR peaks corresponding to protons in 4-Cl-DNBA (*) and 3,5-DNBA (** and ***) are also depicted.

4-Cl-DNBA pilot experiments were performed by transferring one of two volumes of water (4 µL or 10 µL), representing released hemolymph, into a 20 µL droplet of 4 mM 4-Cl-DNBA and recording the NMR spectrum. The signal intensity of 4-Cl-DNBA decreased appropriately as the volume of water transferred to the droplet increased (Figure 3-5). Using 4-Cl-DNBA as the second standard and applying VDTS to determine the volumes of water diluted into the droplet, the principle of estimates returned were: 4.4 ± 0.7 µL and 9.9 ± 0.5 µL respectively (Appendix: Table 5). These values are close (98 %) to the dispensed volumes of water diluted into the droplet, indicating that 4-Cl-DNBA is potentially an acceptable alternative to ^{13}C-formate as a second standard for use in VDTS. The degree of imprecision in the measured versus the theoretical volumes of the water samples may well be within that associated with the Hamilton syringe pipetting imprecision.

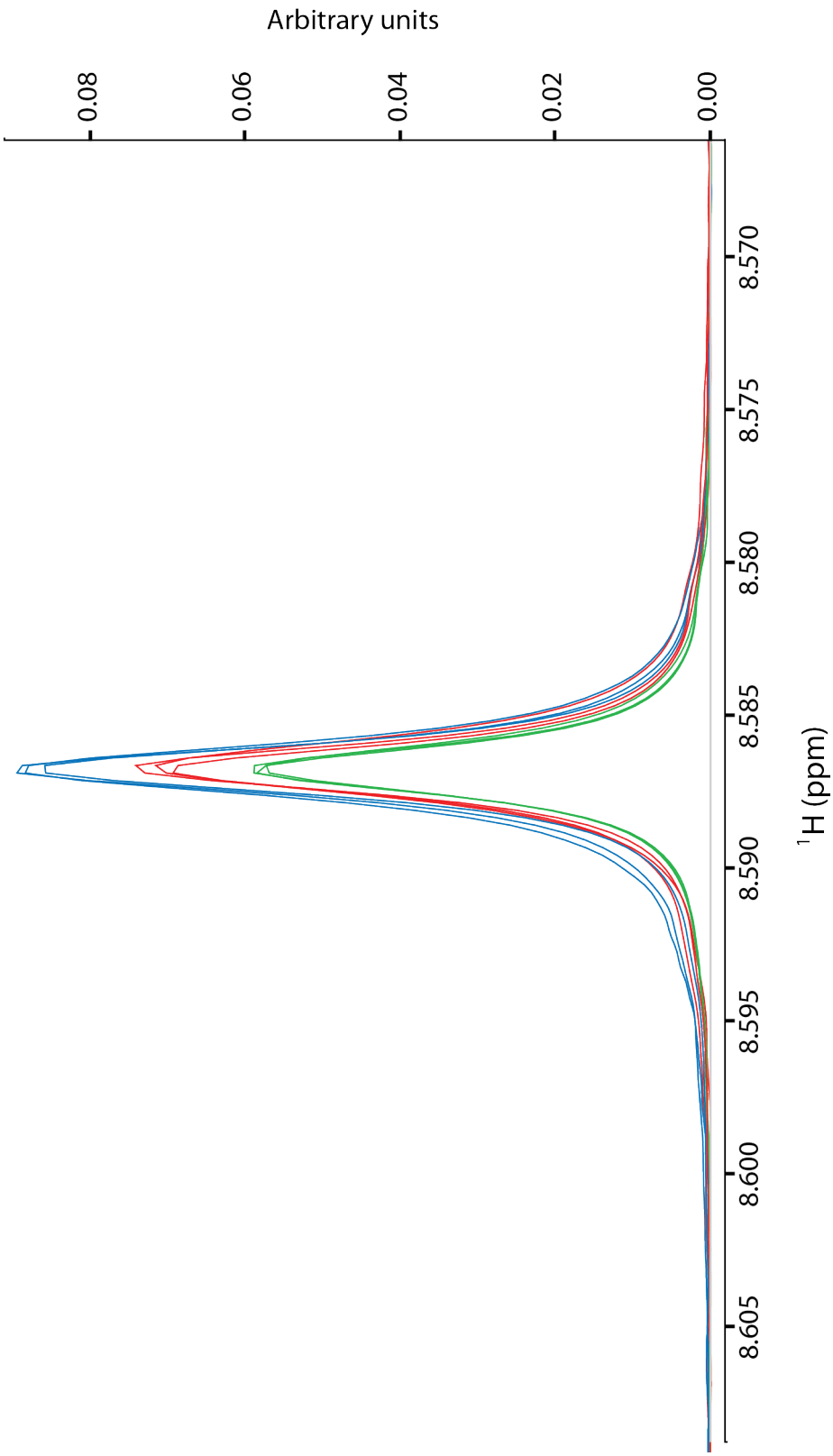

Figure 3-5: 4-Cl-DNBA signal decreases with increasing droplet dilution.

700 MHz ^{1}H NMR spectra of 20 µL 4 mM 4-Cl-DNBA droplets diluted with either 0 µL (blue; n=3), 4 µL (red; n=3) or 10 µL (green; n=3) water.

If the 4-Cl-DNBA was to prove useful for real biological samples, then the 4-Cl-DNBA signal should not be appreciably altered by interactions with components of the hemolymph. To test this, hemolymph was diluted into a droplet of 4-Cl-DNBA. An interaction between a component in the hemolymph and the standard could result in a shift in the signal position for 4-Cl-DNBA and/or a peak shape change. The hemolymph VDTS method developed by Ragan et al. (2013) was performed, exchanging 20 µL of 100 µM ^{13}C-formate for 10 µL of 4 mM 4-Cl-DNBA. For the "opened" sample the cuticles of 10 late L3 fed female larvae were ruptured in the 4-Cl-DNBA droplet. It was observed that the intensity of the 4-Cl-DNBA is decreased in the "opened" (extracted hemolymph) spectra, relative to the "blank" spectra, and the shape and position of the 4-Cl-DNBA signal had barely been altered (Figure 3-6). Hence, 4-Cl-DNBA did not undergo any significant chemical change upon contact with hemolymph. Furthermore, the position of the 4-Cl-DNBA signal was also not crowded by the signals of other hemolymph components, so its quantification was not compromised. VDTS optimised to use 4-Cl-DNBA as a standard was utilised for estimation of two separate fed female larval hemolymph volumes. The volumes yielded were 652 and 889 nL respectively**.** These values are broadly consistent with the average value reported in Ragan et al., (2013) for the hemolymph of fed female larvae at the same developmental stage (692 ± 72 nL). A substantial advantage of 4-Cl-DNBA over ^{13}C-formate is that it is not an endogenous component of *Drosophila* hemolymph or present as a labware contaminant. Therefore all of the 4-Cl-DNBA signal observed in the spectra must derive from the second standard. Taken together, 4-Cl-DNBA is not present in and does not interact with *Drosophila* hemolymph and can be used as a standard to measure accurately the volumes of sub-microlitre samples of hemolymph. Therefore, 4-Cl-DNBA was chosen to replace ^{13}C-formate as the second standard in hemolymph VDTS.

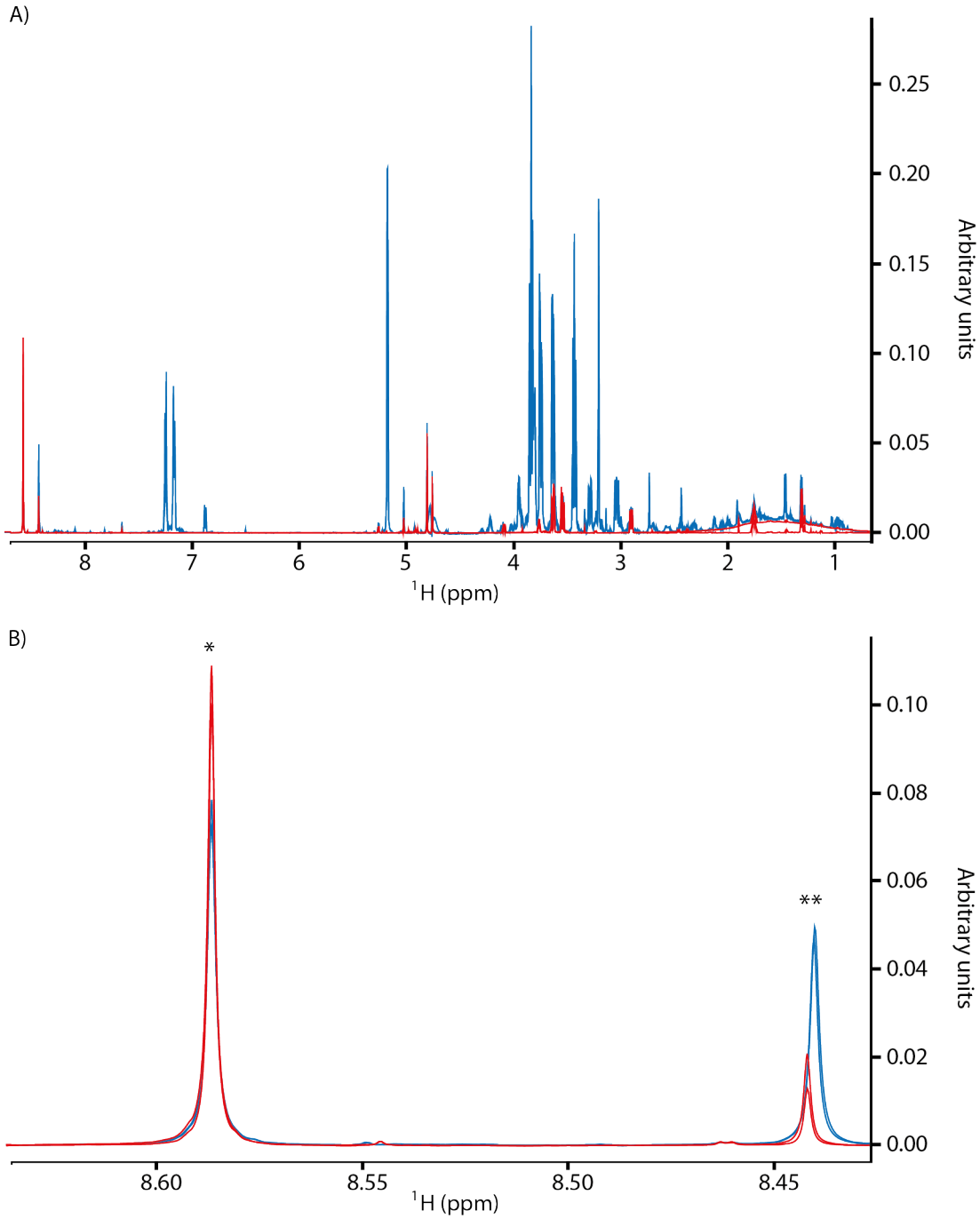

Figure 3-6: The hemolymph chemical environment does not shift the NMR signal of 4-Cl-DNBA.

A) 700 MHz ^{1}H NMR spectra of the extracted hemolymph polar metabolome for batches of "blank" (red; n=3) and "opened" fed female larvae (blue; n=2). B) The region between 8.40 and 8.65 ppm has been expanded vertically to visualise the ^{1}H resonance of 4-Cl-DNBA (*) and H-1 ^{12}C-formate (**) for "opened" (blue) and "blank" controls (red).

3.2 VDTS adaptation to solid tissue samples

Adapting the VDTS technique from extracting metabolites from liquid hemolymph samples, to extracting metabolites from solid whole larval samples involved determination of a method to homogenise the whole larvae (composed of solid tissue and liquid hemolymph). Three homogenisation methods were trialled: sonication, ball bearings and a motorised pellet pestle (Figure 3-7).

Homogenisation using an ultrasonic water bath resulted in incomplete homogenisation of larvae. After a 30 sec sonication, some larvae burst and released hemolymph/tissue but others were still intact and moving (Figure 3-7 A). More consistent homogenisation of larvae between samples can be achieved using ball bearing beating. However, there is a trade off between thorough homogenisation and accessibility to the homogenate. If the microcentrifuge tube used has a smaller base diameter than the ball bearing (as is the case in Figure 3-7 B), the ball bearing can be removed after homogenisation without disturbing the homogenate but large parts of intact whole tissue can remain. If the microcentrifuge tube used has a base diameter equal to or larger to the ball bearing, homogenisation is consistent between the samples but access to the homogenate is compromised by the ball bearing itself. Fortunately, however, homogenisation achieved through use of a motorised pellet pestle with a microcentrifuge tube as a mortar resulted in thorough, consistent homogenisation of whole larvae between samples and homogenate accessibly was retained (see Figure 3-7 C).

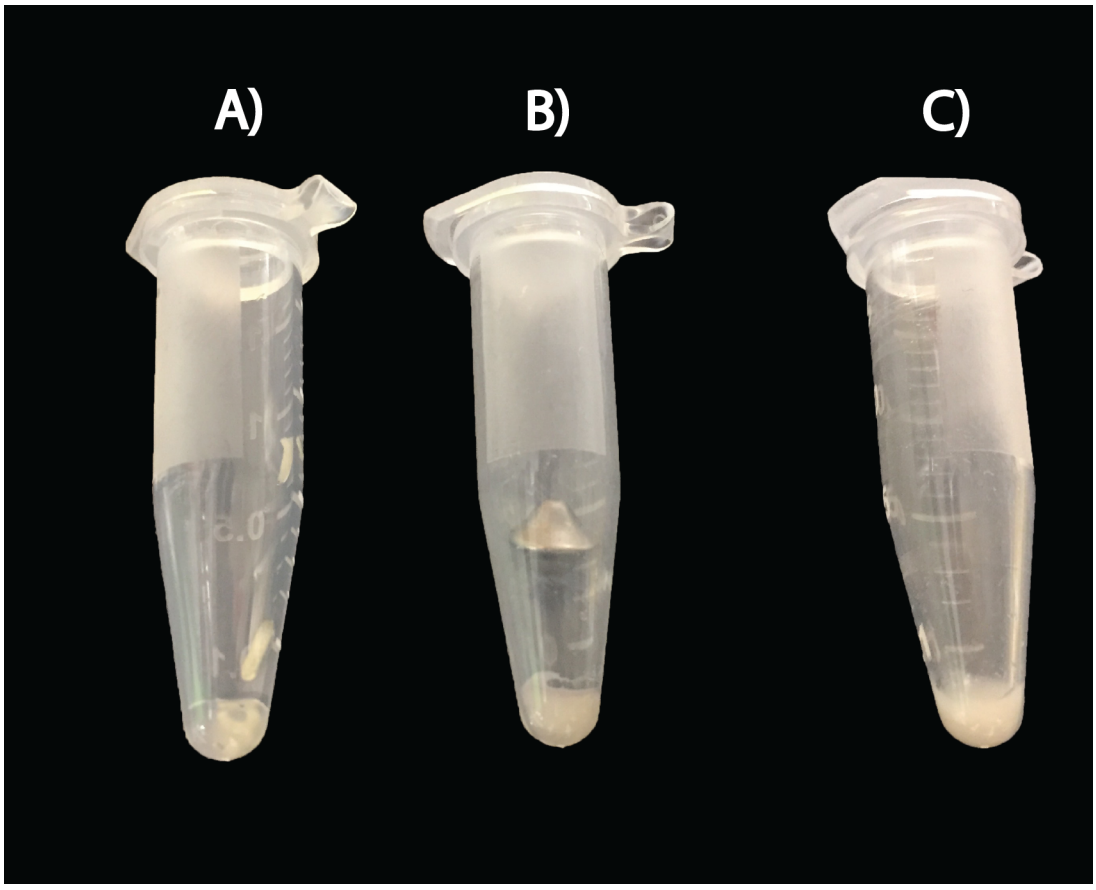

Figure 3-7: Three different methods of larval homogenisation.

Whole larval homogenisation for 30 sec with an ultrasonic water bath (A), ball bearing beating (B) or use of a motorised pellet pestle (C).

In whole larval VDTS, the volume released upon larval homogenisation is determined by comparing the concentration of second standard (determined via *Chenomx*) in homogenised ("opened") versus intact ("blank") larval samples. Although 4-Cl-DNBA was used as the second standard in hemolymph VDTS, a metabolite present in whole larvae (but absent in hemolymph) has a partially overlapping NMR peak adjacent to the NMR peak for 4-Cl-DNBA (Figure 3-8). This unidentified metabolite hinders precise quantification of the 4-Cl-DNBA NMR signal and therefore hinders determination of the absolute concentration of metabolites in whole larval samples. Hence, for whole larval VDTS, I reverted to ^{13}C-formate as the second standard as its NMR peak does not overlap with those of any endogenous larval metabolites. The complete strategy for whole larval metabolite extraction and VDTS is depicted in Figure 3-9.

Figure 3-8: A whole larval metabolite compromises quantification of 4-Cl-DNBA.

The region from 8.60 to 8.58 ppm is shown from the 700 MHz ^{1}H NMR spectrum of the extracted whole larval polar metabolome (black). Reference spectra for 4-Cl-DNBA (red) and the whole larval metabolite (blue) have been fitted to the extracted metabolome spectrum. The sum of the fitted 4-Cl-DNBA and whole larval metabolite reference spectra is also depicted (green).

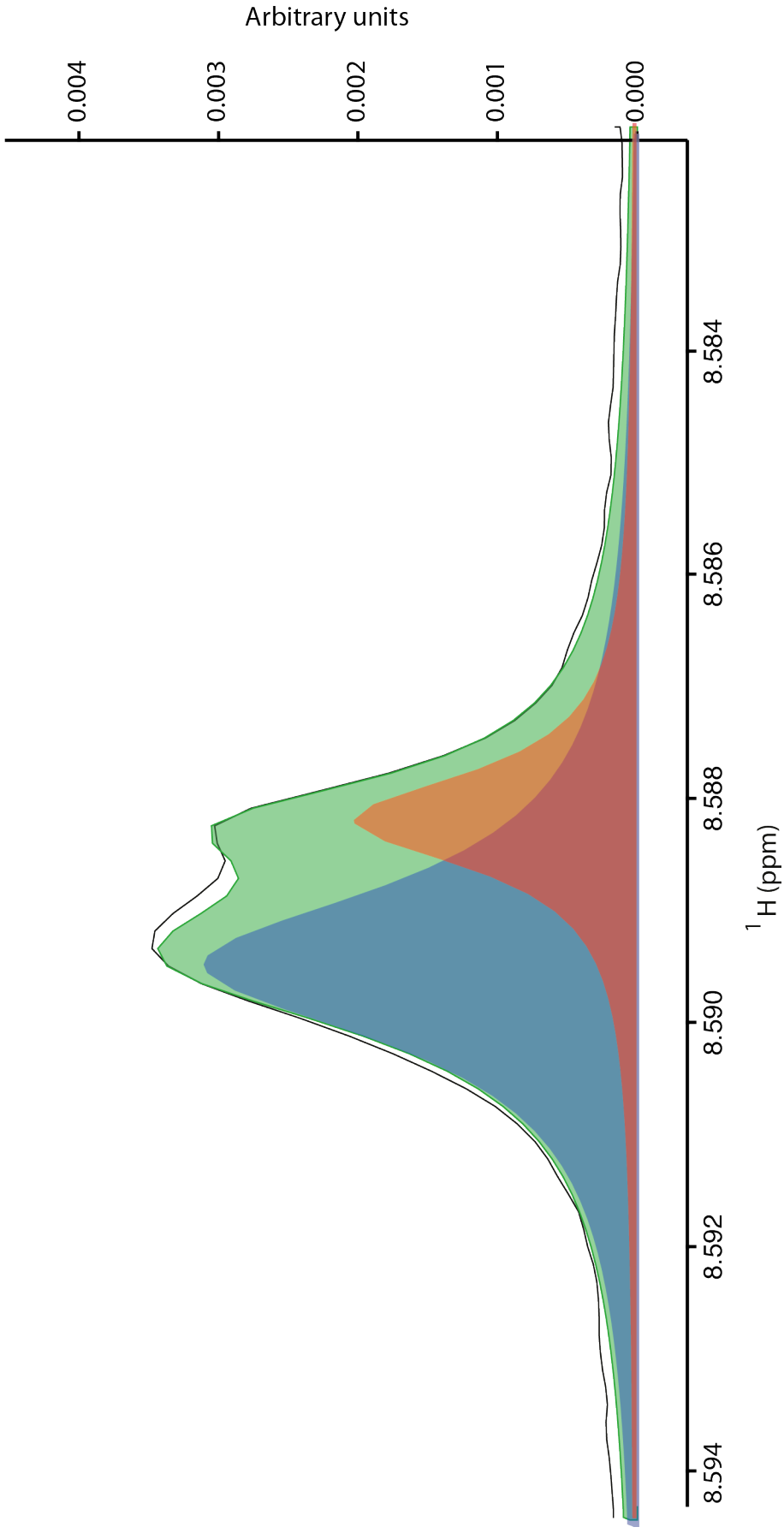
Arbitrary units
0.004
0.003
0.002
0.001
0.000
8.584
8.586
8.588
8.590
8.592
8.594
^{1}H (ppm)

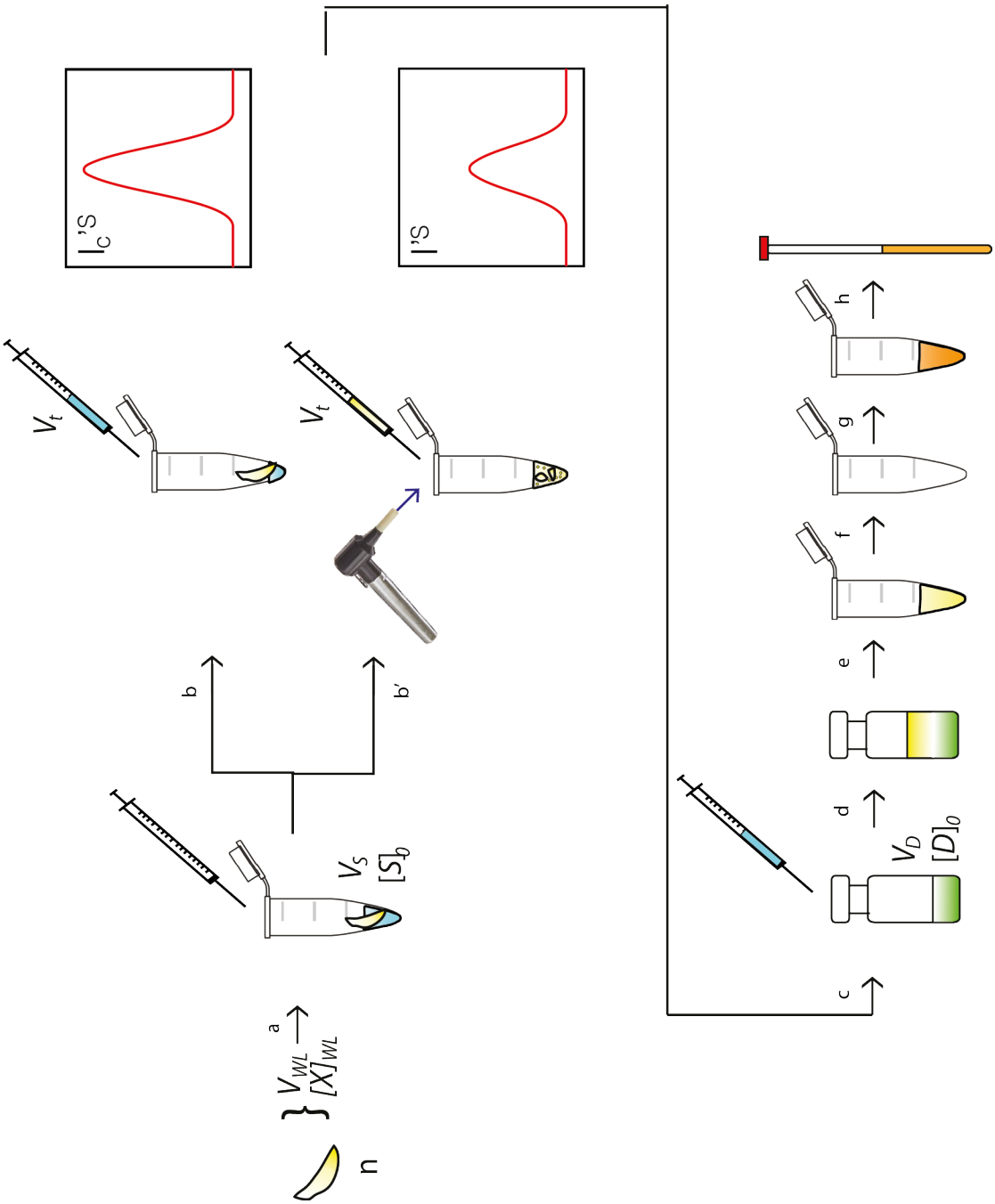
n
a
V_{WL}
$[X]_{WL}$
V_S
$[S]_0$
b
b'
V_t
V_t
I_C'S
I'S
c
V_D
$[D]_0$
d
e
f
g
h

Figure 3-9: Outline of whole larval metabolite extraction and VDTS.

An accurately measured volume (V_S) of saline containing ^{13}C-formate at a known concentration ($[S]_0$) is transferred to a number of larvae (n) in a microcentrifuge tube (a). Larvae are then either homogenised using a motorised pellet pestle and the microcentrifuge as the mortar (b') or left intact (b) to make up the "opened" and "blank" sample respectively. An accurately measured volume (V_t) is then taken from the homogenised or intact larvae and added to a known volume (V_D) of chloroform/methanol/water (green) containing a fixed concentration $[D]_0$ of DSS (c). The remaining steps: d-h are the same as e-i in Figure 3-1. V_{WL}: Volume released from homogenised larva. $[X]_{WL}$: Concentration of metabolite X in the whole larval homogenate. $I_c'^S$: H-1 signal of ^{13}C-formate when larvae are not homogenised into the ^{13}C-formate droplet. I'^S: H-1 signal of ^{13}C-formate when larvae are homogenised into the droplet.

The solid tissue VDTS method was further optimised for the extraction and measurement of metabolites from whole *Drosophila* adults rather than from larva. Again, the motorised pellet pestle method was used to homogenise whole adults that had been immobilised (for a maximum time of 2 minutes) via incubation on a plate chilled with ice. After centrifugation, the whole adult supernatant was treated in the same manner as the whole larval supernatant for the extraction of the polar metabolites (Figure 3-10).

Optimisation of solid tissue VDTS allowed me to compare the polar metabolome from *Drosophila* adults raised under different dietary conditions. Work from our Melbourne collaborator, Louise Cheng (Peter MacCallum Institute), has shown that dietary deprivation of histidine inhibits the growth of tumours caused by the loss of Nerfin-1 or Notch hyperactivation, yet it has minimal effects on the growth of normal stem cells or other tumour types (Szuperák et al., manuscript in preparation). However, to interpret these findings it was necessary to confirm whether dietary histidine deprivation specifically depletes histidine from the adult body or whether the adult has sufficient internal histidine stores to compensate. I therefore compared the polar metabolomes of adults fed on diets differing in their histidine content. It was also necessary to ensure that metabolome differences reflected those in internal tissues and were not simply the result of food trapped in the adult gut lumen. I therefore developed a gut transit assay to determine the time taken for an adult to completely transit the contents of its gut and to replenish it with new food. Pharate adults were transferred into vials containing a holidic diet consisting of entirely purified compounds called chemically defined diet 22 (CDD22, Szuperák et al., manuscript in preparation) that contained bromophenol blue. Adults eclosing onto this food eat it and their (transparent) guts appear blue. If they are then transferred onto CDD22 free from bromophenol blue, the transit time taken for dissected guts to become free from blue colouration can be easily observed. Using this method, I estimated the adult gut transit time as 4.5 hours. I was then able to use this information to design a protocol to measure histidine concentration in whole flies in the absence of histidine "contamination" from the food in the gut (Figure 3-10).

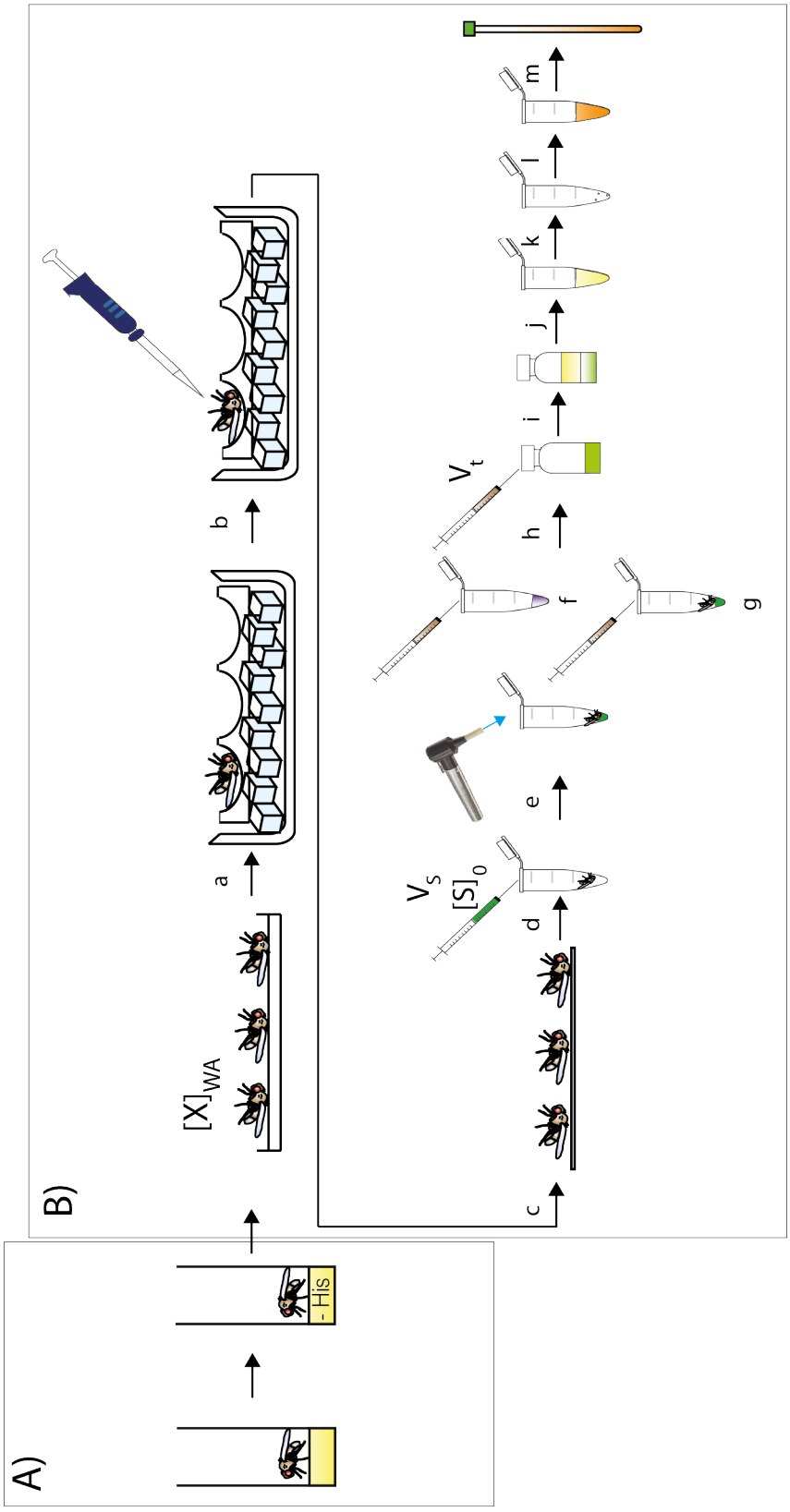
A)
- His
B)
a
b
c
d
e
f
g
h
i
j
k
l
m
$[X]_{WA}$
V_S
$[S]_0$
V_t

Figure 3-10: Outline of whole adult metabolite extraction and VDTS strategy.

A) Gut histidine depletion is achieved by transferring adults from a histidine diet to CDD22 free from histidine (-His) for 4.5 hours. B) Metabolite extraction from whole adults is achieved by sedating adults on a CO_2 pad and then transferring them to a depression dish on ice (a). Adults are then washed with ethanol thrice (b) before transfer to tissue paper and blotting dry (c). An accurately measured volume (V_S) of 4-Cl-DNBA at a known concentration ($[S]_0$) is then transferred to the adults (d). Adults are then either homogenised via a motorised pellet pestle (f) or left intact (g) and an accurate volume of the homogenate or 4-Cl-DNBA solution (V_t) is transferred to a known volume (V_D) of chloroform/methanol/water containing a fixed concentration ($[D]_0$) of DSS (h). After further separation of polar and non-polar components via the Bligh-Dyer method (i), the upper aqueous phase of polar metabolites is aspirated to a microcentrifuge tube (j). The solution is evaporated to dryness (k) and the residue suspended in D_2O (l) prior to transfer to an NMR tube (m). $[X]_{WA}$: concentration of metabolite X in whole adult.

Concentrations of histidine, tyrosine and alanine were determined for adults fed either CDD22 (1 g/L histidine; 6.5 mM), CDD22–His (0 g/L histidine) or CDD22+His (2 g/L histidine; 12.9 mM) (Table 1). Whole body tyrosine and alanine concentrations do no vary drastically between diets or before and after gut depletion of Histidine, even though these two amino acids are present in CDD22 (5 g/L tyrosine (2.8 mM) and 5 g/L alanine (5.6 mM)). For histidine, adults fed throughout on CDD22–His have no detectable whole body histidine whereas those fed on CDD22 have concentrations of 2.5 mM. Adults fed on CDD22+His have a whole body histidine concentration of 4.01 mM, ~1.6 times that seen in adults fed CDD22. However, after gut histidine depletion, adults fed originally on CDD22 or CDD22+His now have much lower and rather similar histidine concentrations (~1.8 and ~1.4 mM respectively). Comparisons before and after gut histidine depletion indicate that food in the gut makes a substantial contribution towards total body histidine. These results also suggest that histidine remaining in the rest of the fly body is strongly lowered by CDD22–His (from 1.83 to 0 mM) but not elevated by CDD22+His.

Metabolite/diet	CDD22		CDD22-His		CDD22+His	
	Concentration (mM)					
	pre-GD	post-GD	pre-GD	post-GD	pre-GD	post-GD
Histidine	2.50	1.83	0	0	4.01	1.39
Tyrosine	0.82	1.26	0.84	1.00	0.74	1.27
Alanine	10.18	13.51	10.27	7.76	10.21	12.56

Table 1: Histidine, tyrosine and alanine concentrations in whole adults, before and after histidine gut depletion (GD).

Entries are average concentrations in mM from two sets of adults fed on either CDD22, CDD22 depleted of histidine (CDD22-His) or CDD22 with twice the amount of histidine (CDD22+His). Pre-GD: whole body metabolite concentrations prior to gut-depletion with CDD22–His. Post-GD: whole body metabolite concentrations post-gut depletion with CDD22 – His.

3.3 Matched VDTS

The VDTS method was further optimised by pairing “opened” (hemolymph released/larvae homogenised) and “blank” (cuticle/larvae intact) samples from the same animal; I refer to this method as matched VDTS (MVDTS). MVDTS ensures that any liquid present of the surface of larvae or any liquid excreted by them prior to cuticle rupturing/homogenisation, would cancel out from the VDTS calculation as it would contribute to diluting the second standard’s proton signal equally in both the “blank” and “opened” samples. This optimisation also “saves” on larvae, requiring only half the number of larvae required in non-matched VDTS experiments. The MVDTS approach can be applied to both whole larvae and hemolymph (Figure 3-11and Figure 3-12).

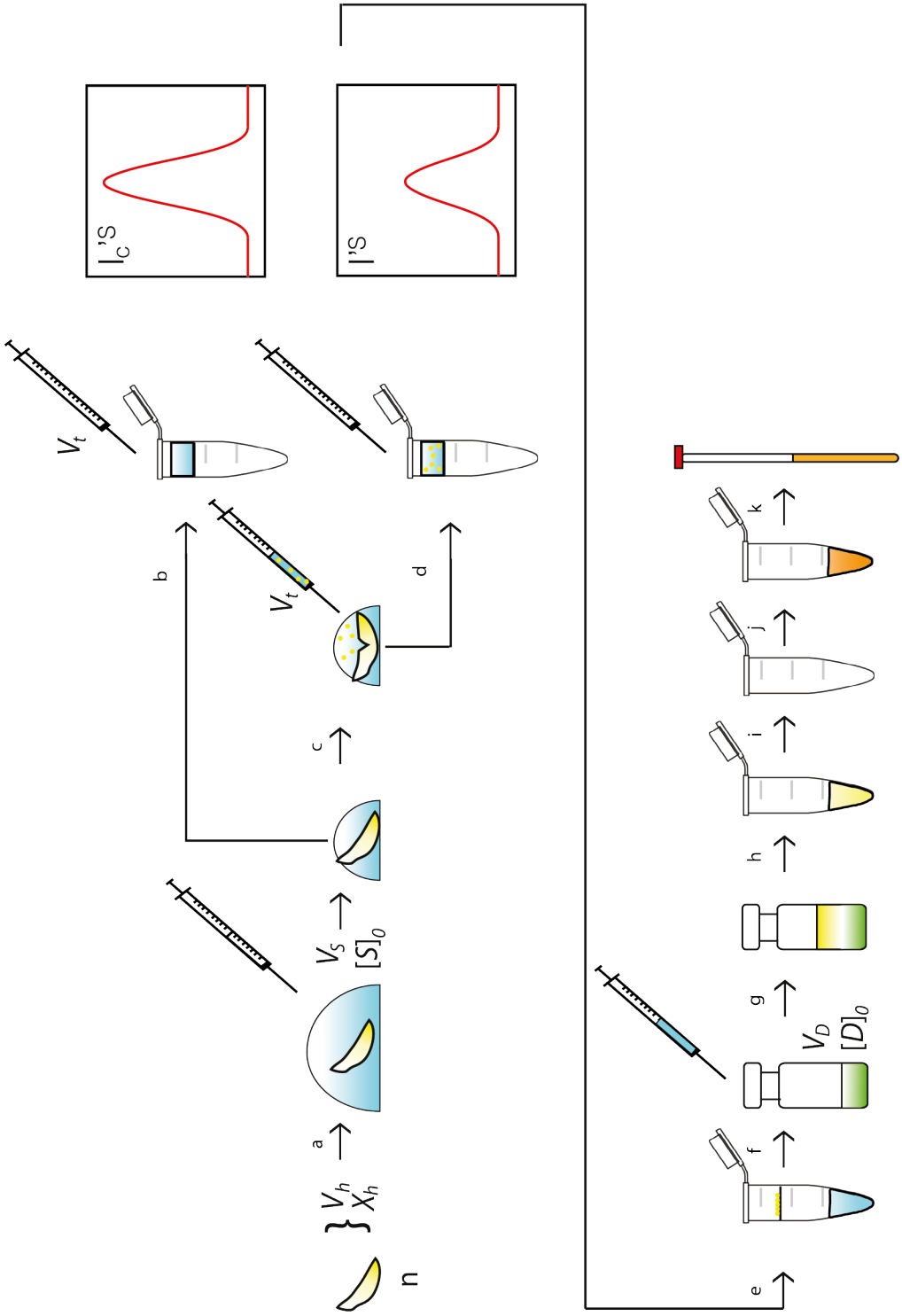
n
a
V_h
X_h
V_S
$[S]_0$
c
b
V_t
d
V_t
I_C'S
I'S
e
f
g
V_D
$[D]_0$
h
i
j
k

Figure 3-11: Outline of matched hemolymph VDTS.

An accurately measured volume (V_S) of saline containing the chosen standard (either ^{13}C formate or 4-Cl-DNBA) at a known concentration ($[S]_0$) is transferred to a number of larvae (n), with a collective hemolymph volume: V_h (a). An accurately measure volume of the droplet (V_t) is removed and transferred into water in a microcentifuge column (b) – this constitutes the "blank" sample. Larval cuticles are then ruptured to release hemolymph into the droplet (c) and an accurately measured volume (V_t) is removed from the droplet and transferred to water in a different microcentifuge column (d) and then cleared of hemocytes (e). The remaining steps: f-k are the same as d-i in Figure 3-1. V_h: Volume of released hemolymph. $[X]_h$: Concentration of metabolite X in the hemolymph. $I_c{}'^S$: ^1H resonance of the standard when larvae do not have their cuticles ruptured. I'^S: ^1H resonance of the standard when larvae have their cuticles ruptured.

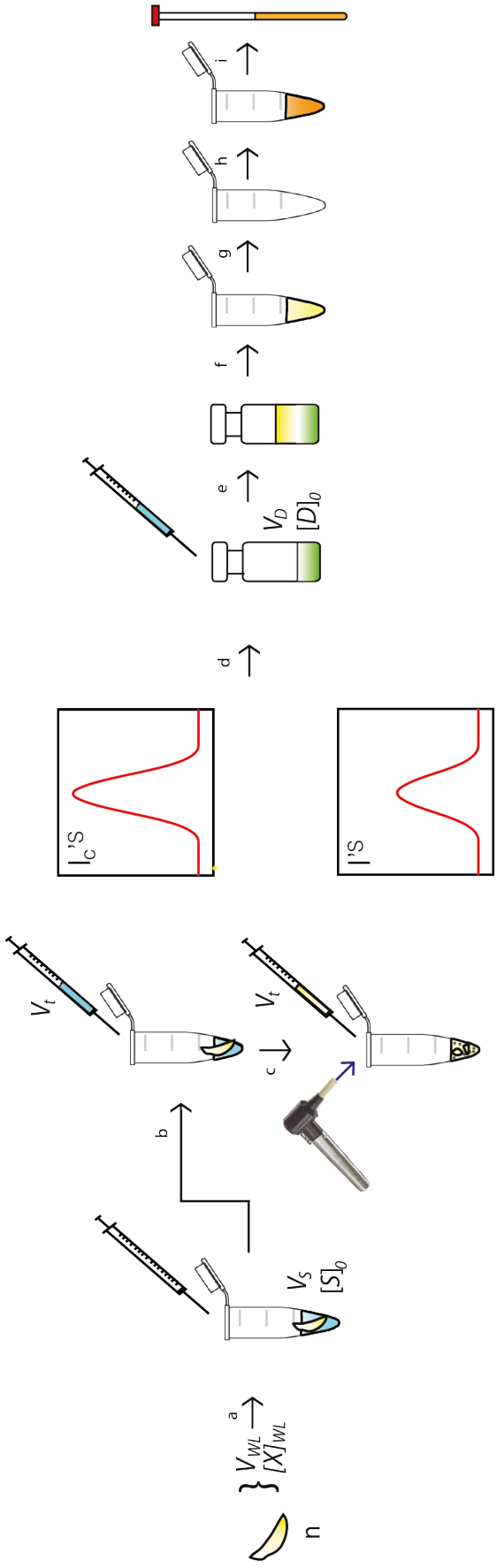
n
a
V_{WL}
$[X]_{WL}$
V_S
$[S]_0$
b
c
V_t
V_t
I_C'S
I'S
d
e
V_D
$[D]_0$
f
g
h
i

Figure 3-12: Outline of the matched whole larval VDTS.

An accurately measured volume (V_S) of saline containing ^{13}C-formate at a known concentration ($[S]_0$) is transferred to a number of larvae (n) in a microcentrifuge tube (a). An accurately measured volume (V_t) is then removed from the larvae in the microcentrifuge tube for the "blank" sample (b). Larvae are then homogenized using a motorized pellet pestle and the microcentrifuge tube as a mortar (c) – this will be the "opened" sample. An accurately measured volume (V_t) is then removed from the homogenised larvae and transferred to a known volume (V_D) of chloroform/methanol/water (green) containing a fixed concentration $[D]_0$ of DSS (d). The remaining steps: e-i are the same as e-i in Figure 3-1. V_{WL}: Volume of homogenised whole larva. $[X]_{WL}$: Concentration of metabolite X in whole larval homogenate. $I_c'^S$: H-1 signal of ^{13}C-formate when larvae are not homogenised into the ^{13}C-formate droplet. I'^S: H-1 signal of ^{13}C-formate when larvae are homogenised into the droplet.

To confirm if the matched optimisation significantly differed from the absolute concentration of hemolymph metabolites determined via the non-matched method, metabolite concentrations from the same sample of late L3 (continuously fed) male and female larvae were determined via the MVDTS and non-matched VDTS method and were compared (Table 2).

Only a single metabolite: succinate was determined to be significantly different when its concentration was determined via non-matched VDTS and MVDTS. However, sarcosine, which is found to be significantly different between continuously fed males and females using non-matched VDTS was not significantly different between fed males and females via MVDTS. Instead, betaine was found to be significantly different between continuously fed males and females, when concentrations were determined via MVDTS. Taken together, it can be observed that metabolite concentrations determined via the non-matched VDTS or MVDTS method do not significantly differ. However, as the MVDTS method minimises the risk of liquid carried over/excreted by the larvae, this method would be used in the future. Unfortunately, I developed the MVDTS method late into my PhD and thus was not able to apply it when calculating the hemolymph and whole larval metabolite concentrations reported in the following chapters.

Table 2: Comparison of absolute hemolymph metabolite concentrations determined via non-matched VDTS and MVDTS for continuously fed larvae.

Entries show mean concentration ± 1 standard deviation for two independent experiments, each with three biological replicates. Bold figures indicate statistically significant ($p \leq 0.01$) differences between:

Continuously fed males and females when metabolite concentrations were determined via VDTS and MVDTS[a] .

VDTS determined metabolite concentrations for continuously fed males and females[b].

MVDTS determined metabolite concentrations for continuously fed males and females[c].

Statistical significance is determined according to Tukey's HSD test in a 2-way ANOVA.

	continuously fed concentration determined via VDTS (mM)		continuously fed concentration determined via MVDTS (mM)	
Metabolite	male	female	male	female
alanine	4.25 ± 1.73	2.37 ± 0.79	4.22 ± 1.51	3.39 ± 1.36
arginine	0.77 ± 0.20	0.83 ± 0.28	0.79 ± 0.21	1.08 ± 0.35
betaine	0.28 ± 0.12	0.48 ± 0.22	**0.19 ± 0.05**[c]	**0.34 ± 0.16**[c]
dimethylamine	0.02 ± 0.01	0.02 ± 0.00	0.03 ± 0.01	0.04 ± 0.01
fumarate	0.15 ± 0.05	0.13 ± 0.04	0.16 ± 0.05	0.17 ± 0.07
glucose	0.57 ± 0.23	0.69 ± 0.26	0.69 ± 0.53	0.87 ± 0.80
glutamine	11.18 ± 5.89	10.46 ± 2.85	9.62 ± 2.97	14.03 ± 3.43
glycine	1.32 ± 0.56	0.89 ± 0.15	1.33 ± 0.51	1.33 ± 0.47
histidine	2.79 ± 1.23	2.54 ± 0.68	2.21 ± 0.45	2.90 ± 0.69
isoleucine	0.29 ± 0.11	0.20 ± 0.05	0.30 ± 0.12	0.25 ± 0.04
leucine	0.52 ± 0.18	0.37 ± 0.06	0.53 ± 0.18	0.43 ± 0.08
lysine	3.14 ± 1.27	2.43 ± 0.46	3.03 ± 0.87	3.42 ± 0.93
malate	2.44 ± 0.91	2.18 ± 0.82	2.26 ± 0.60	2.60 ± 0.89
methionine	0.38 ± 0.25	0.38 ± 0.09	0.32 ± 0.17	0.46 ± 0.05
O-phosphocholine	2.11 ± 0.82	1.51 ± 0.47	1.61 ± 0.29	1.64 ± 0.33
O-phosphoethanolamine	0.49 ± 0.11	0.42 ± 0.19	0.51 ± 0.10	0.44 ± 0.13
o-phosphotyrosine	59.58 ± 25.55	49.11 ± 11.47	50.82 ± 9.62	61.87 ± 9.21
phenylalanine	0.22 ± 0.10	0.16 ± 0.01	0.21 ± 0.07	0.20 ± 0.03
proline	8.14 ± 3.18	6.24 ± 1.68	7.12 ± 1.32	7.67 ± 1.54
sarcosine	**0.36 ± 0.18**[b]	**0.16 ± 0.05**[b]	0.28 ± 0.06	0.21 ± 0.03
succinate	0.98 ± 0.21	**0.67 ± 0.12**[a]	0.90 ± 0.18	**0.82 ± 0.25**[a]
trehalose	63.89 ± 26.29	53.27 ± 11.71	57.46 ± 13.86	65.35 ± 11.50
tyrosine	3.98 ± 2.22	2.59 ± 0.62	3.73 ± 1.55	3.66 ± 1.12
valine	1.11 ± 0.49	0.63 ± 0.11	1.20 ± 0.51	0.95 ± 0.29
β-Alanine	1.21 ± 0.64	1.03 ± 0.26	1.05 ± 0.33	1.40 ± 0.38

3.4 Discussion

I have significantly adapted and optimised VDTS from the original larval hemolymph method developed by Ragan et al., (2013). The first optimisation was to increase the ^{13}C-formate concentration in the droplet and to decrease the volume of the droplet into which hemolymph was released. This increased the difference in the ^{13}C-formate H-1 signal between the "opened" and "blank" samples, allowing a more precise measurement of the hemolymph volume released. The droplet volume optimisation in particular was crucial later in this thesis for accurate and precise determination of the tiny hemolymph volumes (~200 μL) released from smaller larvae (pre-CW) than those originally used by Ragan et al. (post-CW). The second optimisation was to exchange the second standard for hemolymph VDTS from ^{13}C-formate to 4-Cl-DNBA. Use of 4-Cl-DNBA allowed me to sidestep formate contaminations, which can compromise the calculation of hemolymph volume. Formate contamination was found on a number of occasions and traced back to multiple sources - including a batch of Pasteur pipettes and some bottles of distilled water. When used as a standard in hemolymph VDTS, 4-Cl-DNBA could return released hemolymph volumes for late L3 fed female larvae similar to those reported using formate in Ragan et al., (2013).

The VDTS method was further adapted to extract and determine absolute metabolite concentrations from solid adult tissue rather than from hemolymph. ^{13}C-formate was again used as a standard for this VDTS method due to the presence of a metabolite with a large signal, absent in hemolymph that crowded the NMR peak for 4-Cl-DNBA. The new whole adult VDTS method was then applied to a biological question involving histidine metabolism. By developing a gut depletion assay, I was able to estimate how much of the whole body histidine was contained in the gut lumen, which contains undigested, unabsorbed dietary medium. Together the whole body VDTS method coupled with the gut depletion assay revealed that histidine levels are not homeostatically maintained if adults eclose onto a medium devoid of histidine - even if, as larvae they are fed on a standard (histidine containing) medium. In contrast, if adults eclose onto a medium with a standard (CDD22) or double concentration of dietary histidine (CDD22+His) they retain similar whole body histidine concentrations in all tissues but not the gut. This

suggests that augmenting the histidine in the standard CDD22 diet does not significantly alter the overall size of the total body store of histidine.

The final optimisation made to the VDTS method was MVDTS: the use of the same larvae to generate the "blank" and "opened" samples. Use of this new method is likely to improve the precision of determined hemolymph volumes, as illustrated by the findings of Ragan et al., (2013), where it was reported that several hemolymph metabolites were significantly lower in female than in male larvae. It was hypothesised, that these metabolites may be depleted from the hemolymph more in females than in males. This would then fuel the additional growth of females, which grow at a faster rate and are ~1.3 times larger than males. However, a post-doc in the lab, Annick Sawala, and I have repeated the male *versus* female hemolymph experiments and have found statistically significant ($p \leq 0.01$) no sexually dimorphic difference in the hemolymph metabolite concentrations (Table 2). Examining the raw data from Ragan et al., (2013), it can be seen that, on average, "opened" fed male and female spectra share almost identical ^{13}C-formate H-1 signal intensities (n=3 for each), whereas the spectra from "blank" fed males have a lower ^{13}C-formate H-1 signal than "blank" fed females. Theoretically, however, there should be no significant difference between "blank" male and female samples as no hemolymph has been released into the droplet. A possible reason for the lower ^{13}C-formate H-1 signal intensities in "blank" fed male samples could be carry over of PBS on the surface of the larvae due to incomplete drying after a PBS wash or due to increased excretion of liquid by fed male larvae in the droplet, in comparison to fed female larvae. The MVDTS method should theoretically eliminate the possibly of PBS/excrement disproportionately effecting either the "blank" or the "opened" samples as the same larvae are used for both. Any PBS/excrement would dilute the ^{13}C-formate concentration in the "blank" and "opened" sample.

In summary, I have adapted and improved the original VDTS method so that it can be used to measure absolute metabolite concentrations in tiny liquid or solid samples that derive from larvae or from adult *Drosophila.*

Chapter 4. Identifying metabolites that change during development and starvation

The preceding chapter described the optimisation of the VDTS approach and its application to whole body and hemolymph larval samples. The aim of this chapter is to apply these optimised methods to identify polar metabolites that change concentration substantially and significantly during larval development, and in response to NR. A focus was placed on CW, as this developmental checkpoint is known to dramatically affect the larval response to starvation. Before CW, NR arrests larval development but after CW, NR is compatible with developmental progression to pupariation. To determine metabolic changes at CW and how they are modulated in response to NR, a five-way comparison of 1D ^{1}H NMR spectra was used for both male and female larvae (Figure 4-1); thus there were ten conditions in total. This allows for the identification of polar metabolites that change in concentration at different stages of development either side of CW in fed larvae. It also permits the identification of metabolites that change in concentration during starvation and compares this starvation response before and after CW is attained.

For the *w*^{1118} *iso 31* strain used as an inbred isogenised control strain in the Gould lab, CW is attained at approximately 57 hr at a weight of ~0.8 mg (on 2x medium). This isogenic strain pupariates at ~96 hr when reared on a standard diet but pupariates at ~89-90 hr if moved from fully fed conditions to a NR medium post-CW.

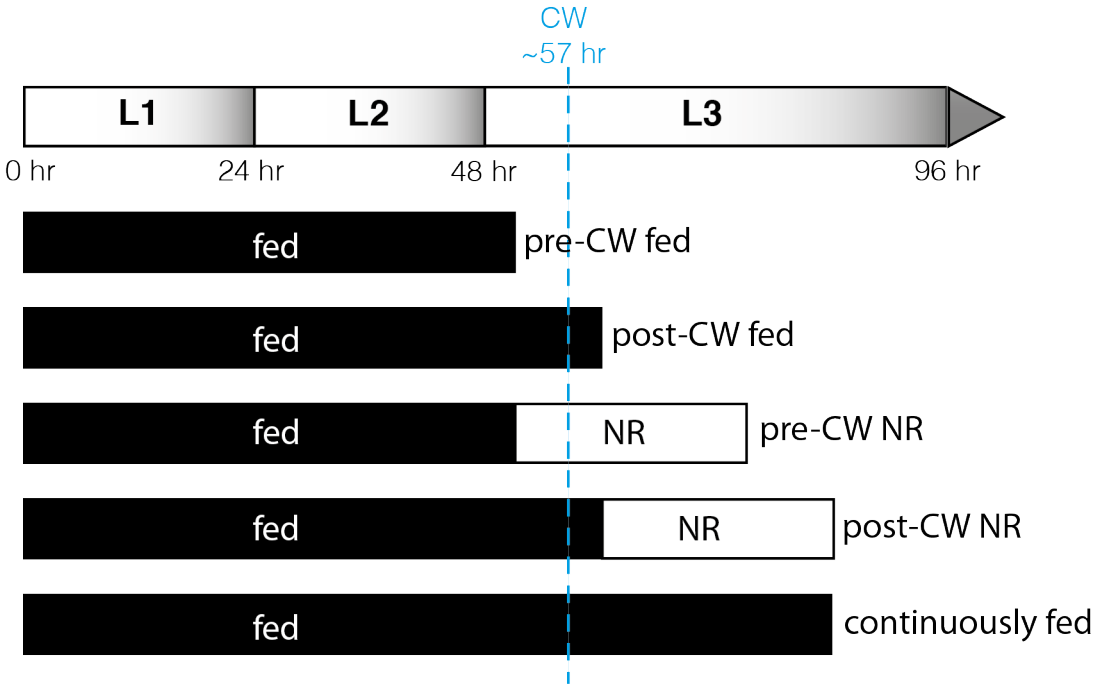

Figure 4-1: Experimental design for the metabolomic analysis of larvae.

Time line of larval development from 0-96 hr; the three larval instars (L1, L2 and L3) are depicted schematically and, below, the five feeding/fasting (fed/NR) regimes used in this experiment. Larvae fed continuously attain CW at ~57 hr.

Pre-CW fed: larvae are fed for 51 hr and then analysed;

Post-CW fed: larvae are fed for 60 hr and then analysed;

Pre-CW NR: larvae are fed for 51 hr and then transferred to NR medium for a further 24 hr before analysis;

Post-CW NR: larvae are fed for 60 hr and then transferred to NR medium for a further 24 hr before analysis;

Continuously fed: larvae are fed for 84 hr and then analysed.

4.1 Hemolymph and whole larval metabolite analysis

The application of PCA effectively allows one to assess whether data contains any high level structure (see Introduction: 1.3.3), and in the context of its application here, whether the NMR spectra corresponding to different sample conditions display distinguishing features reflecting differences in respective metabolomes. In

this application, PCA of larval hemolymph and whole larval polar metabolite NMR spectra was conducted for two independent experiments, with at least three biological replicates for each condition (hemolymph scores: Figure 4-2, hemolymph loadings: Figure 4-3, whole larval scores: Figure 4-4 and whole larval loadings: Figure 4-5). PC1, in the scores of both hemolymph repeats and the first whole larval repeat (Figure 4-2), and PC2 in the second whole larval repeat (Figure 4-4 A), separates pre- and post-CW samples (PC1 in the second whole larval repeat separates fed and NR samples). In the corresponding loadings, large signals for: O-phosphotyrosine (OPT), trehalose, O-phosphocholine and glycine are apparent in the hemolymph loadings (Figure 4-3), whilst: histidine, tyrosine, trehalose and threonine are apparent in the whole larval loadings (Figure 4-5), suggesting these metabolites may be sustainably different between pre- and post-CW samples.

As mentioned in the previous chapter, differing from Ragan et al., (2013), in my hands (and supported by independent experiments conducted by another post-doc in the lab, Annick Sawala) the application of VDTS failed to reveal sexual dimorphism in the polar “NMR metabolomes” for a given set of conditions. In addition, I observed that for either of the whole body or hemolymph experiments that the NMR spectra for fed larvae tend to cluster together whereas the spectra for NR larvae could be separated depending if larvae had attained CW or not (the pre-*versus* post-CW “status”). In other words PCA plot patterns suggested that the response of the polar metabolome to NR appears to be different either side of CW. Furthermore, the two-hemolymph experiments showed that post-CW NR and continuously fed NMR spectra clustered together. This clustering indicates that homeostasis of polar metabolites in the hemolymph is better buffered during NR once that CW has been attained. Taken together, the PCA of the hemolymph and the whole larval NMR data suggest that the attainment of CW correlates with a considerably altered larval response to NR but has less of an effect upon the fed polar metabolome.

Hemolymph analysis

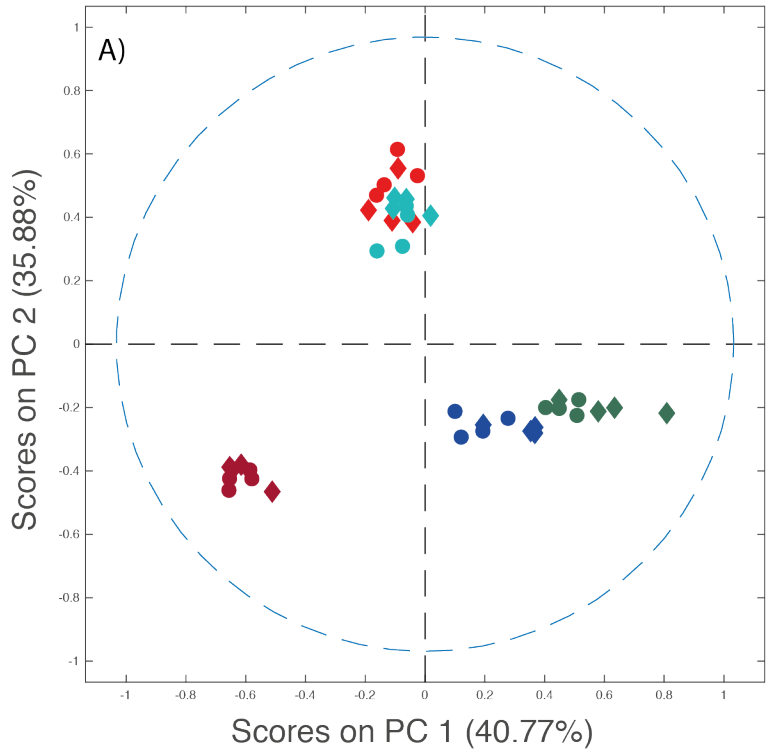

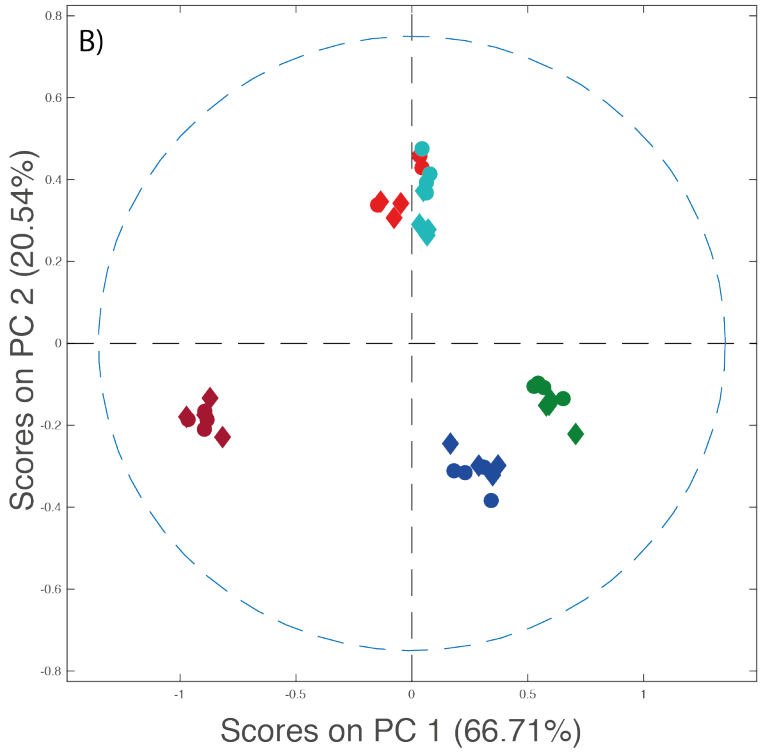

pre-CW fed ♂ pre-CW fed ♀ pre-CW NR ♂ pre-CW NR ♀

post-CW fed ♂ post-CW fed ♀ post-CW NR ♂ post-CW NR ♀

continuously fed ♂ continuously fed ♀

Figure 4-2: PCA scores plots for hemolymph polar metabolome NMR spectra.

PCA scores plots for the NMR spectra from the first (A) and second (B) independent experiments conducted to analyse the polar metabolites in larval hemolymph samples. Diamonds and circles represent data for male and female larvae respectively. Each symbol represents a single “opened” hemolymph NMR spectrum. Red symbols: pre-CW fed samples. Dark red: pre-CW NR samples. Blue symbols: post-CW fed samples. Dark blue symbols: post-CW NR samples. Green: continuously fed samples. Each condition was collected in, at least, triplicate.

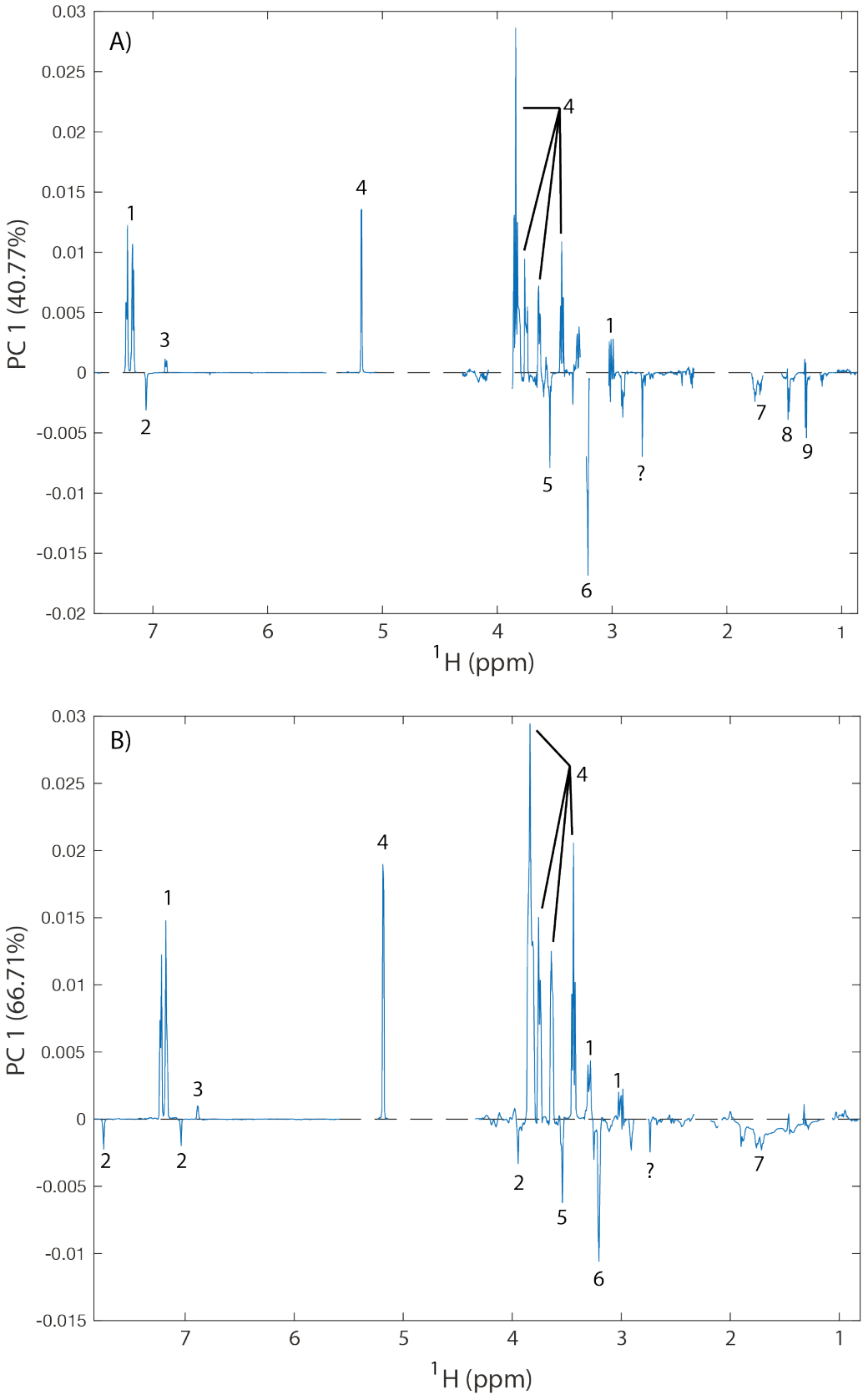

1: OPT; 2: His; 3: Tyr; 4: trehalose; 5: Gly; 6: OPC; 7: Lys; 8: Ala; 9: Thr

Figure 4-3: PCA loadings plots for hemolymph polar metabolome NMR spectra.

PCA loadings plots for the NMR spectra from the first (A) and second (B) independent experiments conducted to analyse the polar metabolites in larval hemolymph samples. Each condition was collected in, at least, triplicate. Numbered loadings correspond to resonances in the recorded NMR spectra that, in turn, correspond to the resonances for: O-phosphotyrosine (1); histidine (2); tyrosine (3); trehaolse (4); glycine (5); O-phosphocholine (6); lysine (7); alanine (8); threonine (9).

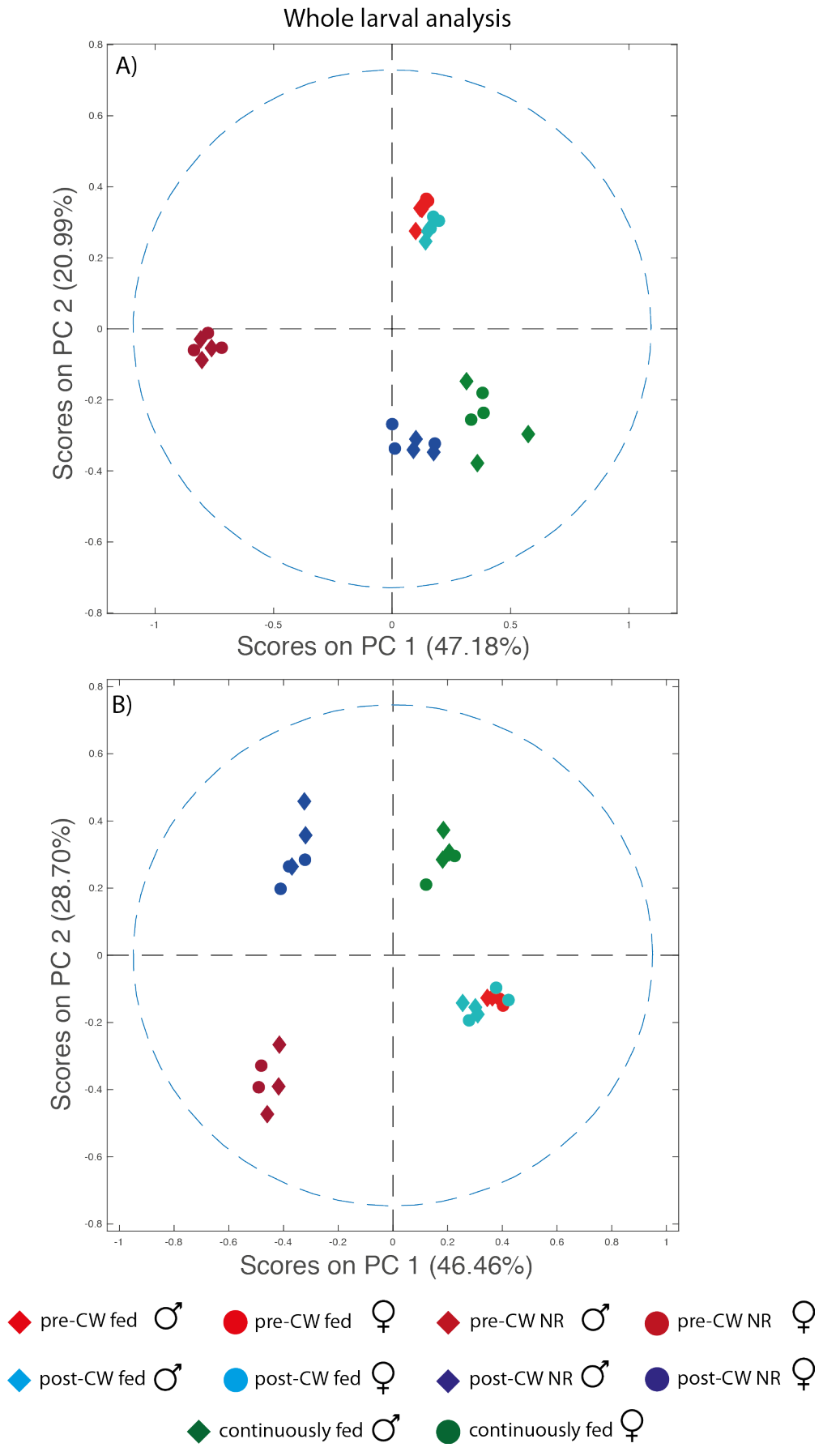
Whole larval analysis
A)
Scores on PC 2 (20.99%)
Scores on PC 1 (47.18%)
B)
Scores on PC 2 (28.70%)
Scores on PC 1 (46.46%)
pre-CW fed ♂
pre-CW fed ♀
pre-CW NR ♂
pre-CW NR ♀
post-CW fed ♂
post-CW fed ♀
post-CW NR ♂
post-CW NR ♀
continuously fed ♂
continuously fed ♀

Figure 4-4: PCA scores plots for whole larval polar metabolome NMR spectra.

PCA scores plots for the NMR spectra from the first (A) and second (B) independent experiments conducted to analyse the polar metabolites in whole larvae. Diamonds and circles represent male and female samples respectively. Each symbol represents a single “opened” whole larval NMR spectrum. Red symbols: pre-CW fed samples. Dark red: pre-CW NR samples. Blue symbols: post-CW fed samples. Dark blue symbols: post-CW NR samples. Green: continuously fed samples. Each condition was collected in triplicate, with the exception, for B only, of continuously fed and pre-CW NR females, which were collected in duplicate.

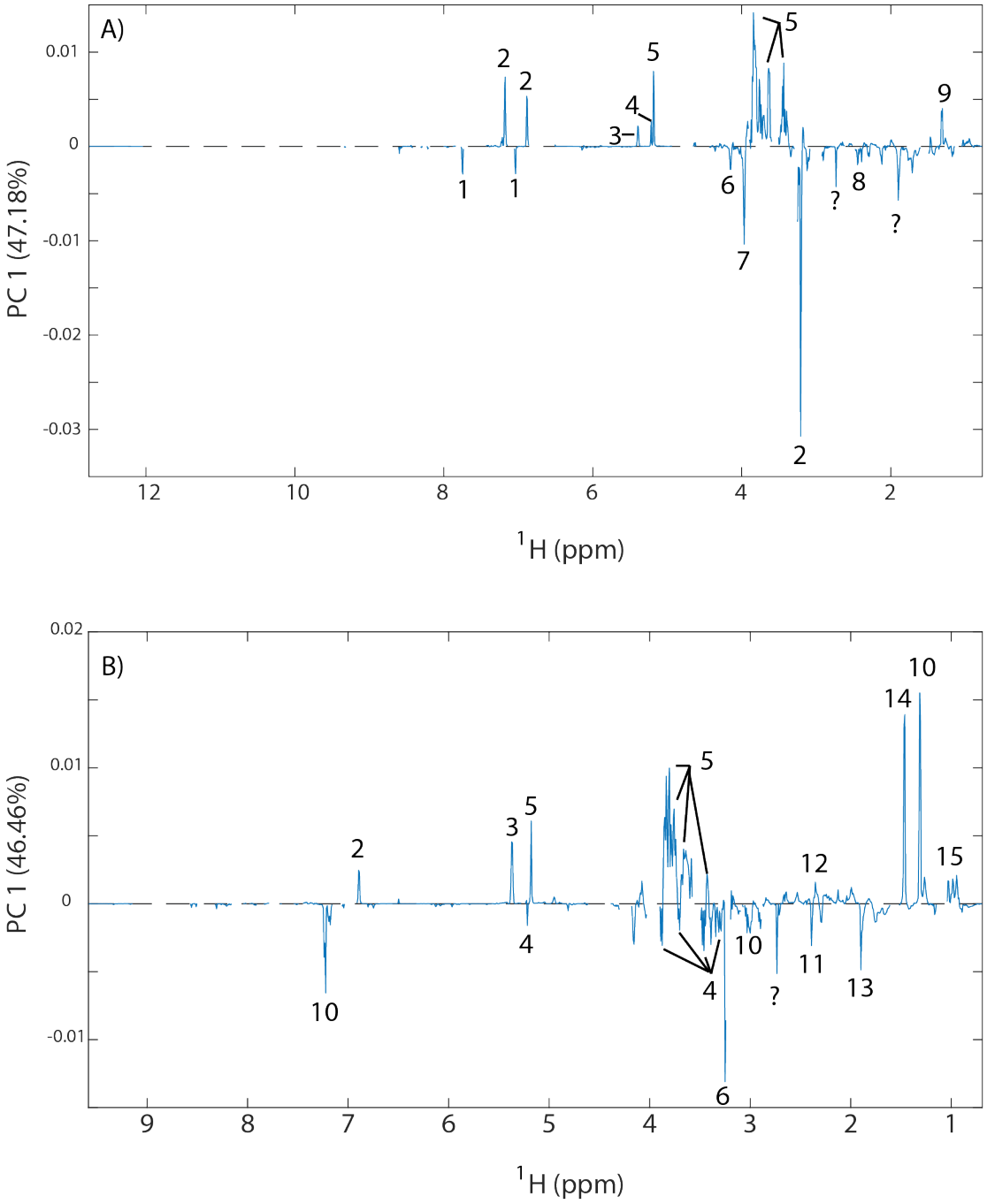

1: His; 2: Tyr; 3: maltose; 4: glucose; 5: trehalose; 6: Pro; 7: OPE; 8: Gln; 9: Thr; 10: OPT; 11: succinate; 12: Glu; 13: acetate; 14: Ala; 15: Val

Figure 4-5: PCA loadings plots for whole larval polar metabolome NMR spectra.

PCA loadings plots for the NMR spectra from the first (A) and second (B) independent experiments conducted to analyse the polar metabolites in whole larval samples. Each condition was collected in, at least, triplicate. Numbered loadings correspond to resonances in the recorded NMR spectra that, in turn, correspond to the resonances for: histidine (1); tyrosine (2); maltose (3); glucose (4); trehalose (5); proline (6); O-phosphoethanomine (7); glutamine (8); threonine (9); O-phosphotyrosine (10); succinate (11); glucose (12); acetate (13); alanine (14) and valine (15).

VDTS was used to determine the volume of hemolymph recovered following cuticle rupture (Appendix: Table 6). With the exception of NR larvae, recovered hemolymph volumes roughly track the larval body mass; a greater amount of hemolymph was recovered from continuously fed larvae (males: ~1.5 mg, 364 ± 88 nL, females: ~1.8 mg, 698 ± 100 nL) in comparison to post-CW fed larvae (males: ~1.1 mg, 292 ± 11 nL, females: ~1.4 mg, 506 ± 83 nL), which in turn yield larger recovered volumes in comparison to pre-CW fed larvae (males: ~0.6 mg, 182 ± 49 nL, females: ~0.7 mg, 312 ± 81 nL). On the basis of the measured volumes, an increase in mass of 1 mg is roughly proportional to a ~300-400 nL increase in hemolymph. Alongside similar determined metabolite concentrations for continuously fed larvae, the released hemolymph volumes determined here for male and female continuously fed larvae are also consistent with those reported by Ragan et al., (2013) (fed males: 406 ± 34 nL and fed females: 692 ± 75 nL). However, released hemolymph volumes for post-CW NR larvae reported here, are larger, by ~1.6-2.0 fold (post-CW NR males: ~0.8 mg, 456 ± 151 nL; females: ~1.0 mg, 368 ± 1 nL), than those reported previously (NR males: 234 ± 57 nL and NR females: 227 ± 64 nL). Interestingly, even though pre-CW NR larvae are ~1.5 fold smaller than post-CW NR larvae, the volume of hemolymph recovered from pre-CW NR larvae is larger than from post-CW NR larvae. Therefore, in my hands, it appears that NR may ease the “escape” of hemolymph from larvae, thus observed as greater recovered hemolymph volumes, in comparison to their fed counterparts.

Absolute metabolite concentrations were determined from the pre- and post-CW samples for hemolymph and whole larvae NMR spectra by fitting metabolite reference spectra as described above (see Materials and Methods: 2.6). The reference spectra database provided by *Chenomx NMR Suite* was supplemented with a 1D ^{1}H NMR reference spectrum created by Dr T.J Ragan for OPT because a reference spectrum for OPT is absent from all metabolite databases examined to date. OPT is, however, a major component of the hemolymph (Table 3) and its presence has been previously observed in *Drosophila* although its function is not yet clear (Mitchell and Lunan, 1964). As indicated by the PCA loadings for the hemolymph samples, OPT, trehalose, O-phosphocholine and glycine were all significantly different between pre- and post-CW NR samples.

Metabolites	pre-CW fed concentartion (mM)		post-CW fed concentartion (mM)		pre-CW NR concentartion (mM)		post-CW NR concentartion (mM)		continously fed concentartion (mM)	
	male	female	male	female	male	female	male	female	male	female
alanine	10.02 ± 2.29	8.70 ± 5.50	9.13 ± 4.18	10.57 ± 6.09	**1.46 ± 0.21**^{a}	**1.31 ± 0.28**^{b}	**2.79 ± 1.16**^{a}	**2.23 ± 0.56**^{b}	5.34 ± 1.91	5.41 ± 1.52
arginine	0.47 ± 0.11	0.41 ± 0.18	0.57 ± 0.23	0.64 ± 0.29	0.52 ± 0.11	0.59 ± 0.20	0.53 ± 0.18	0.42 ± 0.07	1.03 ± 0.52	0.79 ± 0.11
betaine	0.99 ± 0.25	0.75 ± 0.38	0.93 ± 0.17	1.06 ± 0.40	**0.39 ± 0.08**^{a}	**0.35 ± 0.07**^{b}	**0.06 ± 0.03**^{a}	**0.09 ± 0.05**^{b}	0.11 ± 0.03	0.12 ± 0.02
dimethylamine	0.03 ± 0.01	0.03 ± 0.01	0.04 ± 0.01	0.03 ± 0.01	0.11 ± 0.08	0.10 ± 0.07	0.19 ± 0.13	0.18 ± 0.12	0.17 ± 0.15	0.11 ± 0.07
fumarate	0.42 ± 0.11	0.36 ± 0.18	0.34 ± 0.09	0.37 ± 0.14	0.10 ± 0.02	0.09 ± 0.02	0.18 ± 0.06	0.15 ± 0.04	0.25 ± 0.07	0.24 ± 0.03
glucose	1.44 ± 0.87	1.37 ± 0.38	0.90 ± 0.39	1.23 ± 0.76	0.00 ± 0.00	0.00 ± 0.00	0.00 ± 0.00	0.00 ± 0.00	0.62 ± 0.28	0.55 ± 0.17
glutamine	3.24 ± 1.02	2.60 ± 1.98	3.22 ± 2.05	4.03 ± 2.15	2.57 ± 1.24	2.29 ± 0.53	2.97 ± 1.00	3.43 ± 1.70	8.81 ± 4.49	7.50 ± 1.97
glycine	1.26 ± 0.43	1.18 ± 0.88	1.35 ± 1.02	1.74 ± 1.19	**2.47 ± 0.27**^{a}	**2.37 ± 0.58**^{b}	**1.03 ± 0.31**^{a}	**1.19 ± 0.66**^{b}	2.22 ± 0.77	2.08 ± 0.27
histidine	1.04 ± 0.23	0.80 ± 0.41	0.97 ± 0.48	1.25 ± 0.69	**1.64 ± 0.10**^{a}	1.67 ± 0.35	**0.96 ± 0.28**^{a}	1.13 ± 0.42	1.03 ± 0.26	0.96 ± 0.25
isoleucine	0.73 ± 0.18	0.51 ± 0.24	0.45 ± 0.24	0.51 ± 0.29	**0.09 ± 0.01**^{a}	**0.09 ± 0.02**^{b}	**0.37 ± 0.10**^{a}	**0.35 ± 0.09**^{b}	0.66 ± 0.27	0.62 ± 0.11
leucine	1.21 ± 0.31	0.88 ± 0.38	0.76 ± 0.36	0.85 ± 0.47	**0.15 ± 0.02**^{a}	**0.15 ± 0.03**^{b}	**0.48 ± 0.16**^{a}	**0.43 ± 0.17**^{b}	1.04 ± 0.43	0.92 ± 0.29
lysine	2.14 ± 0.69	1.51 ± 0.58	2.55 ± 1.66	2.81 ± 1.36	2.00 ± 0.32	2.23 ± 0.38	1.54 ± 0.37	1.30 ± 0.46	2.45 ± 1.26	2.64 ± 1.35
malate	1.53 ± 0.43	1.28 ± 0.47	1.30 ± 0.37	1.44 ± 0.19	0.72 ± 0.20	0.64 ± 0.12	1.04 ± 0.38	0.80 ± 0.21	0.65 ± 0.19	0.73 ± 0.09
methionine	0.16 ± 0.06	0.11 ± 0.05	0.11 ± 0.06	0.16 ± 0.09	0.08 ± 0.02	0.07 ± 0.01	0.11 ± 0.04	0.12 ± 0.05	0.07 ± 0.02	0.07 ± 0.01
O-phosphocholine	0.66 ± 0.15	0.45 ± 0.20	0.78 ± 0.59	0.68 ± 0.54	**1.24 ± 0.13**^{a}	**1.19 ± 0.30**^{b}	**3.11 ± 1.18**^{a}	**2.80 ± 1.21**^{b}	1.23 ± 0.34	0.97 ± 0.13
O-phosphoethanolamine	1.57 ± 0.54	1.49 ± 0.67	1.42 ± 0.40	1.36 ± 0.52	**5.41 ± 0.52**^{a}	**5.66 ± 1.15**^{b}	**1.13 ± 0.57**^{a}	**1.80 ± 1.07**^{b}	0.47 ± 0.42	0.34 ± 0.13
O-phosphotyrosine	13.81 ± 3.42	9.68 ± 4.37	17.86 ± 10.34	17.21 ± 10.21	**5.76 ± 1.51**^{a}	**5.66 ± 1.11**^{b}	**38.39 ± 12.21**^{a}	**33.81 ± 11.80**^{b}	68.08 ± 29.35	49.86 ± 4.92
phenylalanine	0.20 ± 0.05	0.15 ± 0.06	0.16 ± 0.11	0.17 ± 0.11	**0.00 ± 0.00**^{a}	**0.00 ± 0.00**^{b}	**0.16 ± 0.05**^{a}	**0.14 ± 0.04**^{b}	0.31 ± 0.15	0.27 ± 0.06
proline	2.20 ± 0.45	1.57 ± 0.70	2.16 ± 0.77	1.94 ± 0.65	**0.51 ± 0.08**^{a}	**0.50 ± 0.12**^{b}	**1.64 ± 0.33**^{a}	**1.29 ± 0.36**^{b}	4.30 ± 2.53	3.28 ± 1.14
sarcosine	0.32 ± 0.10	0.22 ± 0.17	0.26 ± 0.11	0.20 ± 0.11	**0.15 ± 0.03**^{a}	**0.13 ± 0.03**^{b}	**0.07 ± 0.02**^{a}	**0.03 ± 0.02**^{b}	**0.24 ± 0.09**^{c}	**0.11 ± 0.02**^{c}
succinate	0.78 ± 0.24	0.73 ± 0.37	0.65 ± 0.20	0.66 ± 0.26	**0.36 ± 0.03**^{a}	**0.31 ± 0.03**^{b}	**0.71 ± 0.17**^{a}	**0.65 ± 0.20**^{b}	0.79 ± 0.21	0.74 ± 0.12
trehalose	27.39 ± 5.14	22.94 ± 11.08	25.44 ± 9.91	24.37 ± 11.35	**5.60 ± 1.46**^{a}	**4.79 ± 1.68**^{b}	**41.14 ± 14.51**^{a}	**37.02 ± 12.56**^{b}	63.31 ± 21.36	43.48 ± 3.49
tyrosine	0.89 ± 0.27	0.65 ± 0.40	0.82 ± 0.53	0.83 ± 0.58	**0.38 ± 0.07**^{a}	**0.34 ± 0.08**^{b}	**2.66 ± 0.49**^{a}	**2.17 ± 0.64**^{b}	4.32 ± 1.89	2.95 ± 0.37
valine	1.96 ± 0.45	1.44 ± 0.83	1.36 ± 0.57	1.46 ± 0.77	**0.28 ± 0.02**^{a}	**0.27 ± 0.06**^{b}	**0.79 ± 0.18**^{a}	**0.78 ± 0.23**^{b}	1.73 ± 0.71	1.59 ± 0.37
β-alanine	0.81 ± 0.15	0.61 ± 0.27	0.80 ± 0.18	0.77 ± 0.30	0.22 ± 0.05	0.22 ± 0.04	0.32 ± 0.08	0.32 ± 0.07	0.58 ± 0.25	0.43 ± 0.09

Table 3: Hemolymph metabolite concentrations.

Entries show mean concentration ± 1 standard deviation for two independent experiments, each with three biological replicates. Bold figures indicate statistically significant ($p \leq 0.01$) differences between:

pre-CW NR males and post-CW NR males[a]

pre-CW NR females and post-CW NR females[b]

male and female continuously fed larvae[c].

Statistical significance is determined according to Tukey's HSD test in a 2-way ANOVA.

For the hemolymph NMR spectra, a total of 25 polar metabolites were unambiguously identified and the absolute concentrations of these were determined according to the VDTS procedure (Table 3). As mentioned in the preceding chapter, and consistent with the unsupervised PCA, the concentrations of the majority of identified metabolites were not significantly different between continuously fed males and females (Table 3). However, consistent with their larger body mass, greater hemolymph volumes were extracted from females than males, indicating that the total amount of each metabolite is likely to be greater in female hemolymph than for males (Appendix: Table 6). Only sarcosine was at a significant higher (~2.2 fold, $p < 0.0003$) concentration in the hemolymph of continuously fed males compared to females. Moreover, none of the 25 metabolites were significantly different ($p \leq 0.01$) between the pre- and post-CW fed hemolymph metabolomes. In contrast, 15 of the 25 metabolites displayed significantly ($p \leq 0.01$) different concentrations between pre- and post-CW NR hemolymph metabolomes in both males and females (Figure 4-6). Sarcosine (~3 fold), glycine (~2 fold), betaine (~5 fold) and O-phosphoethanolamine (OPE, ~4 fold) were all at a significantly higher concentration in pre-CW NR larvae. On the other hand, phenylalanine (from undetectable to 0.2 mM), valine (~3 fold), proline (~3 fold), isoleucine (~4 fold), leucine (~3 fold), succinate (~2 fold), alanine (~2 fold), O-phosphocholine (OPC, ~2 fold), trehalose (~8 fold), tyrosine (~7 fold) and OPT (~6 fold) were all present at a significantly higher concentration in post-CW NR larvae. Therefore, again consistent with the PCA outcome, the results of the metabolite-by-metabolite VDTS analysis shows that the attainment of CW correlates with significant alterations in the absolute concentrations of many larval hemolymph metabolites during NR but not fed conditions.

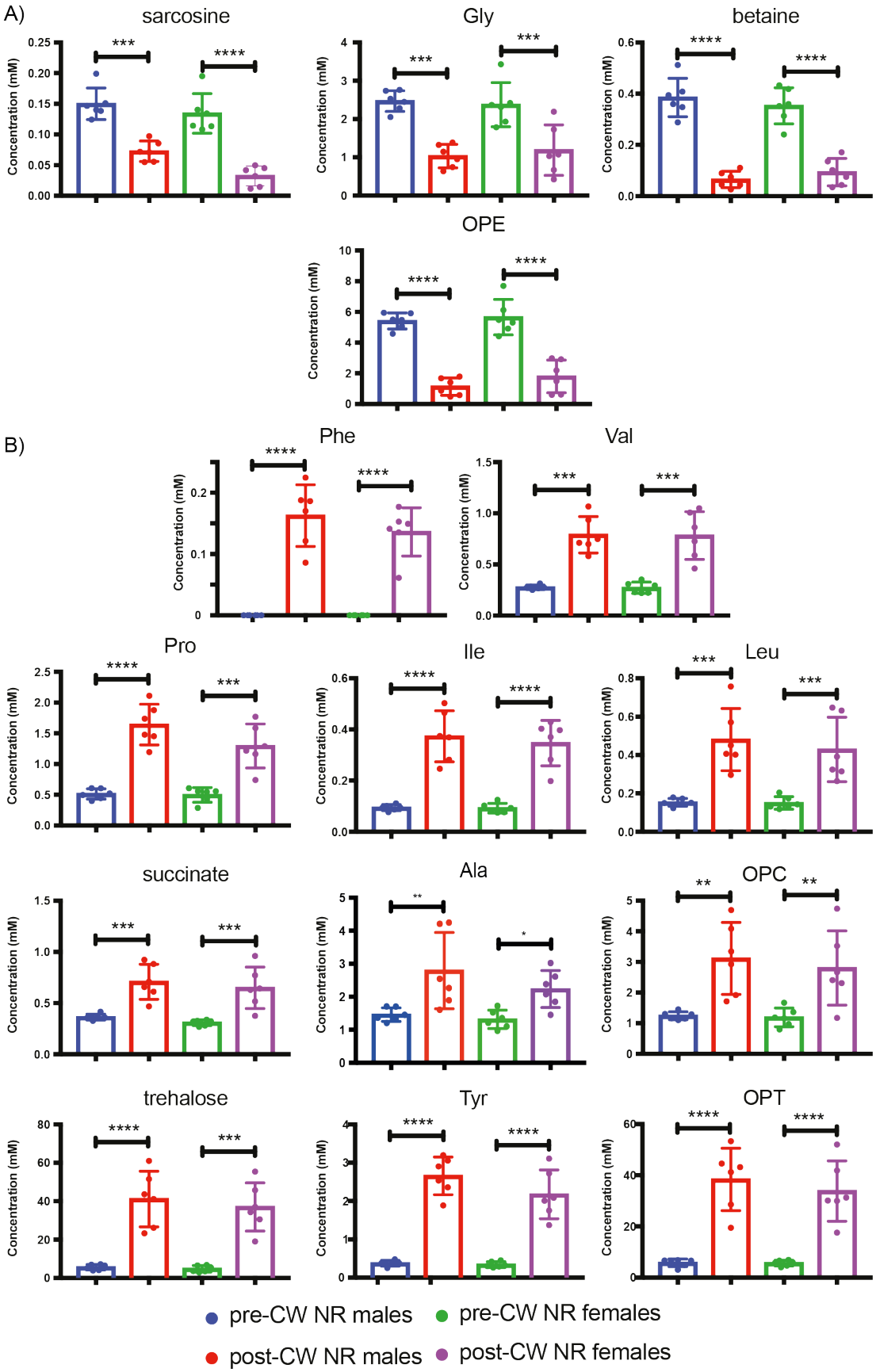
A)
sarcosine
Gly
betaine
OPE
B)
Phe
Val
Pro
Ile
Leu
succinate
Ala
OPC
trehalose
Tyr
OPT
Concentration (mM)
pre-CW NR males
pre-CW NR females
post-CW NR males
post-CW NR females

Figure 4-6: Hemolymph metabolite concentrations in pre- and post-CW NR larvae.

Comparison of absolute hemolymph metabolite concentrations, determined via VDTS, for the 15 metabolites that were statistically significantly different in concentration between pre-CW NR and post-CW NR larval NMR samples. A) Metabolites that were significantly higher in pre-CW NR larvae in comparison to post-CW NR larvae. B) Metabolites that were significantly higher in post-CW NR larvae in comparison to pre-CW NR larvae. Each condition was composed of six replicates (three each from two independent experiments). Statistical significance was determined according to Tukey's HSD test in a 2-way ANOVA with an alpha-value of 1%. Gly: glycine; Phe: phenylalanine; Val: valine; Pro: proline; Ile: isoleucine; Leu: leucine; and Tyr: tyrosine. **: p-value $\leq$ 0.01; ***: p-value $\leq$ 0.001; and ****: p-value: $\leq$ 0.0001.

VDTS was used to determine the liquid volume recovered after whole larval homogenisation (Appendix: Table 7). Consistent with recovered hemolymph values, recovered larval tissue volumes after homogenisation track larval body mass. It appears a 1 mg increase in mass, equates to a ~0.5 μL increase in homogenate volume recovered.

For the whole larval NMR spectra, 26 metabolites could be unambiguously identified (Table 4). In addition to the 25 metabolites identified in hemolymph spectra, the resonances for glutamate were now clearly observable in whole larval NMR spectra. In contrast to the situation for hemolymph, following VDTS analysis, some sex-specific differences in whole larval metabolite concentrations were observed. Whereas, none of the 25 metabolites were significantly different ($p \leq 0.01$) between males and females in the pre- and post-CW hemolymph metabolomes (fed or NR), 8 metabolites were found to have significantly ($p \leq 0.01$) different concentrations between males and females for the whole larva spectra. Hence, glutamate (~1.7 fold, $p < 0.003$), glutamine (~1.6 fold, $p < 0.01$), histidine (~1.4 fold, $p < 0.01$), leucine (~1.7 fold, $p < 0.01$), valine (~1.5 fold, $p < 0.01$) and β-alanine (~1.7 fold, $p < 0.002$) were significantly higher in post-CW NR females than males. Furthermore, betaine (~1.6 fold, $p < 0.003$) and sarcosine (~1.7 fold, $p < 0.002$) are significantly higher in pre-CW fed males than females.

Metabolite	pre-CW fed concentration (mM)		post-CW fed concentration (mM)		pre-CW NR concentration (mM)		post-CW NR concentration (mM)		continously fed concentration (mM)	
	male	female	male	female	male	female	male	female	male	female
alanine	8.49 ± 1.32	6.02 ± 4.48	8.89 ± 2.22	6.86 ± 2.39	2.83 ± 0.95	2.24 ± 0.93	2.86 ± 1.08	3.68 ± 2.04	7.61 ± 2.22	5.92 ± 0.97
arginine	4.16 ± 0.92	3.22 ± 1.60	3.45 ± 1.00	3.22 ± 1.09	2.14 ± 1.40	**2.03 ± 1.31**^{f}	3.10 ± 0.76	**4.97 ± 2.26**^{h}	5.53 ± 1.50	5.15 ± 0.66
betaine	**2.22 ± 0.34**^{a}	1.42 ± 0.27	**1.32 ± 0.45**^{c}	1.28 ± 0.51	**0.46 ± 0.17**^{e}	**0.43 ± 0.15**^{f}	**0.12 ± 0.07**^{g}	**0.18 ± 0.15**^{h}	0.31 ± 0.09	0.31 ± 0.03
dimethylamine	**0.04 ± 0.01**^{a}	**0.03 ± 0.01**^{b}	**0.02 ± 0.00**^{c}	**0.02 ± 0.01**^{d}	**0.02 ± 0.01**^{e}	**0.02 ± 0.01**^{f}	**0.01 ± 0.00**^{g}	**0.02 ± 0.01**^{h}	0.02 ± 0.01	0.02 ± 0.01
fumarate	**0.41 ± 0.01**^{a}	0.33 ± 0.15	**0.25 ± 0.04**^{c}	0.26 ± 0.08	**0.07 ± 0.06**^{e}	**0.06 ± 0.04**^{f}	**0.16 ± 0.05**^{g}	**0.23 ± 0.10**^{h}	0.46 ± 0.13	0.41 ± 0.05
glucose	**8.49 ± 1.35**^{a}	5.81 ± 2.04	**4.83 ± 2.19**^{c}	4.89 ± 2.18	**7.36 ± 4.47**^{e}	5.60 ± 3.78	**3.49 ± 0.90**^{g}	4.70 ± 1.51	5.50 ± 0.87	5.49 ± 0.78
glutamate	13.49 ± 3.13	9.46 ± 4.18	9.48 ± 2.59	9.51 ± 3.27	2.70 ± 0.95	**2.22 ± 0.78**^{f}	4.04 ± 0.48	**6.72 ± 2.40**^{h}	9.41 ± 2.79	8.33 ± 0.87
glutamine	8.56 ± 2.92	7.76 ± 4.09	8.77 ± 2.13	8.78 ± 2.93	2.88 ± 0.85	**2.65 ± 0.88**^{f}	2.77 ± 0.78	**4.46 ± 1.51**^{h}	8.83 ± 3.07	8.34 ± 2.09
glycine	1.96 ± 0.72	1.73 ± 1.22	1.91 ± 0.21	1.81 ± 0.59	**2.12 ± 0.52**^{e}	**2.01 ± 0.37**^{f}	**0.76 ± 0.38**^{g}	**1.06 ± 0.46**^{h}	2.10 ± 0.99	1.73 ± 0.37
histidine	4.36 ± 1.87	3.71 ± 2.39	2.88 ± 0.59	2.75 ± 0.93	**1.97 ± 0.38**^{e}	**1.89 ± 0.13**^{f}	**0.97 ± 0.26**^{g}	**1.26 ± 0.30**^{h}	1.34 ± 0.39	1.31 ± 0.41
isoleucine	0.36 ± 0.04	0.30 ± 0.22	0.27 ± 0.11	0.26 ± 0.09	0.18 ± 0.06	0.16 ± 0.04	0.28 ± 0.09	0.45 ± 0.21	0.48 ± 0.19	0.38 ± 0.09
leucine	0.82 ± 0.09	0.62 ± 0.40	0.61 ± 0.20	0.54 ± 0.17	0.36 ± 0.13	0.31 ± 0.09	0.51 ± 0.13	0.85 ± 0.38	0.99 ± 0.26	0.88 ± 0.14
lysine	2.88 ± 1.05	2.41 ± 1.48	2.88 ± 0.27	3.03 ± 1.05	1.81 ± 0.47	1.84 ± 0.37	1.22 ± 0.33	1.87 ± 0.72	2.19 ± 0.67	2.18 ± 0.49
malate	**5.23 ± 1.71**^{a}	4.28 ± 2.00	**3.30 ± 0.75**^{c}	3.34 ± 1.30	**0.83 ± 0.69**^{e}	**0.82 ± 0.67**^{f}	**2.36 ± 0.96**^{g}	**3.04 ± 1.53**^{h}	5.47 ± 1.91	4.80 ± 0.73
methionine	0.42 ± 0.15	0.38 ± 0.23	0.25 ± 0.09	0.27 ± 0.16	**0.07 ± 0.03**^{e}	**0.09 ± 0.05**^{f}	**0.23 ± 0.09**^{g}	**0.28 ± 0.16**^{h}	0.63 ± 0.13	0.67 ± 0.08
O-phosphocholine	1.74 ± 0.62	1.52 ± 0.86	1.76 ± 0.44	1.44 ± 0.50	2.41 ± 0.48	**2.09 ± 0.62**^{f}	3.12 ± 1.04	**4.57 ± 1.93**^{h}	0.93 ± 0.36	0.65 ± 0.20
O-phosphoethanolamine	**3.13 ± 1.18**^{a}	2.48 ± 1.68	**1.77 ± 0.39**^{c}	1.45 ± 0.38	**4.59 ± 1.12**^{e}	**4.15 ± 0.54**^{f}	**1.24 ± 0.36**^{g}	**1.81 ± 0.84**^{h}	1.38 ± 0.52	1.14 ± 0.15
O-phosphotyrosine	**5.87 ± 1.01**^{a}	**4.35 ± 1.43**^{b}	**11.77 ± 1.27**^{c}	**12.27 ± 1.90**^{d}	**4.52 ± 1.00**^{e}	**4.19 ± 1.41**^{f}	**8.69 ± 3.81**^{g}	**9.64 ± 4.30**^{h}	3.07 ± 1.43	1.87 ± 1.18
phenylalanine	0.17 ± 0.03	0.22 ± 0.22	0.18 ± 0.04	0.21 ± 0.05	**0.07 ± 0.02**^{e}	**0.05 ± 0.03**^{f}	**0.18 ± 0.05**^{g}	**0.31 ± 0.16**^{h}	0.48 ± 0.15	0.50 ± 0.12
proline	4.32 ± 0.85	**3.34 ± 1.26**^{b}	4.73 ± 0.83	**4.84 ± 1.72**^{d}	**0.56 ± 0.14**^{e}	**0.60 ± 0.19**^{f}	**2.02 ± 0.71**^{g}	**2.64 ± 1.44**^{h}	6.24 ± 2.52	5.39 ± 0.97
sarcosine	**0.53 ± 0.11**^{a}	**0.32 ± 0.15**^{b}	**0.29 ± 0.03**^{c}	**0.15 ± 0.05**^{d}	0.09 ± 0.09	0.08 ± 0.07	0.04 ± 0.02	0.03 ± 0.02	**0.25 ± 0.04**	**0.15 ± 0.02**^{i}
succinate	0.91 ± 0.24	0.73 ± 0.49	0.65 ± 0.13	0.63 ± 0.19	0.54 ± 0.23	0.48 ± 0.28	0.56 ± 0.30	0.83 ± 0.51	2.37 ± 1.15	2.19 ± 0.86
trehalose	24.23 ± 4.00	19.53 ± 7.75	21.52 ± 3.74	18.79 ± 6.65	**1.43 ± 1.49**^{e}	**1.88 ± 2.50**^{f}	**20.81 ± 7.27**^{g}	**29.92 ± 15.06**^{h}	41.21 ± 11.37	36.02 ± 5.67
tyrosine	3.28 ± 0.85	**2.36 ± 1.29**^{b}	3.99 ± 1.26	**4.04 ± 1.57**^{d}	**0.73 ± 0.45**^{e}	**0.67 ± 0.50**^{f}	**8.95 ± 2.58**^{g}	**14.20 ± 7.51**^{h}	19.85 ± 3.55	18.61 ± 2.28
valine	1.51 ± 0.21	1.04 ± 0.69	1.18 ± 0.24	0.87 ± 0.29	0.44 ± 0.11	**0.39 ± 0.10**^{f}	0.64 ± 0.16	**0.99 ± 0.39**^{h}	1.44 ± 0.45	1.18 ± 0.25
β-alanine	1.59 ± 0.46	1.14 ± 0.55	2.08 ± 0.69	1.69 ± 0.66	**0.31 ± 0.08**^{e}	**0.32 ± 0.07**^{f}	**0.77 ± 0.18**^{g}	**1.29 ± 0.45**^{h}	2.07 ± 0.49	1.86 ± 0.26

Table 4: Whole larval metabolite concentrations.

Entries show mean concentration ± 1 standard deviation for two independent experiments, each with three biological replicates. Bold figures indicate statistically significant ($p \leq 0.01$) differences between:

pre-CW fed males and post-CW fed males[a]

pre-CW fed females and post-CW fed females[b]

pre-CW NR males and post-CW NR males[c]

pre-CW NR females and post-CW NR females[d].

male and female continuously fed larvae[e].

Statistical significance is determined according to Tukey's HSD test in a 2-way ANOVA.

Overall, these findings demonstrate that although body tissue metabolite concentrations may vary dependent on sex, hemolymph metabolite levels are tightly regulated to nullify major differences between the sexes. Interestingly, although such a sexually dimorphic difference is observed in post-CW NR whole larval metabolites, in continuously fed larvae, only sarcosine (~2 fold, $p < 0.0003$) was observed to be significantly different between males and females. The absence of a sexually dimorphic difference in whole larvae concentrations in fed compared to NR larvae is worthy of further investigation but, at present, I cannot rule out that NMR signals originating from food in the gut of fed and not NR larvae, masks sex-specific differences. In others words, as food is not present in the gut of NR larvae, the NMR spectra may more faithfully reflect the body tissue metabolome than in the case of fed animals.

Comparing fed larvae pre- and post-CW, the absolute concentrations of only three of the 26 identified metabolites were significantly ($p \leq 0.01$) different in both males and females: dimethylamine ($p < 0.008$), sarcosine ($p < 0.0005$) and OPT ($p < 0.0006$). OPT was ~2.2 fold higher in post-CW fed larvae whereas dimethylamine and sarcosine were both significantly lower by ~1.8 and ~1.9 fold respectively in post-CW fed larvae. In contrast, a much larger number of the identified metabolites (13 of 26) were significantly different ($p \leq 0.01$) between pre- and post-CW in NR than fed larvae (Figure 4-7). Histidine (~2.1 fold), glycine (~2.3 fold), OPE (~2.9 fold) and betaine (~3 fold) were all significantly lower in NR larvae after CW. Whilst, OPT (~2.3 fold), fumarate (~3 fold), malate (~3.3. fold), β-alanine (~3.3. fold), methionine (~3.4 fold), proline (~4 fold) phenylalanine (~4 fold), trehalose (~15.3 fold) and tyrosine (~16.5 fold), are all significantly higher in NR larvae after CW. Therefore, the attainment of CW has a more dramatic effect on whole larval metabolite concentrations during NR than during fed conditions. This conclusion about the whole larval metabolites concentrations is broadly similar to that arrived at for hemolymph concentrations, although there are clear differences in which metabolites are most affected in the two larval compartments, if the assumption is made that the whole larval concentrations generally represent the body tissue over the hemolymph.

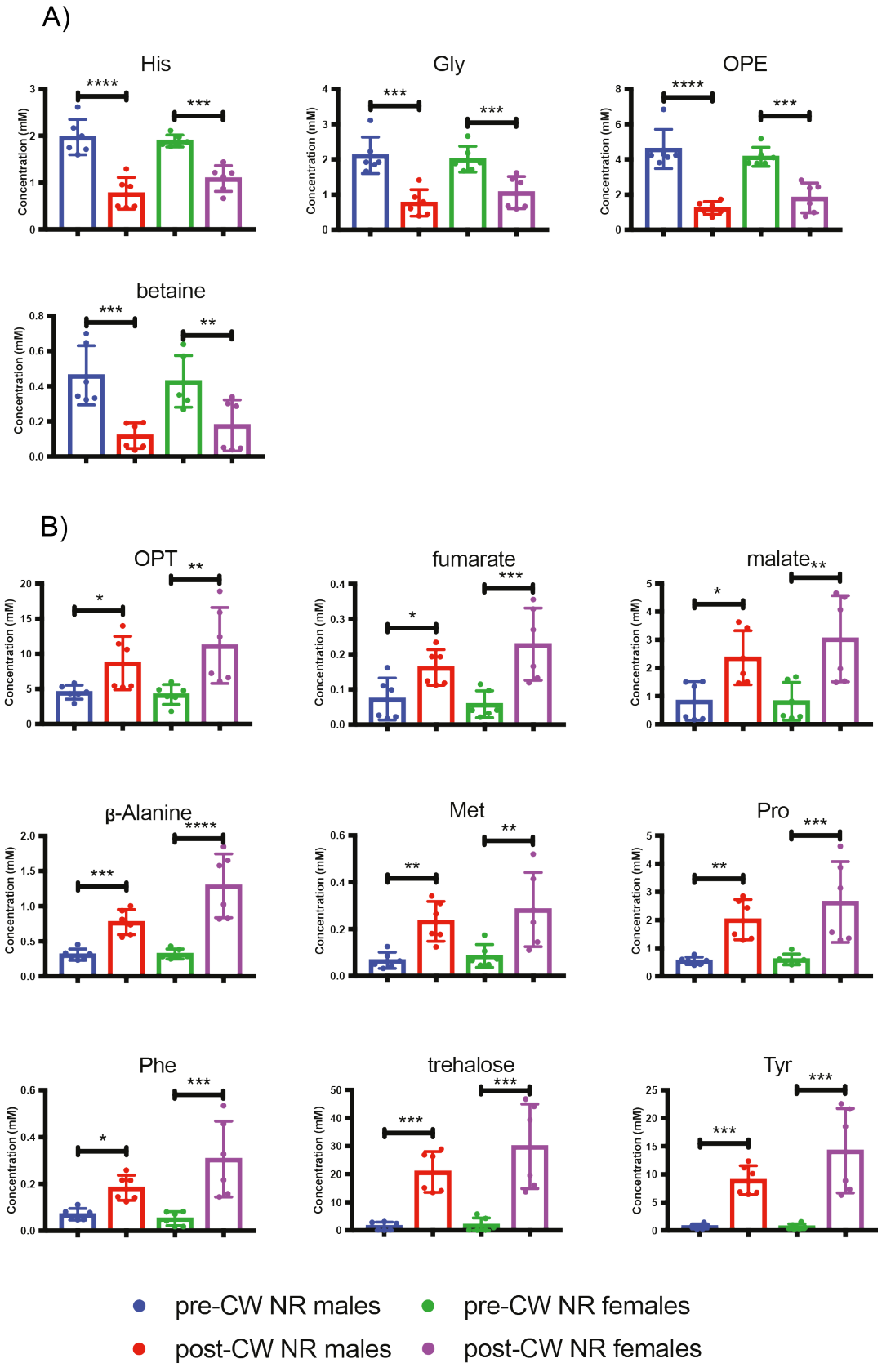
A)
His
Gly
OPE
betaine
B)
OPT
fumarate
malate
β-Alanine
Met
Pro
Phe
trehalose
Tyr
Concentration (mM)
pre-CW NR males
pre-CW NR females
post-CW NR males
post-CW NR females

Figure 4-7: Whole larval metabolite concentrations in pre- and post-CW NR larvae.

Comparison of absolute whole larval metabolite concentrations determined via VDTS that were statistically significantly different between pre-CW NR and post-CW NR larvae. A) Metabolites that were significantly higher in pre-CW NR larvae in comparison to post-CW NR larvae. B) Metabolites that were significantly higher in post-CW NR larvae in comparison to pre-CW NR larvae. Each condition was assessed using six replicates (three each from two independent experiments). Statistical significance was determined according to Tukey's HSD test in a 2-way ANOVA. His: histidine; Gly: glycine; Met: methionine; Pro: proline; Phe: phenyalanine; and Tyr: tyrosine. *: p-value $\leq$ 0.05; **: p-value $\leq$ 0.01; ***: p-value $\leq$ 0.001; and ****: p-value: $\leq$ 0.0001.

Comparing NR larvae pre- and post-CW, proline and trehalose are at a higher concentrations in the hemolymph and the whole larva after the attainment of CW. Interestingly, this pattern is also the case for three metabolites that lie in metabolic pathways connecting to tyrosine, namely: phenylalanine, OPT and tyrosine. To visualise the trajectories of the concentration of these three metabolites in the hemolymph and also in the whole larva during development and starvation, the fold increase in their absolute concentration was plotted relative to their concentration measured at the pre-CW time point (i.e. 51 hr) (Figure 4-8). It can be observed during normal development that whole larval phenylalanine and tyrosine levels remained stable until CW is reached and then increased ~3 fold and ~7 fold respectively, whilst OPT levels slightly rose slightly in the run-up-to CW and then fall (~ 5 fold, relative to the post-CW fed time-point) as larvae approach pupariation (Figure 4-8 A, i and iv). Within the hemolymph, tyrosine and phenylalanine follow a similar trajectory to that observed in the whole larva. In contrast to its behaviour in the whole larva, the OPT level rose dramatically (~5 fold) in the hemolymph after the post-CW time point (i.e. 60 hr) (Figure 4-8 B, i and iv). When starvation was administered before the attainment of CW, the whole larval and hemolymph levels of all three of these metabolites decreased (Figure 4-8 A, ii and v and Figure 4-8 B, ii and v respectively); this is especially so for hemolymph phenylalanine levels, which drop to below the detection limit. However, when starvation was administered after CW, the trajectories of tyrosine and OPT in the whole larva and in the hemolymph, were found to resemble the situation in normal development Figure 4-8 A iii and vi, and Figure 4-8 B iii and vi). Taken together, the fold changes in OPT concentration post-CW, during NR or further feeding, follow opposing directions in the whole larva and in the hemolymph. Where OPT levels fall moderately after CW in the whole larva but rise strongly in the hemolymph. In other words, OPT can rise in the hemolymph of (post-CW) NR larvae even in the absence of exogenous dietary sources of tyrosine or its metabolites. The fall in OPT levels in the whole larva could indicate release of OPT from non-liquid tissue stores once CW is attained, subsequently resulting in a concomitant rise in hemolymph OPT.

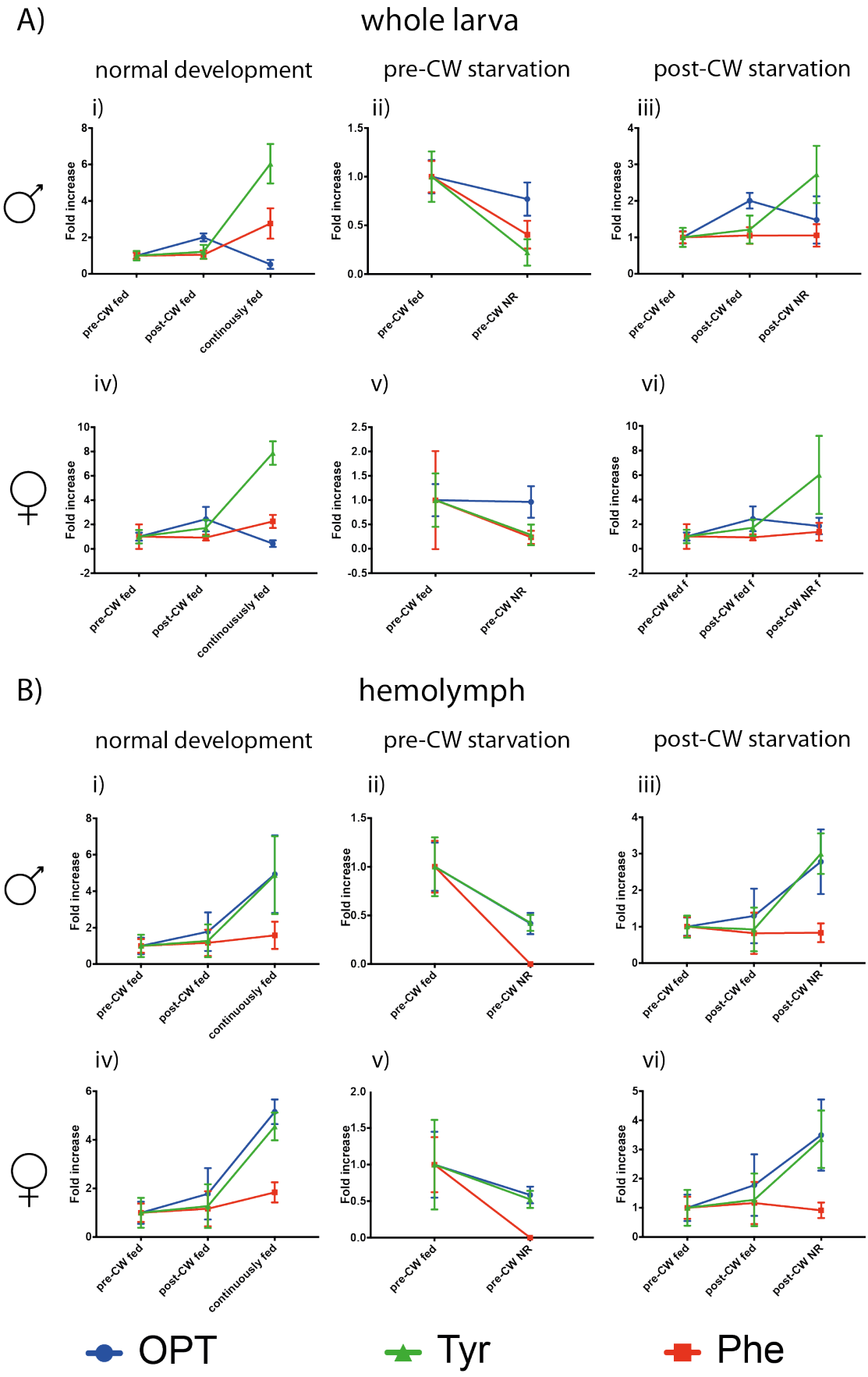
A)
whole larva
normal development
pre-CW starvation
post-CW starvation
i)
ii)
iii)
iv)
v)
vi)
Fold increase
pre-CW fed
post-CW fed
continously fed
pre-CW NR
post-CW NR
pre-CW fed f
post-CW fed f
post-CW NR f
B)
hemolymph
normal development
pre-CW starvation
post-CW starvation
continuously fed
OPT
Tyr
Phe

Figure 4-8: Fold changes in phenylalanine, tyrosine and OPT concentration.

Fold increase in the absolute metabolite concentrations in the whole larva (A) or hemolymph (B) for phenylalanine, OPT and tyrosine during normal development (i and iv), and during NR administered pre-CW (ii and v) or post-CW (iii and vi) for male (i, ii and iii) and in female (iv, v and vi) larvae. OPT: O-phosphotyrosine; Tyr: tyrosine; and Phe: phenylalanine.

4.2 Discussion

In this chapter, the refined VDTS technique (See Chapter 3) was adopted to determine absolute hemolymph and whole larval polar metabolite concentrations from male and female larvae subjected to five different fed/NR regimes (Figure 4-1). PCA was applied to unassigned NMR spectra collected under the different conditions, to assess the global structure of the data. The PCA scores plots indicated that CW attainment altered the NR but not the fed larval hemolymph and whole larval metabolomes. PCA findings were followed up by determination of the absolute concentrations of 26 unambiguously identified polar metabolites using the full VDTS analysis. Significant differences between metabolite concentrations were determined using Tukey's HSD test: a post-hoc analysis used in conjunction with a 2-way ANOVA (2-way as the two variables under consideration were gender and dietary regime – diet also encompassed developmental age, as pre-CW fed and post-CW fed were considered for this analysis as two different "diets"). Ragan et al., (2013) also used Tukey's HSD test to determine significant differences in metabolite concentrations between conditions. Therefore, a direct comparison could be made between the results reported here and those in Ragan et al.. However, unlike in Ragan et al., (2013), in this work an alpha value of 1% (instead of 5%) was selected as a more robust protection against false positive indications in the context of the multiple comparisons of the different metabolites. The likelihood of false positive discovery would be reduced from 1 in 20 to 1 in 100.

For both the hemolymph and the whole larval samples, very few metabolite concentrations were significantly different ($p \leq 0.01$) pre- and post-CW in fed animals whereas almost half of them differed for samples obtained under the NR dietary regime. Hence the attainment of CW appears to dramatically change the larval response to the onset of NR. As post-CW NR larvae go on to pupariate under NR, whereas pre-CW NR larvae arrest, metabolites that display a significantly higher concentration in NR larvae after, but not before, CW could potentially be required in order to permit developmental progression to pupariation. Alternatively, these elevated metabolite concentrations may simply be a consequence of progression to pupariation (i.e. products along pathways permitting pupariation rather than direct actors). Three tyrosine metabolites (phenylalanine, tyrosine and

OPT) were found to have significantly variant concentrations ($p \leq 0.01$) either side of CW, in both the hemolymph and in the whole larva. OPT and tyrosine levels rise in the hemolymph as normal development proceeds and this also happens during post-CW NR, indicating that internal resources, not the diet, must fuel this increase. One possibility is that OPT is stored in tissue and then released into the hemolymph, a scenario that is consistent with the observation that the OPT concentration decreases somewhat in whole larval homogenates as it increases strongly in the hemolymph. Once released from the tissues, OPT could conceivably be converted to tyrosine, by hydrolysis or phosphatase action, resulting in the concomitant rise of tyrosine in the hemolymph. Interestingly, I observe that when OPT is not “released from tissue storage”, such as during pre-CW NR, the phenylalanine level is observed to fall. Therefore, it could be suggested when tyrosine is not sufficiently generated from OPT, phenylalanine may act as a tyrosine reserve. These changing levels of tyrosine-related metabolites during development truly demonstrate how the response to starvation is affected by the attainment of CW.

In support of the hypothecated OPT released from tissue, hemolymph contains ~7% (~15 nmole/larvae) of the number of moles of OPT in the whole larva (~218 nmole/larvae) at the post-CW fed time-point and ~80% of the number of moles of OPT in the whole larva at the post-CW NR time point. Interestingly, the rise of OPT and a concomitant rise of inorganic phosphate during larval development was observed nearly 50 years ago, although it's functional significance has since remained elusive (Lunan and Mitchell, 1969; Mitchell and Lunan, 1964).

Chapter 5. A function for tyrosine in developmental timing

I showed in chapter 4.1 that post-CW larvae that are progressing towards pupariation, display a decrease in whole-body OPT and a concomitant rise in whole-body and hemolymph tyrosine. This suggested a hypothesis for progression towards pupariation involving a release of OPT from tissue stores and a subsequent conversion of released OPT into tyrosine. Before exploring the function(s) of OPT and tyrosine in developmental progression, I review the *Drosophila* literature in this area.

5.1 OPT and tyrosine in *Drosophila*

OPT was identified as a prominent constituent of *Drosophila* larvae, which rises after the second larval moult and then falls rapidly around puparium formation (Mitchell and Lunan, 1964). The majority of OPT in late L3 larvae was later observed to reside in the hemolymph and its fall at pupariation is associated with a concomitant rise in inorganic phosphate, suggestive of a phosphatase reaction (Lunan and Mitchell, 1969). To uncover where the large amount of free tyrosine generated during this process might be utilised, Lunan and Mitchell (1969) fed ^{14}C-labelled tyrosine to late L3 larvae. It could be seen from ^{14}C counts/minute/milligram of larva, that there was specific activity in the cuticle during the tanning of the early puparial case. Lunan and Mitchell (1969) therefore proposed that OPT in *Drosophila* is an inert storage form of tyrosine, ultilised to provide this amino acid for the sclerotization process. Previously, it had been documented that in another dipteran, *Calliphora,* there is a conversion of tyrosine to N-acetyldopamine, providing a precursor for sclerotization or tanning of the cuticle (Karlson and Sekeris, 1962). No OPT is observed in *Calliphora*, although the sclerotization process involves the cross linking of diphenolic compounds as it does in *Drosophila* (Sugumaran et al., 1992) (Figure 5-1). Other “tyrosine-storage” molecules have been described in other insects, such as: β-glucosyl-O-tyrosine in *Drosophila busckii*; β-alanyl-L-tyrosine in *Sarcophaga bullata*; and γ-L-glutamyl-L-phenylalanine in *Musca domestica* (Bodnaryk, 1970; Chen et al., 1978; Parker et

al., 1969). As these molecules gradually increase in the hemolymph through the larval period, peaking before a rapid decline at the white puparium stage, they have all been proposed to provide precursors for cuticle tanning. Alternatively, in the Lepidopteran: *Calpodes ethlius*, tyrosine is thought to be stored in “vacuoles” in the larval fat body, which disappear at the same time as tyrosine rises in the hemolymph prior to the moult (McDermid and Locke, 1983). The intermoult generation and disappearance of these tyrosine vacuoles suggested that they may provide the large amounts of tyrosine required to generate the phenolic compounds necessary for cuticular tanning. In summary, there is evidence that tyrosine is not only an important nutrient but that its metabolism is an important part of the process of insect cuticle sclerotization.

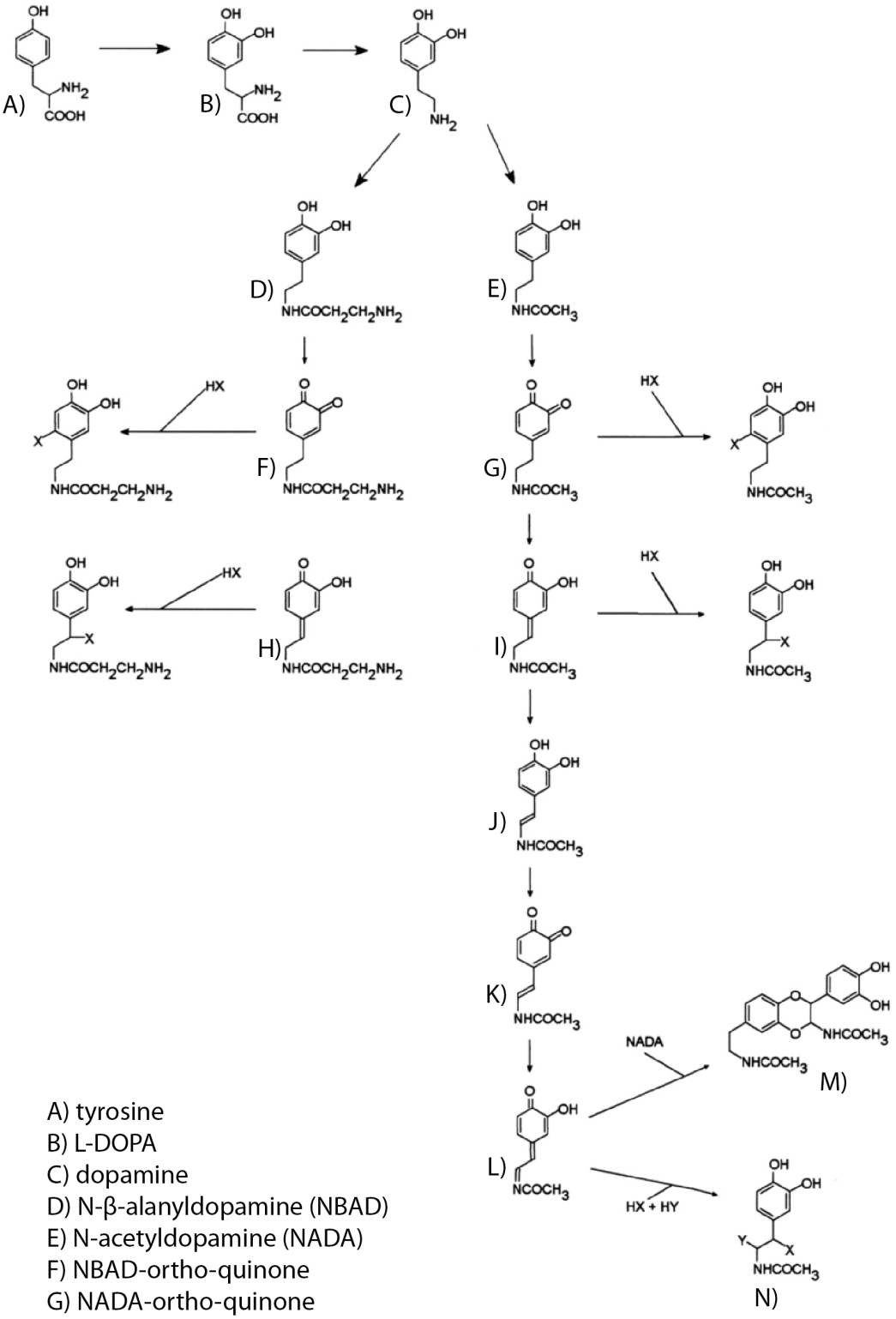

A) tyrosine
B) L-DOPA
C) dopamine
D) N-β-alanyldopamine (NBAD)
E) N-acetyldopamine (NADA)
F) NBAD-ortho-quinone
G) NADA-ortho-quinone
H) NBAD-para-quinone methide
I) NADA-para-quinone methide
J) α,β-dehydro-NADA
K) α,β-dehydro-NADA-ortho-quinone
L) α,β-dehydro-NADA-para-quinone methide

Figure 5-1: Proposed pathways for sclerotization of the insect cuticle.

Tyrosine (A) is converted into L-DOPA (B) by tyrosine hydroxylase. L-DOPA is decarboxylated to dopamine (C), which in turn can be acylated to N-acetyldopamine (E, NADA), or to N-β-alanyldopamine (D, NBAD). Laccase can oxidise E and D to NADA-ortho-quinone (G) and NBAD-ortho-quinone (F). These ortho-quinones can be isomerised to NADA-para-quinone methide (I) and NBAD-para-quinone methide (H), respectively. Tautomerase can convert I to to α,β-dehydro-NADA (J), which can be oxidised to α,β-dehydro-NADA-ortho-quinone (K) and α,β-dehydro-NADA-para-quinone methide (L). L can spontaneously react with NADA to give 2-(3', 4'-dihydroxyphenyl)-3-acetylamino-6-(N-acetyl-2'-aminoethyl)-2,3-dihydro-1,4-benzodioxine (M). L) may also react with nucleophilic reactants (HX and HY) to give N), which is a suggested crosslink, thought to stabilise the cuticle. Permission to adapt this figure has been granted by Insect Biochemistry and Molecular Biology (adapted from Andersen, (2010)).

As mentioned in Chapter 1, ecdysone is the steroid hormone responsible for orchestrating the transitions (moults) between developmental stages in *Drosophila* larvae. Recently, another role for tyrosine metabolism in the synthesis of ecdysone was reported (Ohhara et al., 2015) (Figure 5-2). In this context, inhibition in the conversion of tyrosine to tyramine, via RNAi-mediated knock down (KD) of *Tyrosine decarboxylase 2* (*Tdc2*) in the PG, resulted in a significant reduction in 20E concentration and a delay or block in pupariation (Ohhara et al., 2015). Lower 20E concentrations are likely to be a consequence of reduced expression of the Halloween genes, involved in ecdysone biosynthesis in the PG. This is thought to result from insufficient activation of the GPCR Octβ3R in the PG by its ligand tyramine, as KD of *Octβ3R* in the PG, resulted in a similar significant reduction in 20E concentration and a block in pupariation (Ohhara et al., 2015). Anti-tyramine antibody staining suggests that tyramine accumulates in PG cells during the final larval instar but is then released late in L3, to activate Octβ3R, in an autocrine manner. The lack of Octβ3R signalling in the PG decreases its responsiveness to dIlps and PTTH signalling, in turn decreasing Halloween gene expression and thus ecdysone biosynthesis. As it was observed in this study that arrested/delayed pupariation in *Oregon-R* larvae could be rescued by 20E re-feeding, it was indicated that the fault in the larval to pupal transition was solely due to insufficient 20E (Ohhara et al., 2015). This study shows that tyrosine metabolism plays an important and specific role in developmental timing not just in cuticle sclerotization (Figure 5-4).

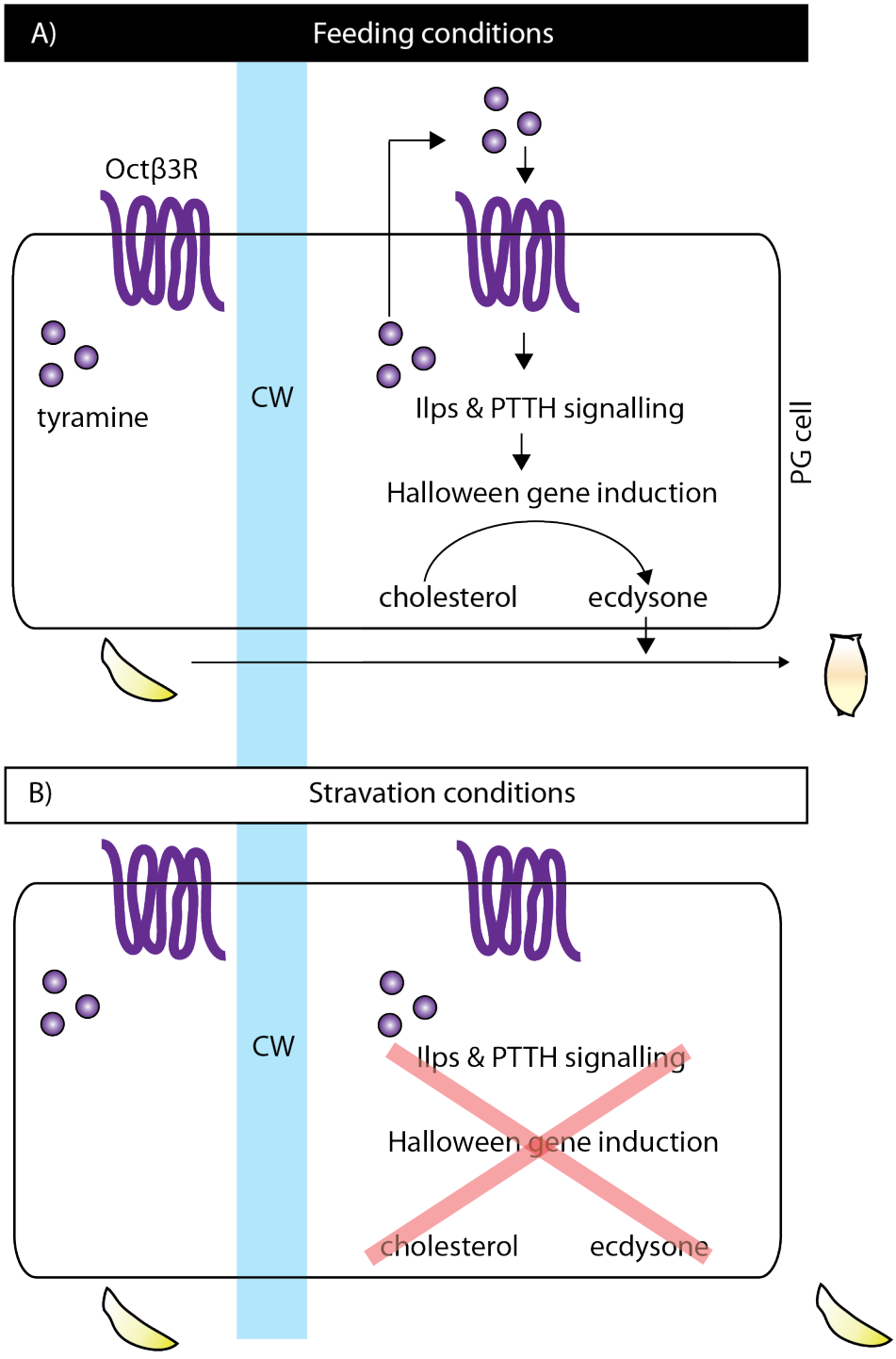
A)
Feeding conditions
Octβ3R
tyramine
CW
Ilps & PTTH signalling
Halloween gene induction
cholesterol
ecdysone
PG cell
B)
Stravation conditions
CW
Ilps & PTTH signalling
Halloween gene induction
cholesterol
ecdysone

Figure 5-2: A model for the regulation of pupariation by Octβ3R signalling.
A) During feeding conditions, after the attainment of CW, tyramine is secreted from the PG cells and activates Octβ3R in an autocrine manner, leading to insulin like peptide (Ilp) and PTTH signalling, subsequent Halloween gene induction, ecdysone biosynthesis and the larval to pre-pupal moult. B) When fail to attain CW during starvation conditions, tyramine is sequestered inside the PG cells, the lack of Octβ3R activation via tyramine, consequently results in reduced ecdysone biosynthesis and thus an arrest at the final larval instar. This figure was adapted from Ohhara et al., 2015.

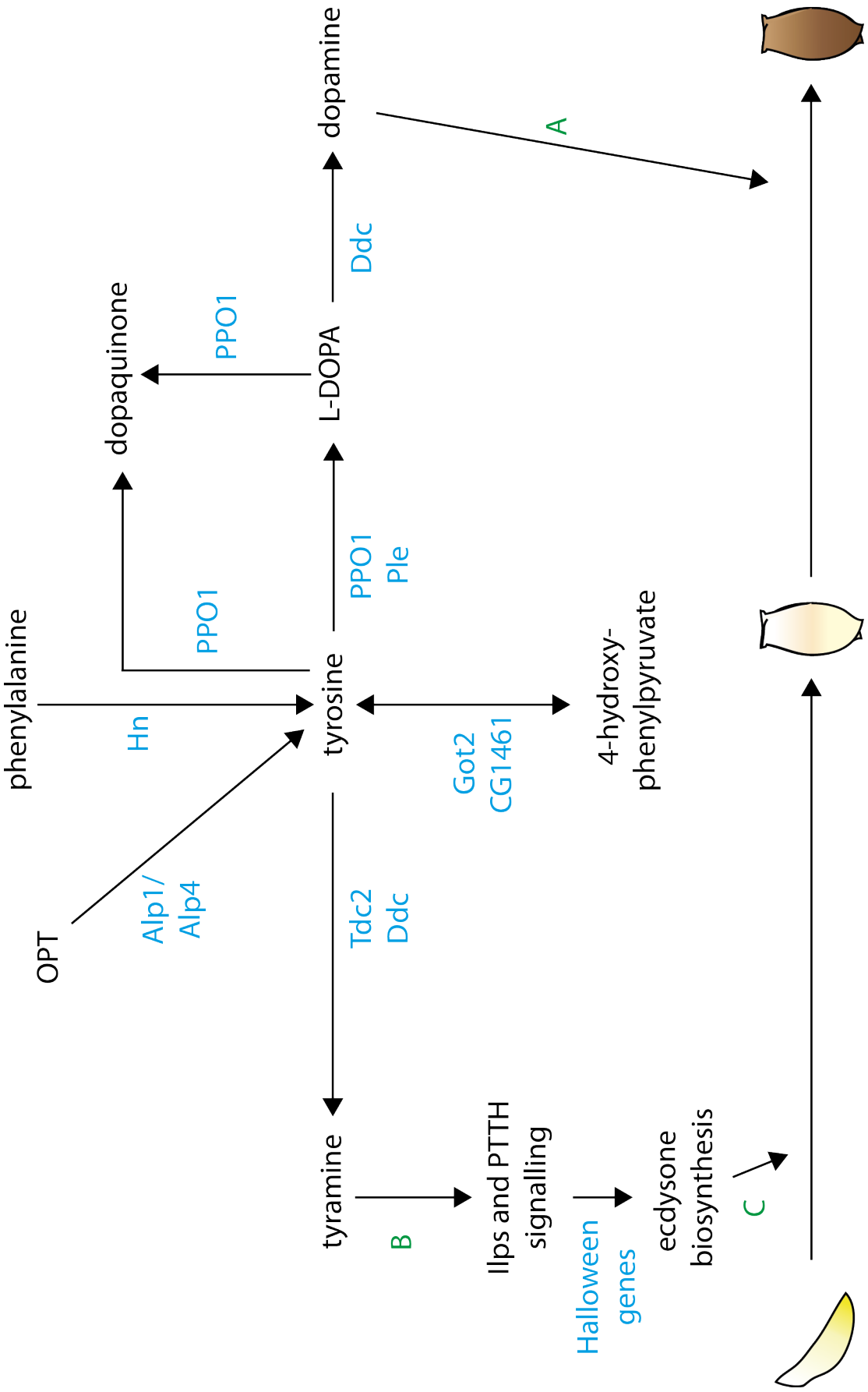
dopamine
A
dopaquinone
PPO1
L-DOPA
Ddc
phenylalanine
Hn
PPO1
PPO1
Ple
tyrosine
4-hydroxy-
phenylpyruvate
Got2
CG1461
OPT
Alp1/
Alp4
Tdc2
Ddc
tyramine
B
Ilps and PTTH
signalling
Halloween
genes
ecdysone
biosynthesis
C

Figure 5-3: Tyrosine metabolism in *Drosophila*.

Tyrosine can be generated from o-phosphtyrosine (OPT), phenylalanine and 4-hydroxy-phenylpyruvate by Alkaline phosphatase (Alp1: CG5656 and Alp4: CG1462), Henna (Hn: CG7399), Glutamate oxaloacetate transaminase 2 (Got2: CG4233) and CG1461 respectively. Tyrosine can then be converted into 4-hydroxy-phenylpyruvate, dopaquinone or L-DOPA by Got2, CG1461, Prophenoloxidase 1 (PPO1: CG42639) or Pale (Ple: CG10118), respectively. L-DOPA can subsequently be converted into dopaquinone or dopamine by PPO1 or Dopa decarboxylase (Ddc: CG10697), respectively. Dopamine is then enzymatically converted through a series of reactions resulting in the diphenolic compounds generated for cuticle tanning detailed in Figure 5-1 (A). Tyrosine can also be converted into tyramine via Ddc and Tyrosine decarboxylase 2 (Tdc2). Monoaminergic autocrine activation of Octβ3R by tyramine (B) has been reported to increase responsiveness of PG cells to IIS and PTTH signalling and stimulate Halloween gene expression and thus ecdysone biosynthesis. A burst of ecdysone and its conversion to 20-hydroxyecdysone in peripheral cells, then mediate the larval to pupal moult (C). Redrawn using information: from the *Drosophila* tyrosine metabolism pathway (http://www.genome.jp/kegg/pathway.html), Harper and Armstrong, 1972 and Ohhara et al., 2015. Enzyme names appear in blue. Pathways mentioned in green are explained in the text.

5.1.1 Literature search for enzymes converting OPT into tyrosine

Beckman and Johnson (1964) identified alkaline phosphatase activities, expressed in extracts from L3 *Drosophila* larvae, which can catalyse the conversion of OPT into tyrosine in, *in vitro* enzymatic assays. Two alkaline phosphatases: Alp1 and Alp4, expressed during the larval instars were identified and a further Alp, Alp2, was reported to be expressed in the adult but not in the larva (Beckman and Johnson, 1964; Harper and Armstrong, 1972; Schneiderman et al., 1966). Later it was shown that larval Alp1 activities are maximal at a pH of ~8, are significantly inhibited by potassium cyanide and L-cysteine but not by 1 mM inorganic phosphate, 2 mM L-phenylalanine or L-tyrosine (Harper and Armstrong, 1973, 1972). A number of biological and synthetic substrates were tested *in vitro* with the biochemically purified Alp protein to define the substrate reaction velocity and specificity. Using this approach, it was observed that OPT is the only known biological substrate that exhibits a reaction velocity equal to that of the synthetic substrate p-nitrophenyphosphate (Harper and Armstrong, 1973, 1972).

Schneiderman et al., (1966), dissected the internal organs away from second and third instar *Drosophila* larvae, leaving a "shell" or carcass of the hypoderm, muscle and cuticle. In this carcass preparation they detected very low Alp activity in second and young third instars, via electrophoretic studies and zymography, but an increase in this activity in mature third instar larvae. Schneiderman et al., inferred this enzyme to be Alp1, the same enzyme previously detected by Beckman and Johnson (1964). Taking together, the concomitant rise of inorganic phosphate, the fall of OPT and the increased activity of Alp1, Harper and Armstrong (1972) suggested that carcass expression of this Alp, functioned to provide precursors for cuticle tanning (sclerotization). Many years later, sequencing of the *Drosophila* genome and expression analysis of predicted Alp genes strongly suggested that Alp1 corresponds to CG5656 and Alp4 corresponds to CG1462 (Flybase: Marygold, 2015).

Flybase transcript analysis indicates that Alp1 (CG5656) is maximally expressed in two developmental peaks, one during mid-embryogenesis and the other during late non-feeding L3 stages, when larvae have begun to wander just prior to pupariation. Expression of Alp4 (CG1462) transcripts shows a largely complementary pattern of maximal expression, peaking during the L1 to early-L3 larval feeding stages and then again during adulthood (Figure 5-4). In terms of tissue specificity, Alp1 is predicted to be expressed in the larval salivary gland and larval carcass (Figure 1-3). More is known about Alp4 expression and function. Alp4 expression has been observed in the "digestive system" of larvae and adults and in the accessory gland of adult males (Figure 5-5). Sözen et al., (1997) and Yang et al., (2000), subsequently narrowed the "digestive system" expression of Alp4 to the lower malpighian tubules, the fly equivalent to renal cells, as well as to neurons in the ellipsoid body of the adult brain. The zone of the lower malpighian tubules that expresses Alp4 is known to play a role in fluid re-absorption (O'Donnell and Maddrell, 1995). Moreover, ectopic expression of Alp4 in the main segment of the malpighian tubules (rather than the lower segment) results in reduced fluid secretion rates (Yang et al., 2000). Transposon insertions into the Alp4 gene, which appear not to lead to complete loss of function of Alp4, resulted in a semi-lethal phenotype (Yang et al. 2000). An association between Alp4 action in the tubules and OPT conversion has not yet been made, rather the phosphatase action of Alp4

in the tubules was proposed to be involved in reclaiming calcium from calcium phosphates, a function that may be relevant for adult physiology (Yang et al., 2000). In summary, the activity of Alp1 and Alp4 as OPT phosphatases has been shown in enzymatic assays, their expression has been partially characterised but their *in vivo* physiological functions during development remain unknown.

Figure 5-4: Developmental time course of Alp1 and Alp4 expression.

Alp1 and Alp4 transcript abundance from embryo to 30 day-old adults. Redrawn from Flybase (flybase.org) using RNA sequencing data recorded by Celniker et al., 2009.

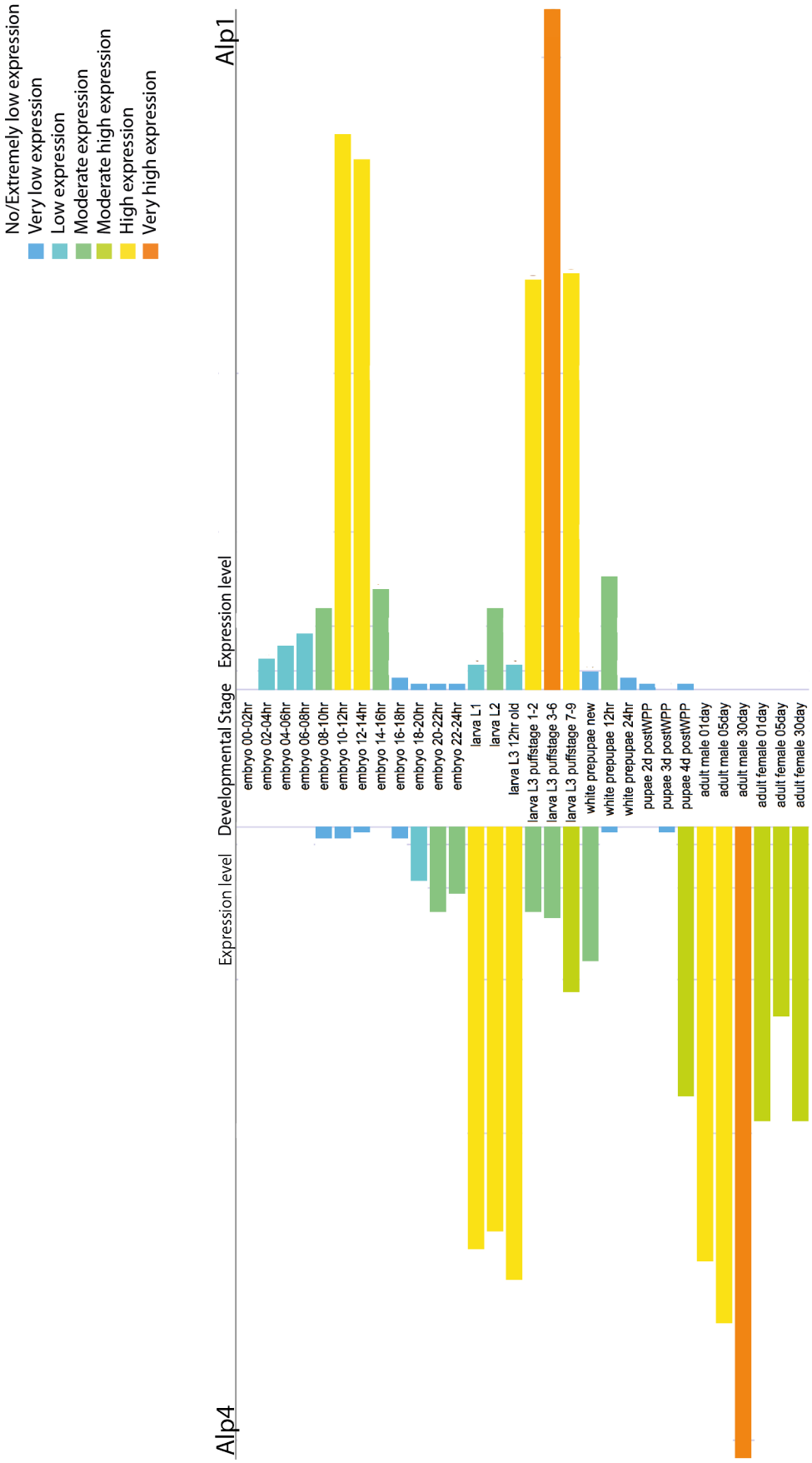
No/Extremely low expression
Very low expression
Low expression
Moderate expression
Moderate high expression
High expression
Very high expression
Alp1
Expression level
Developmental Stage
embryo 00-02hr
embryo 02-04hr
embryo 04-06hr
embryo 06-08hr
embryo 08-10hr
embryo 10-12hr
embryo 12-14hr
embryo 14-16hr
embryo 16-18hr
embryo 18-20hr
embryo 20-22hr
embryo 22-24hr
larva L1
larva L2
larva L3 12hr old
larva L3 puffstage 1-2
larva L3 puffstage 3-6
larva L3 puffstage 7-9
white prepupae new
white prepupae 12hr
white prepupae 24hr
pupae 2d postWPP
pupae 3d postWPP
pupae 4d postWPP
adult male 01day
adult male 05day
adult male 30day
adult female 01day
adult female 05day
adult female 30day
Expression level
Alp4

Figure 5-5: Tissue expression of Alp1 and Alp4.

Excerpt of the *Drosophila* transcriptome displaying Alp1 and Alp4 spatial transcript abundance. Redrawn from Flybase (flybase.org) using RNA sequencing data recorded by Celniker et al., 2009.

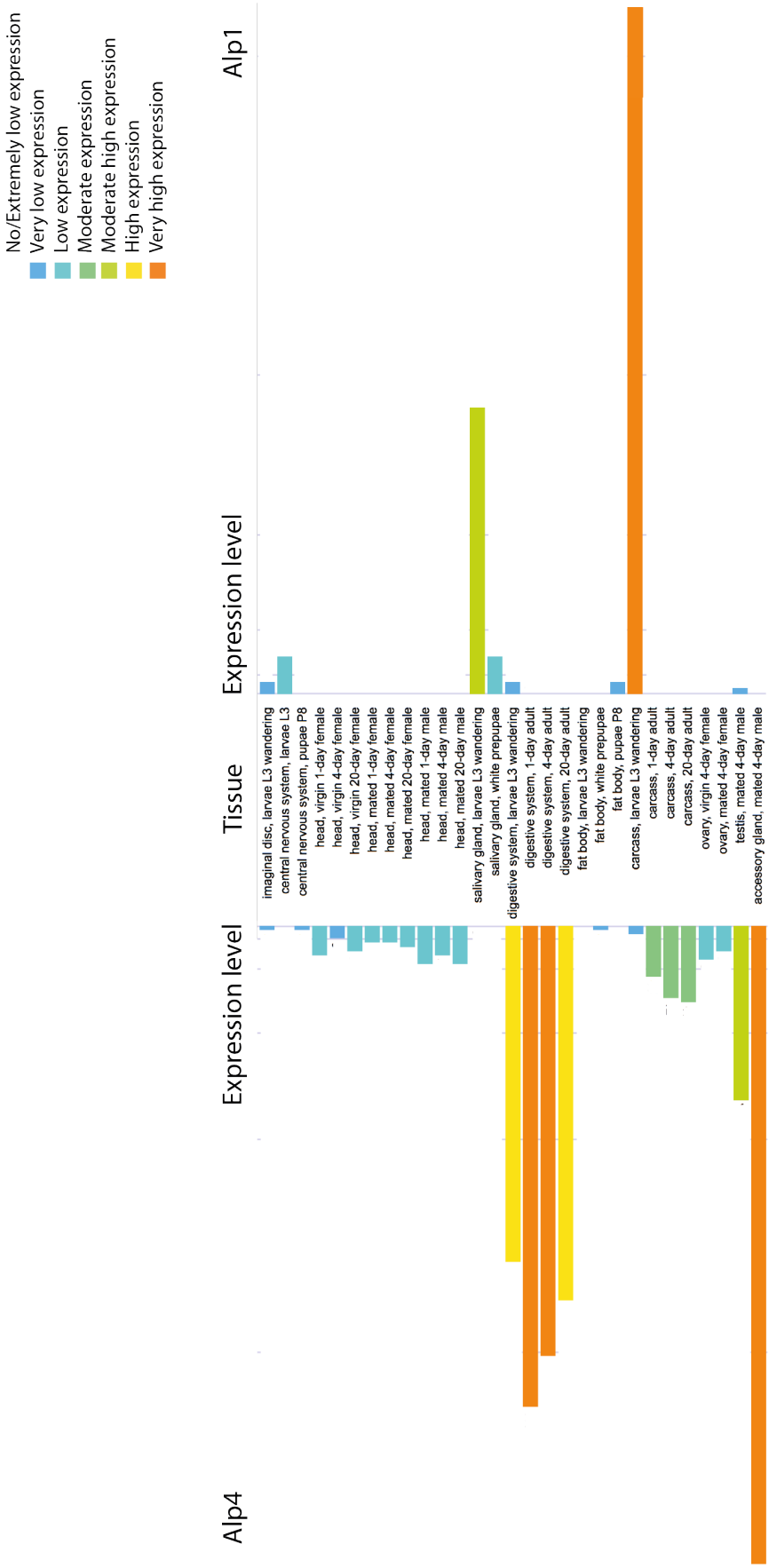
No/Extremely low expression
Very low expression
Low expression
Moderate expression
Moderate high expression
High expression
Very high expression
Alp1
Expression level
Tissue
imaginal disc, larvae L3 wandering
central nervous system, larvae L3
central nervous system, pupae P8
head, virgin 1-day female
head, virgin 4-day female
head, virgin 20-day female
head, mated 1-day female
head, mated 4-day female
head, mated 20-day female
head, mated 1-day male
head, mated 4-day male
head, mated 20-day male
salivary gland, larvae L3 wandering
salivary gland, white prepupae
digestive system, larvae L3 wandering
digestive system, 1-day adult
digestive system, 4-day adult
digestive system, 20-day adult
fat body, larvae L3 wandering
fat body, white prepupae
fat body, pupae P8
carcass, larvae L3 wandering
carcass, 1-day adult
carcass, 4-day adult
carcass, 20-day adult
ovary, virgin 4-day female
ovary, mated 4-day female
testis, mated 4-day male
accessory gland, mated 4-day male
Expression level
Alp4

5.2 Alp1 and Alp4 are required for timely pupariation

In the previous results chapters, I showed using VDTS metabolomics that tissue OPT levels fall and hemolymph tyrosine levels rise towards the end of the third larval instar. These events are blocked by NR before CW but proceed in a timely fashion if NR is applied after CW. The following chapter focuses on testing whether the events of falling tissue OPT, rising hemolymph tyrosine and progression to pupariation might not just be associated in time but also functionally linked. My observations combined with those of Ohhara et al., (2015), information on Alp1/4 from previous literature and from Flybase, suggest a hypothesis that I will explore in this chapter. The hypothesis is that Alp1 and/or Alp4 act upon OPT larval stores to liberate free tyrosine, which in turn provides the tyramine necessary for Octβ3R signalling in the PG and thus for ecdysone biosynthesis and timely pupariation.

Initially, I tested whether the post-CW rise in tyrosine plays an important role in developmental timing by applying genetic manipulations to a panel of *Drosophila* tyrosine metabolism enzymes. The GAL4-UAS system was used with *tub-GAL4*, to ubiquitously KD the expression of each tyrosine-metabolism enzyme via RNAi (Brand and Perrimon, 1993; Dietzl et al., 2007) . The panel of tyrosine metabolism enzymes was selected from the KEGG pathway database (http://www.genome.jp/kegg/pathway.html, Kanehisa et al., 2000) plus the manual addition of Alp1 and Alp4 (Figure 5-3). This included: Prophenoloxidase 1 (PPO1), Dopa decarboxylase (Ddc), Tyrosine decarboxylase (Tdc), Glutamate oxaloacetate transaminase 2 (Got2), CG1461 (a theorised tyrosine Aminotransferase), Alp1 and Alp4. To assay how KD of the enzymes affected developmental timing, the time taken for larvae to reach pupariation (time to pupariation: TTP) was measured; the time when 50% of larvae reached pupariation was then calculated from the graph generated (Figure 5-6 and Figure 5-7). It was observed that, during fed conditions, ubiquitous larval KD of *PPO1, Ddc, Tdc, Got2* and *CG1461* had little or no delay in TTP but KD of *Alp4* (*Alp4i*) resulted in a robust delay in TTP (~9.5 hours), in comparison to the control (*tub>TRiP Ctrl*). Interestingly, if NR is administered after attainment of CW (66 hr, *Alp4i*: ~0.94 mg), *Alp4i* no longer delays TTP. Conversely, during NR but not fed conditions *Alp1* KD (*Alp1i*, at 66 hr: ~1.07 mg) delays TTP (~7 hours). Together these results demonstrate that Alp1 and Alp4 regulate the

timing of the larval to pupal transition but that Alp1 is required during NR whereas Alp4 is required during fed conditions. The NR-specific delay in TTP via KD of *Alp1* is especially interesting, as administration of NR once CW has been attained, is known to accelerate TTP (here by ~2.5 hours when comparing *tub>Ctrls*) – therefore, it may be that Alp1 action plays a role in this accelerated TTP.

To test whether the functions of Alp1 and Alp4 are additive or overlapping, both enzymes were together inactivated (*tub>Alp4i;;Alp1i*). The resulting delay in TTP of double KD of *Alp1* and *Alp4* was larger than the single KD of *Alp4* during fed conditions (~2.5 hours more) (Figure 5-8). During post-CW (~72 hr) NR, the TTP delay in the double knockdown was also larger than that in the single KD of *Alp1* (~8 hours more) (Figure 5-8). The larger delays in TTP observed in the double versus the single KDs, suggest that Alp1 and Alp4 have partially overlapping or redundant functions. In other words, Alp1 is most important during NR but may nevertheless have some degree of function during fed conditions. Conversely, Alp4 plays a major role during fed conditions but may also make a smaller contribution during NR.

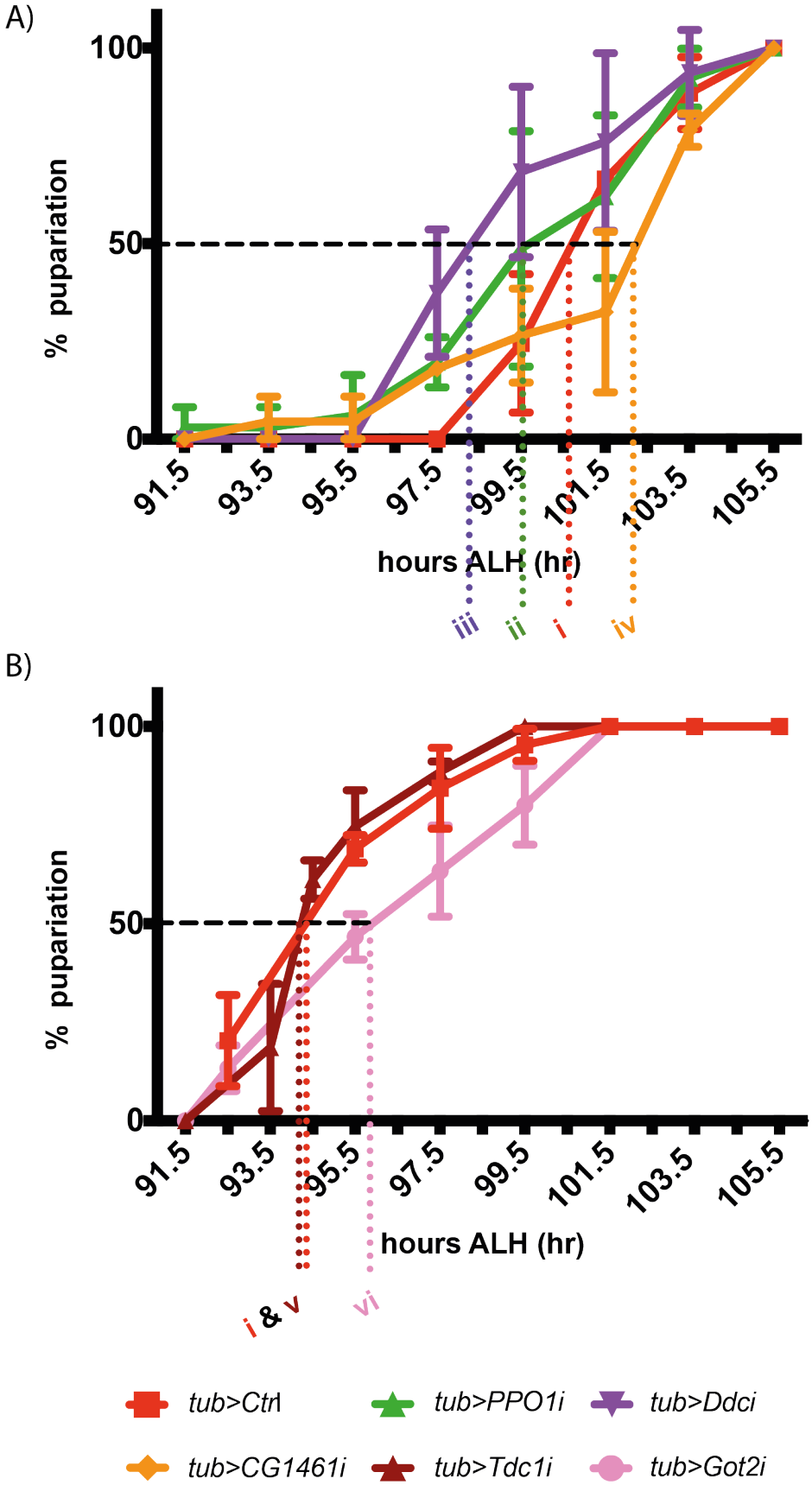
A)
100
50
0
% pupariation
91.5
93.5
95.5
97.5
99.5
101.5
103.5
105.5
hours ALH (hr)
iii
ii
i
iv
B)
100
50
0
% pupariation
91.5
93.5
95.5
97.5
99.5
101.5
103.5
105.5
hours ALH (hr)
i & v
vi
tub>Ctrl
tub>PPO1i
tub>Ddci
tub>CG1461i
tub>Tdc1i
tub>Got2i

Figure 5-6: Knock down of four tyrosine-metabolism enzymes does not delay TTP.

A) During continuously fed conditions, 50% of ubiquitously knocked down *PPO1, Ddc* and *CG1461* larvae pupariate at approximately the same time as the control line (TTP for: *control* ~100.5 hr (i), *PPO1* ~99.5 hr (ii), *Ddc* ~98.5 hr (iii) and *CG1461* ~102.5 hr (iv)). B) During continuously fed conditions, 50% of ubiquitously knocked down *Tdc1* and *Got2* larvae pupariate at approximately the same time as the control line (TTP for: control ~ 94.5 hr (i), *Tdc1* ~94.5 hr (v) and *Got2* ~95.5 hr (vi)). *tub>Ctrl*: *α-tubulin*-GAL4 crossed to *TRiP Ctrl*. Each point on each curve is the average % of larvae that have reached pupariation at that time, recorded using 15 larvae per vial, with 3 vials per condition (45 larvae per condition) - error bars represent one standard deviation.

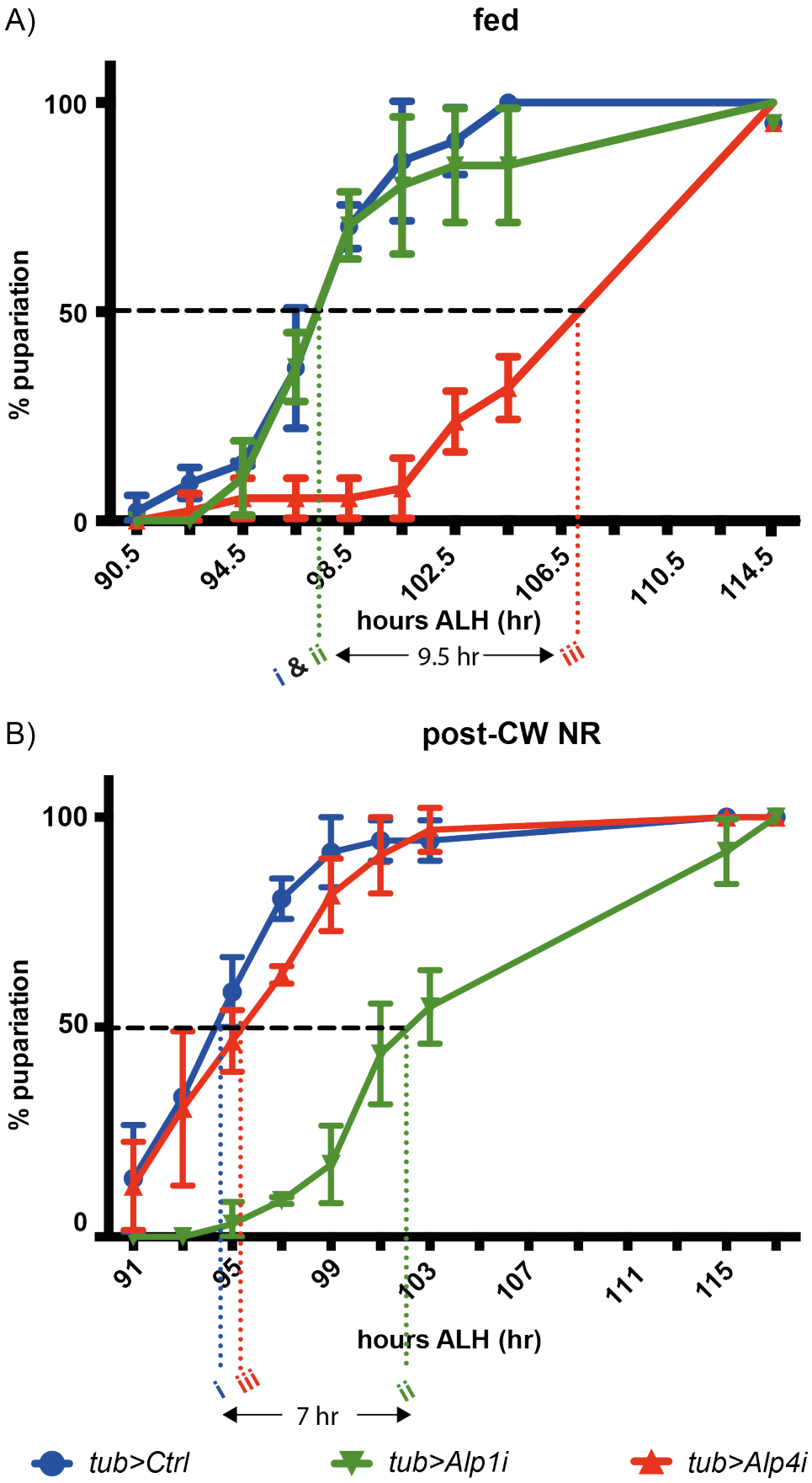
A)
fed
100
50
0
% pupariation
90.5
94.5
98.5
102.5
106.5
110.5
114.5
hours ALH (hr)
i & ii
9.5 hr
iii
B)
post-CW NR
100
50
0
% pupariation
91
95
99
103
107
111
115
hours ALH (hr)
i
iii
ii
7 hr
tub>Ctrl
tub>Alp1i
tub>Alp4i

Figure 5-7: KD of *Alp1* or *Alp4* delays TTP in NR and fed larvae respectively.

A) During continuously fed conditions 50% of ubiquitously knocked down *Alp4* larvae (*tub>Alp 4i*) pupariate ~107 hr (iii) whilst control and *Alp1* KD larvae (*tub>Alp1i*) reach 50% pupariation at ~ 97.5 hr (i & ii). B) If NR is administered after CW has been attained, 50% of *tub>Alp1i* larvae pupariate at ~102 hr (ii) whilst control and *tub>Alp4i* larvae reach 50% pupariation at ~95 hr (i & iii). *tub>Ctrl*: *α-tubulin*-GAL4 crossed to TRiP Ctrl. Each point on each curve is the average % of larvae that have reached pupariation at that time, recorded using 15 larvae per vial, with 3 vials per condition (45 larvae per condition) - error bars represent one standard deviation. A) and B) are graphs representative of an experiment that was repeated on three independent occasions.

A)

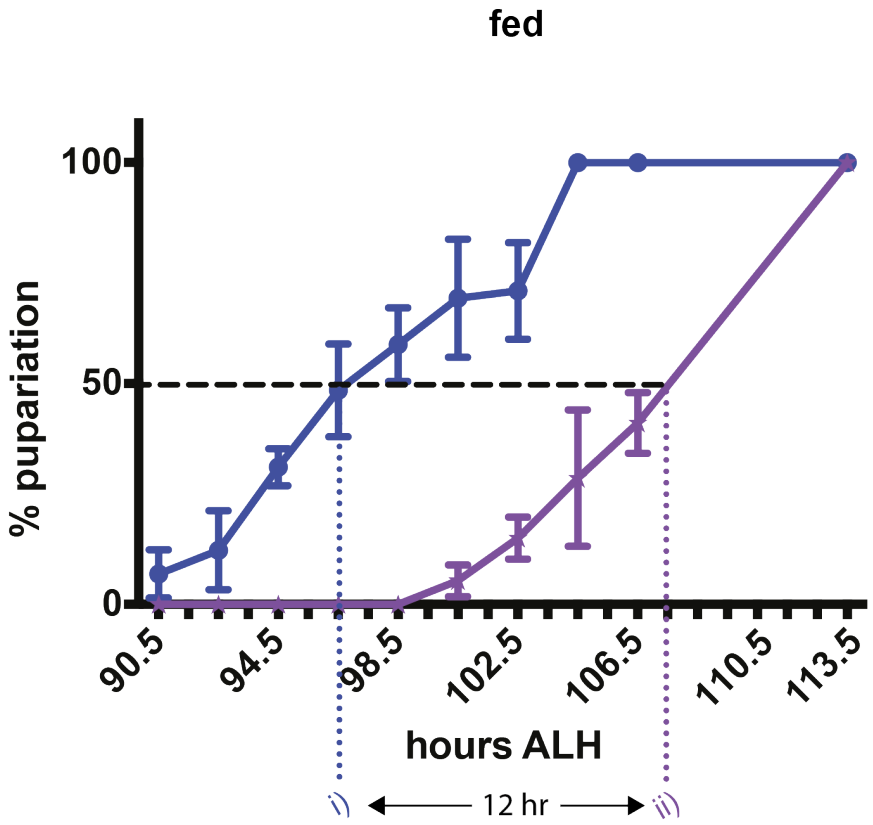
fed
100
50
0
% pupariation
90.5
94.5
98.5
102.5
106.5
110.5
113.5
hours ALH
12 hr

B)

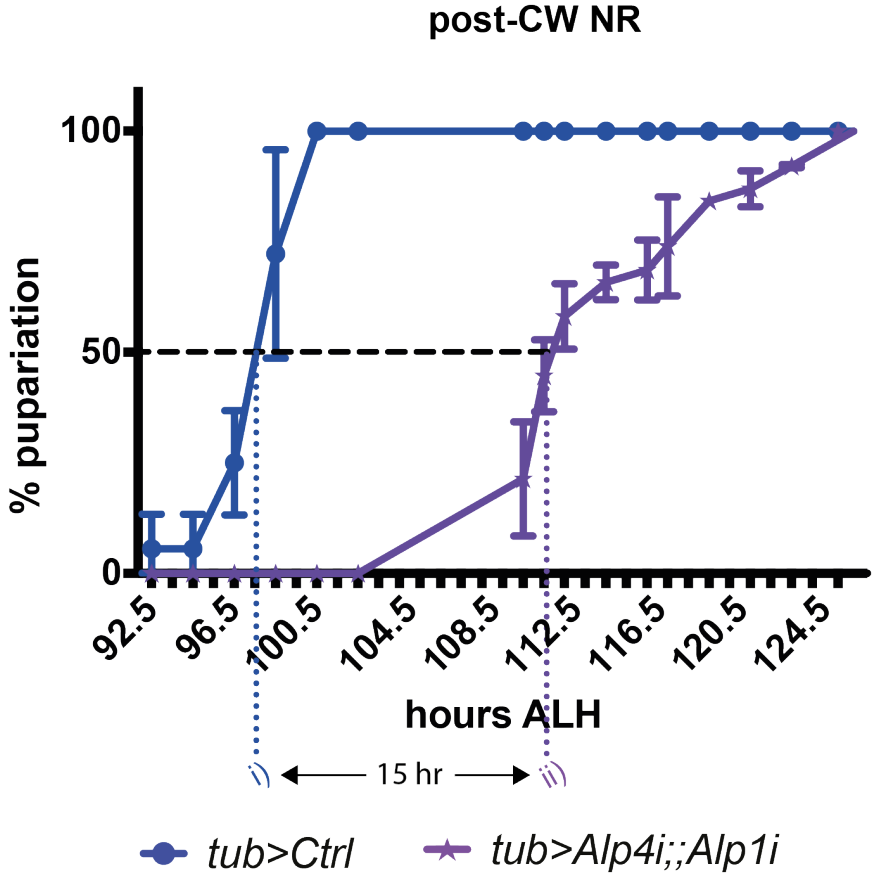
post-CW NR
100
50
0
% pupariation
92.5
96.5
100.5
104.5
108.5
112.5
116.5
120.5
124.5
hours ALH
15 hr
tub>Ctrl
tub>Alp4i;;Alp1i

Figure 5-8: Double KD of *Alp1* and *Alp4* delays TTP in fed and NR larvae.

A) During continuously fed conditions 50% of ubiquitously knocked down *Alp1* and *Alp4* larvae (*tub>Alp4i;;Alp1i*) pupariate ~108.5 hr (ii) whilst control larvae (*tub>Ctrl*) reach 50% pupariation at ~96.5 hr (i). B) If NR is administered after CW has been attained, 50% of *tub>Alp4i;;Alp1i* larvae pupariate at ~112.5 hr (ii) whilst *tub>Ctrl* larvae reach 50% pupariation at ~97.5 hr (i). *tub>Ctrl*: *α-tubulin*-GAL4 crossed to w^{1118}. Each point on each curve is the average % of larvae that have reached pupariation at that time, recorded using 15 larvae per vial, with 3 vials per condition - error bars represent one standard deviation.

Next, the GAL4/UAS system was used to assess the tissue-specific requirements of Alp1 and Alp4 in developmental progression. Alp1 expression has been observed in the "carcass" – a collection of the cuticle, epidermis and muscle. I tested for a tissue-specific role using the *A58-GAL4* driver (abbreviated *A58>),* which expresses GAL4 specifically in the epidermis (Galko and Krasnow, 2004). Like *tub>Alp1i* larvae, *A58>Alp1i* larvae moved to NR post CW (66hr ~1.01 mg), also demonstrated a delayed TTP in comparison to controls (Figure 5-9). Therefore, the area of Alp1 expression can be narrowed from the "carcass" to (at least) the epidermis. As the delay in TTP was larger (by ~4 hours) in *A58>Alp1i* larvae in comparison to *tub>Alp1i* larvae, it may be suggested that *A58>* may express more strongly than *tub>* and thus give a greater RNAi KD. Again it is observed that post-CW NR accelerates TTP in controls, in comparison to controls on continuously fed conditions (here by ~9.5 hours). Therefore, this adds further support to the suggestion that Alp1 action may play a role in the (post-CW) NR-induced acceleration in TTP. As Alp4 expression was observed in the malpighian tubules (Yang et al., 2000), it is perhaps unsurprising that *A58>Alp4i* larvae do not display a delayed TTP in comparison to controls when continuously fed, unlike *tub>Alp4i* larvae.

Figure 5-9: Specific KD of *Alp1* in the epidermis delays TTP in NR larvae.

A) During continuously fed conditions 50% of controls (*A58>Ctrl*, i: ~109 hr), epidermis knocked down *Alp1* (*A58>Alp1i*, ii: ~105.5. hr) and *Alp4* (*A58>Alp4i*, iii: ~109.5 hr) larvae pupariate around the same time. B) If NR is administered after CW has been attained, 50% of *A58>Alp1i* larvae pupariate at ~110 hr (ii) whilst *A58>Ctrl* and *A58>Alp4i* larvae reach 50% pupariation at ~99.5 hr (i) and 97.5 hr (iii) respectively. *A58>Ctrl*: *A58-GAL4* crossed to *TRiP Ctrl*. Each point on each curve is the average % of larvae that have reached pupariation at that time, recorded using 15 larvae per vial, with 3 vials per condition - error bars represent one standard deviation.

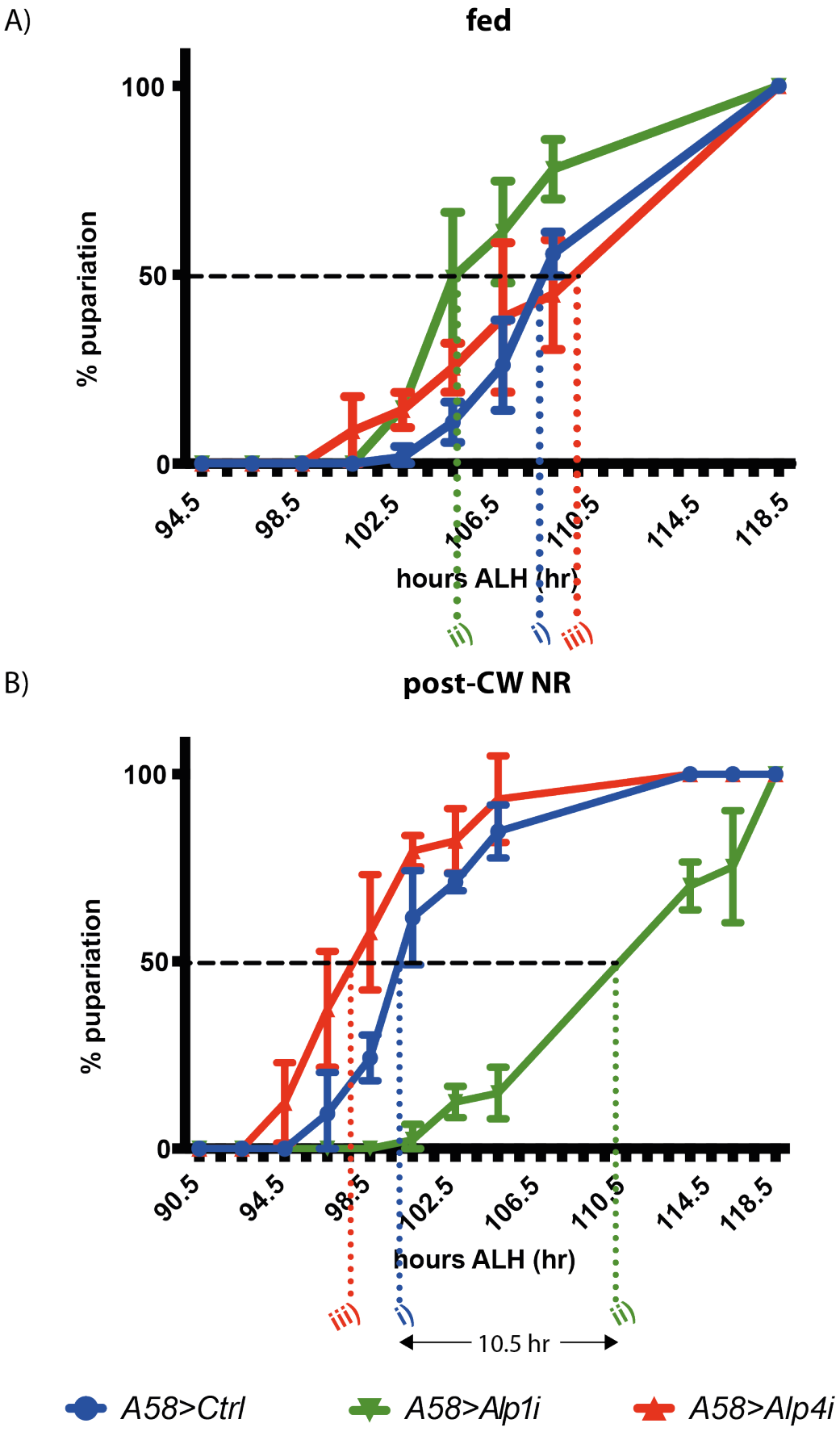
A)
fed
100
50
0
% pupariation
94.5
98.5
102.5
106.5
110.5
114.5
118.5
hours ALH (hr)
ii)
i)
iii)
B)
post-CW NR
100
50
0
% pupariation
90.5
94.5
98.5
102.5
106.5
110.5
114.5
118.5
hours ALH (hr)
iii)
i)
ii)
10.5 hr
A58>Ctrl
A58>Alp1i
A58>Alp4i

5.2.1 *Alp* KD effects tyrosine-related metabolite concentrations

To test whether Alp1 and Alp4 are required in an *in vivo* context for the conversion of OPT to tyrosine, metabolomics was used to measure the ratio of whole body OPT to tyrosine in control (*tub>w*^{1118}) versus double KD (*tub>Alp4i;;Alp1i*) fed larvae. Double KD larvae are delayed developmentally, so they were compared to control wandering L3 (wL3) larvae in two different ways: double KD larvae (early L3 larvae (pre-wL3), ~1.65 mg per larva) chronologically matched with wL3 controls (~1.97 mg per larva) and double KD larvae developmental-stage matched with wL3 controls (i.e. also wL3, ~1.86 mg per larvae) (Figure 5-10). The whole body OPT:Tyr ratio at early L3 in double KD larvae was significantly (~6 fold) higher than chronologically matched wL3 controls. In contrast, the OPT:Tyr ratio determined from double KD larvae at the wL3 stage did not significantly differ from that of developmental-stage matched wL3 controls. Hence, these experiments do not distinguish whether the OPT:Tyr ratio change is a direct consequence of decreased Alp activity or a more indirect effect mediated by Alp1/4 acting upon another process, itself required for larval progression. Nevertheless, these experiments show that Alp1 and Alp4 are required for the decrease in the OPT:Tyr ratio that normally accompanies larval progression during L3.

I also measured the tyramine concentration in the fed whole body in controls and in double KDs. In controls, tyramine concentration decreases during early L3. This revealed a similar pattern to the OPT:Tyr ratio, such that the tyramine concentration is similar between wL3 double KD and controls but ~3 fold higher in early L3 double KDs chronologically matched with wL3 controls. This indicates that Alp1 and Alp4 are required, directly or indirectly, for the normal decrease in tyramine during L3 progression. Unlike OPT and tyrosine, tyramine cannot be detected in the hemolymph suggesting that it may be largely sequestered in body tissue(s) and released in an Alp1/4-dependent fashion during L3 larval progression.

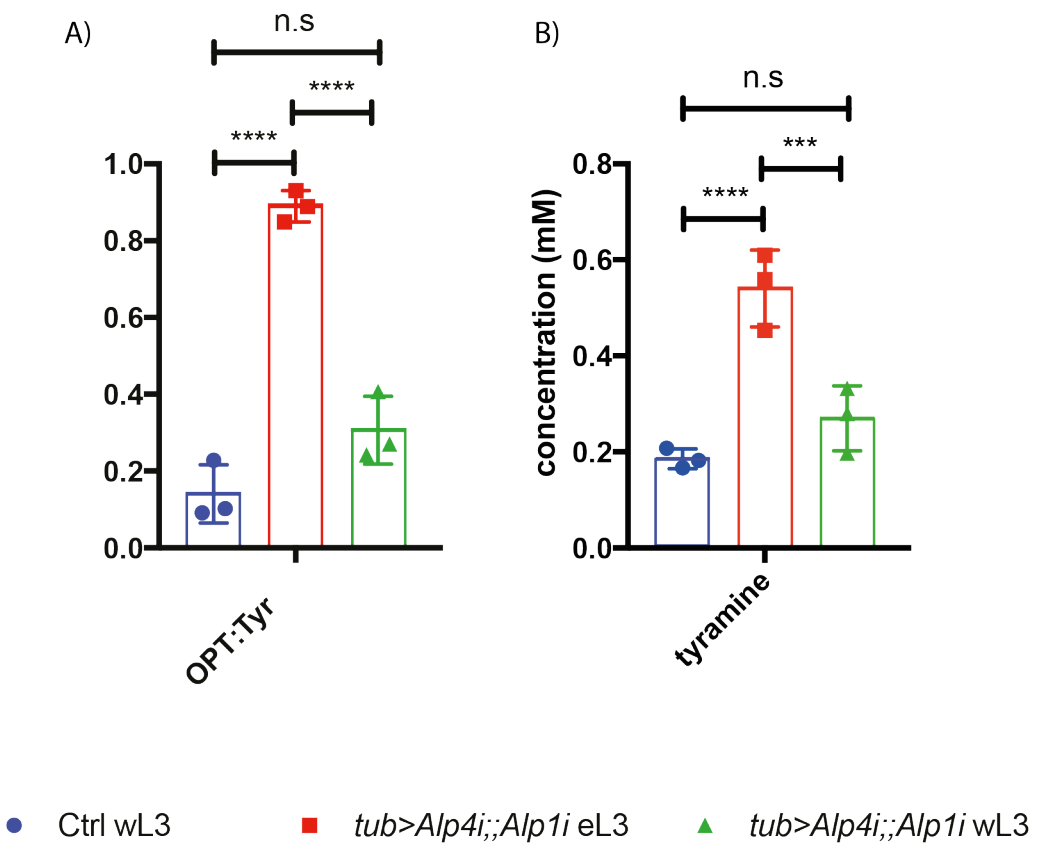

Figure 5-10: Alp1 and Alp4 regulate the OPT:Tyr ratio and tyramine.

A) Ratio of whole larval OPT to tyrosine concentration (OPT:Tyr) in wandering L3 *tub>w*^{1118} larvae (Ctrl wL3), chronologically matched early L3 Alp double KD (tub>*Alp4i;;Alp1i* eL3) and developmentally matched wandering L3 Alp double KD (tub>*Alp4i;;Alp1i* wL3). B) Whole larval concentration of tyramine in Ctrl wL3, *tub>Alp4i;;Alp1i* eL3 and *tub>Alp4i;;Alp1i* wL3 larvae. Metabolite concentrations were determined for each condition from 15 larvae collected in three replicates. Then ratio of OPT to tyrosine was calculated for each individual spectrum from the whole larval OPT concentration over the whole larval tyrosine concentration. Statistical significance was determined according to Tukey's HSD test in a 2-way ANOVA with an Alpha-value of 5 %. *: p-value $\leq$ 0.05; ****: p-value: $\leq$ 0.0001; and n.s.: not significant (p > 0.05).

5.3 Rescue of Alp1/4 phenotypes with dietary tyrosine

The preceding genetic analysis suggests the hypothesis that Alp1 and Alp4 function to release tyrosine from its OPT storage form, in turn promoting larval developmental progression to pupariation. If the only function of Alp1/4 relevant to TTP is to provide a source of tyrosine, then it should be possible to rescue the *Alp1i* and *Alp4i* delayed TTP phenotypes by boosting dietary tyrosine. I first showed that a diet supplemented with tyrosine results in a ~6 fold increase in hemolymph tyrosine concentration (Figure 5-11). Interestingly, hemolymph OPT also increases following supplementation, suggesting but not proving that "excess" tyrosine taken up via the gut can be converted back to OPT as a "storage" form. The kinase enzyme(s) responsible for converting free tyrosine to OPT have yet to be identified.

To conduct tyrosine supplementation rescue experiments, *Alp4i* larvae were reared on standard medium supplemented with 1.5 g/L tyrosine (2x+Tyr) (Figure 5-12). Tyrosine supplementation did not accelerate the TTP of genetic control larvae (in compared to controls raised on standard food) but it did strongly reduce the TTP delay in fed *Alp4i* larvae (from ~10 to 1.5 hours, an 84% reduction). For Alp1, the rescue experiments were conducted on NR medium supplemented with tyrosine. This NR-supplementation strategy reduced the delay of Alp1i larvae moved to NR after CW (72 hr: ~1.28 mg) by ~50-67% (Figure 5-13). This indicates that dietary tyrosine partially rescues the *Alp1i* delay in NR larvae but the degree of rescue is less complete than with fed *Alp4i* larvae.

These results show that tyrosine insufficiency contributes to the developmental delay of *Alp1* KD and *Alp4* KD larvae. Together with previous studies showing that Alp1 and Alp4 have intrinsic OPT phosphatase activity *in vitro* (Harper and Armstrong, 1972), I conclude that efficient OPT to tyrosine conversion is required for timely developmental progression to pupariation in both fed and NR larvae and that this requires a different Alp enzyme in each condition.

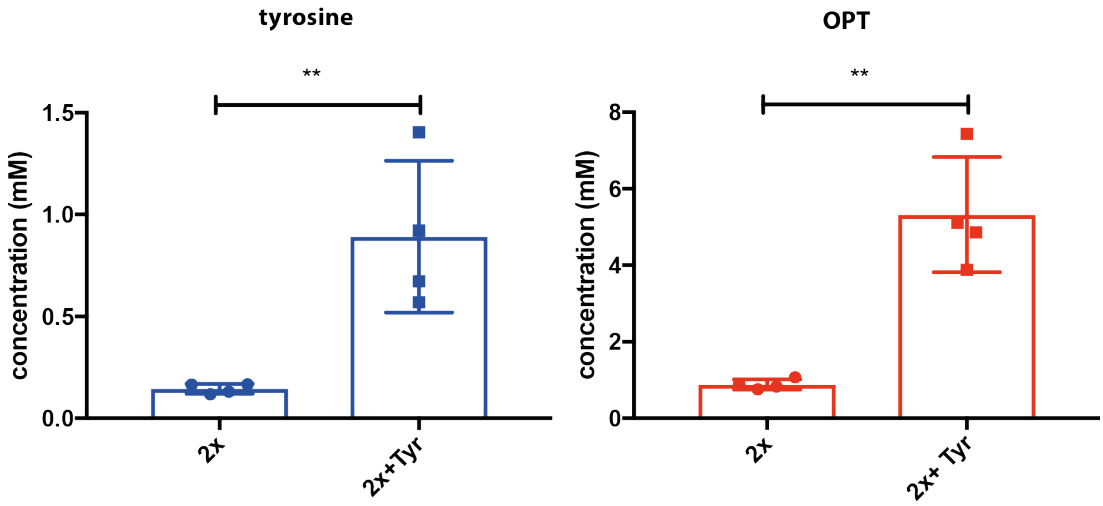

Figure 5-11: Dietary supplementation increases hemolymph tyrosine and OPT.

Hemolymph OPT and tyrosine concentrations determined via VDTS from w^{1118} larvae reared on standard (2x) or tyrosine supplemented (2x + Tyr) medium, for 51 hr. Each condition is the average metabolite concentration from 15 larvae, from four biological replicates. Statistical significance was determined according to Tukey's HSD test in a 2-way ANOVA with an Alpha-value of 5 %. **: p-value $\leq$ 0.01.

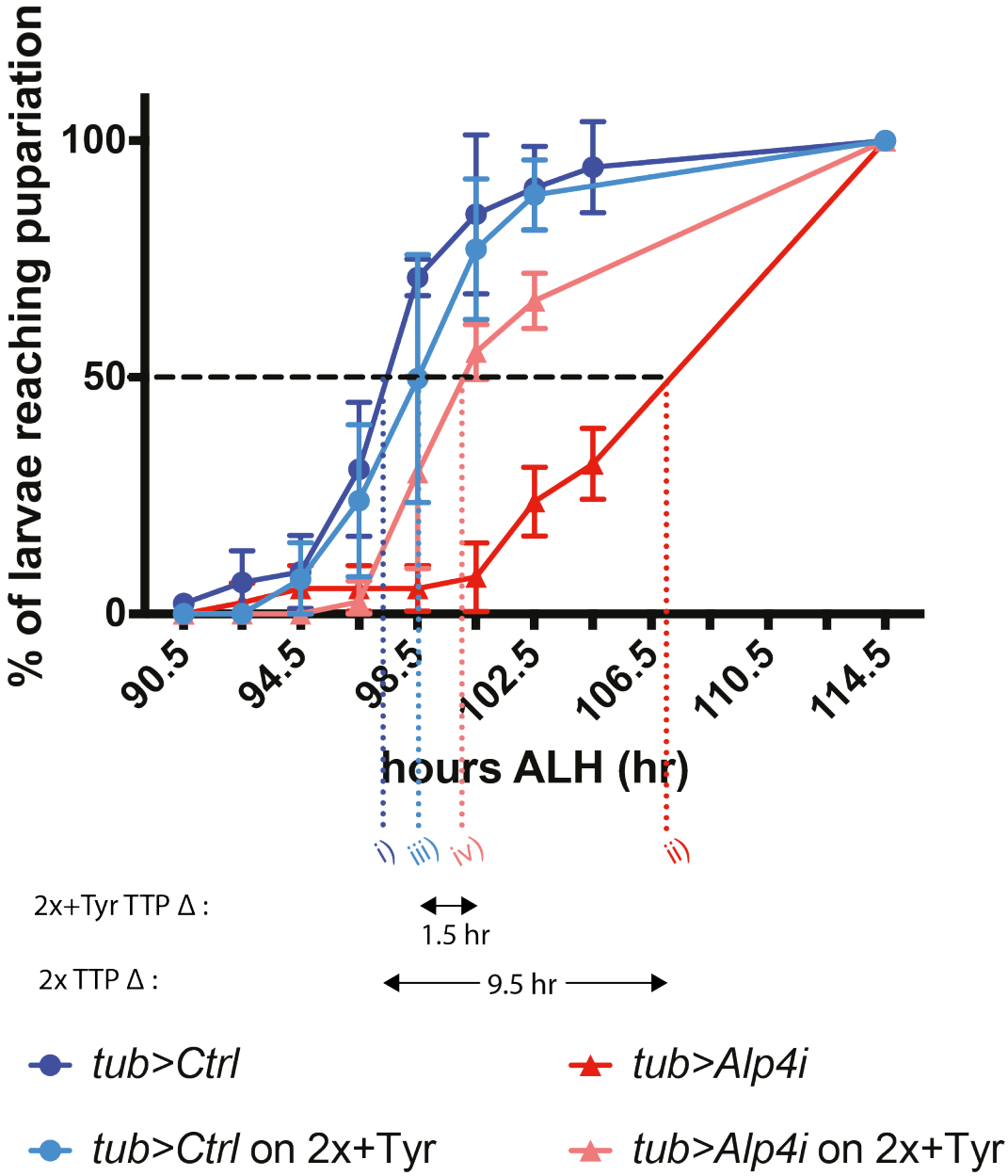
% of larvae reaching pupariation
100
50
0
90.5
94.5
98.5
102.5
106.5
110.5
114.5
hours ALH (hr)
i)
iii)
iv)
ii)
2x+Tyr TTP Δ :
1.5 hr
2x TTP Δ :
9.5 hr
tub>Ctrl
tub>Alp4i
tub>Ctrl on 2x+Tyr
tub>Alp4i on 2x+Tyr

Figure 5-12: Tyrosine rescues the *Alp4* KD delay in fed larvae.

During continuously fed conditions on 2x medium, 50% of controls (*tub>Ctrl*) pupariate at ~97 hr (i), whilst ubiquitously knocked down Alp4 (*tub>Alp4i*) larvae pupariate at ~106.5 hr. During continuously fed conditions on 2x supplemented with 1.5 g/L tyrosine (2x + Tyr), 50% of controls (*tub>Ctrl* on 2x+Tyr) pupariate at ~98.5 hr (iii), whilst ubiquitously knocked down Alp4 (tub>Alp4i on 2x+Tyr) larvae pupariate at ~100 hr (iv). *Ctrl: TRiP Ctrl* larvae. 2x+Tyr TTP Δ: difference in TTP between Ctrl and *Alp4i* on 2x+Tyr. 2x TTP Δ: difference in TTP between Ctrl and *Alp4i* on 2x. Each point on each curve is the average % of larvae that have reached pupariation at that time, recorded using 15 larvae per vial, with 3 vials per condition - error bars represent one standard deviation.

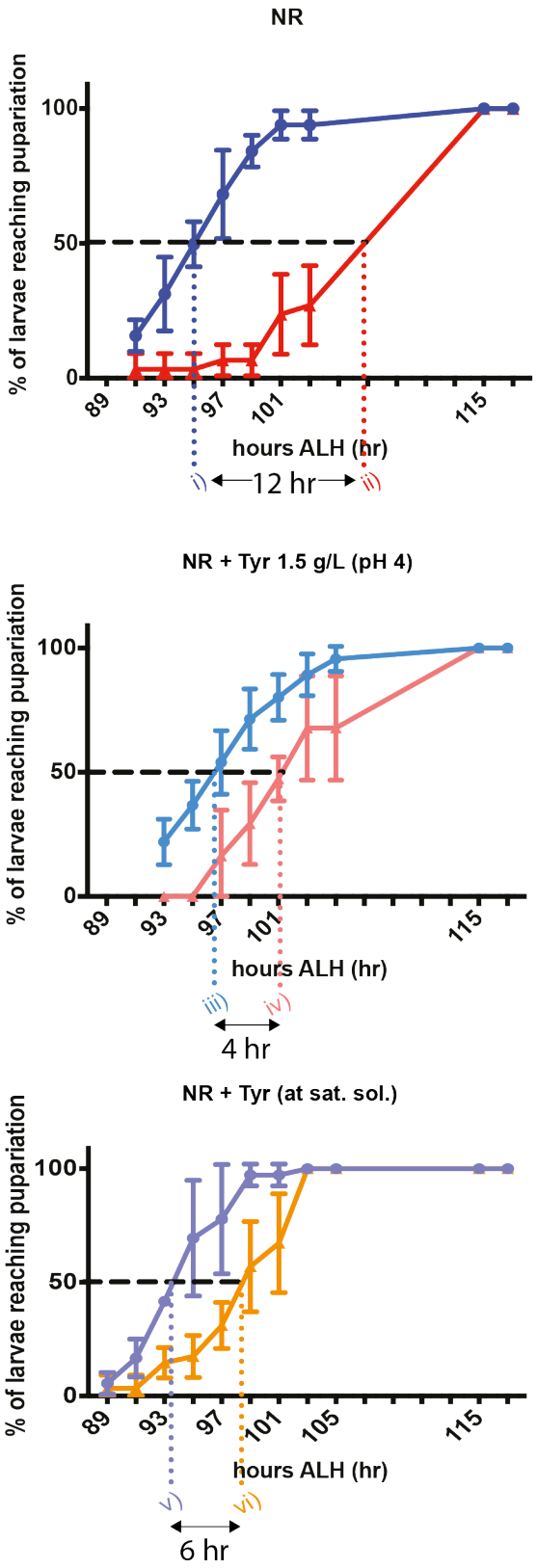

NR: *tub>Ctrl* *tub>Alp1i*

NR + Tyr (pH 4): *tub>Ctrl* *tub>Alp1i*

NR + Tyr (at sat. sol.): *tub>Ctrl* *tub>Alp1i*

Figure 5-13: Tyrosine partially rescues the *Alp1* KD delay in NR larvae.

If NR is administered after CW has been attained, 50% of ubiquitously knocked down *Alp1* (*tub>Alp1i*) larvae pupariate at ~107 hr (ii) whilst controls (*tub>Ctrl*) reach 50% pupariation at ~95 hr (i). If larvae are transferred to NR medium supplemented with 1.5 g/L tyrosine (NR + Tyr (pH4)) post CW attainment, 50% of *tub>Alp1i* larvae pupariate at ~101 hr (iv) whilst *tub>Ctrl* larvae reach 50% pupariation at ~97 hr (iii). If larvae are transferred to NR medium supplemented with tyrosine at saturating solubility (NR + Tyr (at sat. sol.)) post CW attainment, 50% of *tub>Alp1i* larvae pupariate at ~99 hr (vi) whilst *tub>Ctrl* larvae reach 50% pupariation at ~93 hr (iii). *Ctrl*: *TRiP Ctrl* larvae. 1.5 g/L was solubilised in NR media via either acidification with HCl (taking the final pH of the solution to pH 4) or through generating a NR solution saturated with tyrosine, at pH 7 (see Methods and Materials: 2.2.1). Each point on each curve is the average % of larvae that have reached pupariation at that time, recorded using 15 larvae per vial, with 3 vials per condition - error bars represent one standard deviation.

5.4 Discussion

This chapter identifies a function for the developmental changes in OPT and tyrosine concentration observed using metabolomics in the previous chapters. I knocked down various metabolic enzymes involved in tyrosine metabolism and found that Alp enzymes were required for timely developmental progression. Double KD of both *Alp1* and *Alp4* resulted in a delay in TTP during continuous feeding and post-CW NR. In these *Alp4i;;Alp1i* larvae, a reduced rate of OPT to tyrosine conversion was inferred, indicated that the fall in OPT and concomitant rise in tyrosine during the final larval instar may be due to the phosphatase action via the Alps. Higher whole larval tyramine concentrations were observed in delayed *Alp4i;;Alp1i* larvae. However, as tyramine cannot be detected in the hemolymph, tyramine may be retained in the body tissue of delayed Alp4i;;Alp1i larvae, chronologically matched to wandering controls. Therefore, the action of both Alps is proposed to be necessary for lowering the OPT:Tyr ratio and (perhaps as a consequence) lowering whole body tyramine concentrations, which may in turn become necessary for progression through to pupariation.

The results of individual KDs of *Alp1* and *Alp4* indicate that they are not completely redundant. Instead, for timely pupariation, Alp1 is more strongly required during NR and Alp4 more strongly during fed conditions. Therefore, It will be interesting in the future to examine whether Alp1 and Alp4 expression are regulated differentially by the nutritional status of the larva. In the case of Alp1, this regulation may occur in the epidermis, as tissue-specific KD experiments mapped the requirement for timely pupariation during NR to this tissue - the very same tissue that also utilises tyrosine in cuticle sclerotization.

Insufficient tyrosine was demonstrated to result in the delayed TTP induced by Alp KD, as dietary supplementation with tyrosine rescued or partially rescued TTP. Larvae moved to NR pre-CW, arrest development; this developmental arrest cannot be rescued by transferring pre-CW larvae to NR supplemented with tyrosine. Therefore, as NR supplemented with tyrosine can partially rescue TTP in *Alp1* KD larvae, the delay observed in *Alp1* KD larvae is not thought to be a result of movement to NR pre-CW. Our standard fly food has a tyrosine concentration of 0.5

g/L (Szuperák et al., manuscript in preparation), therefore an addition of (3x) 1.5 g/L tyrosine was chosen for the supplementation experiments. The additional tyrosine solubilised easily into the standard food, however, 1.5 g/L tyrosine is insoluble in NR medium at pH 7. Therefore, supplementation of the NR medium with tyrosine was achieved by acidifying the solution (to pH 4 with 1M HCl) and through creation of a NR solution saturated with tyrosine (see Methods and Materials 2.2.1). Both methods of NR supplementation resulted in a partial rescue in the delayed TTP induced by *Alp1* KD. However, supplementation of standard feed with tyrosine resulted in an almost complete rescue of TTP induced by *Alp4* KD. The lack of a complete rescue in the *Alp1* KD induced delay, may still be a result of insufficient hemolymph tyrosine concentrations. After the transfer to the supplemented NR media, in the TGP, larvae have a limited time to ingest tyrosine (in the media) before the onset of wandering (a period of non-feeding). It could be suggested the period between the move to supplemented NR media and the onset of wandering is too short to ingest sufficient tyrosine for the complete rescue of TTP.

Although, Alp1 has previously been associated with OPT conversion in *Drosophila,* with an aim to provide tyrosine for the process of sclerotization (Harper and Armstrong, 1972), Alp4 has not. I propose the reciprocal action of Alp1 and Alp4, dependent on the feeding state, generates sufficient tyrosine from OPT for sclerotization and tyramine for funnelling into the ecdysone biosynthesis pathway - thus enabling timely developmental progression.

Chapter 6. Discussion

In this thesis, I refined the VDTS method of NMR metabolomics for small sample sizes and then used it to study developmental progression in *Drosophila*. Comparison of the metabolomes from larvae either side of the CW transition identified several polar metabolites that significantly change during fed and/or NR conditions. The functional significance of changes in metabolites in the tyrosine pathway (phenylalanine, tyrosine and OPT) were then explored using genetic analysis. This identified new roles in developmental progression for two OPT phosphatase enzymes, Alp1 and Alp4. I now discuss the main findings of the thesis and their wider implications.

6.1 VDTS is a powerful method for quantifying metabolite concentrations

The VDTS method was initially developed by Ragan et al. (2013) for liquid samples of *Drosophila* hemolymph. Non-specific variation between samples, as a result of variable dilution can mask specific, perhaps significant, variation. PQN has proven itself a robust method to account for overall non-specific variation, delivering greater accuracy for following chemometeric analysis, such as PCA. However, when comparing samples of very different overall signal strengths (a “spectral mass difference” of >50%), such as analysed in this thesis (fed *versus* NR), PQN performs poorly in comparison to normalisation with sample volumes determined via VDTS. The determination of absolute metabolite concentrations back calculated from determined volumes via VDTS provides an additional advantage over relative normalisation methods such as PQN, as absolute metabolite concentrations enable the comparison of results between experiments and between investigators - delivering a means of standardisation to NMR-metabolomics experiments.

Previously, determination of the volume of hemolymph released after cuticle tearing had been comprised by formate contamination. To

increase the accuracy of determined hemolymph volumes, the ^{13}C-formate standard was replaced with a standard not endogenously found in *Drosophila* or on lab-wear: 4-Cl-DNBA. Mock dilution of 4-Cl-DNBA returned precisely determined (via VDTS) volumes of the diluent (water). Furthermore, components of hemolymph were observed not to interact with the standard, avoiding a compromise in volume determinations.

I also adapted the VDTS method for solid samples of whole larvae and adults, optimising a method to achieve thorough and consistent sample homogenisation, through the use of a motorised pellet pestle and the microcentrifuge tube the sample is contained with as a mortar. I also developed a sample variant of the method (MVDTS) where unopened and opened larval samples are paired so as to reduce errors from liquid carry over or larval excretion, which can significantly effect the back calculation of absolute metabolite concentrations. The optimised hemolymph and whole-larval VDTS are powerful metabolomics techniques, enabling the determination of absolute metabolite concentrations in sub-microlitre samples. I anticipate that VDTS and MVDTS can be extended beyond *Drosophila* to other types of liquid and solid samples where volumes are not known or are imprecise.

6.2 The polar metabolome changes at CW

I found that the hemolymph and whole-body metabolite profiles of starved larvae change significantly upon attainment of CW. Although I observed that metabolite level trajectories during NR, more closely match normal development, if NR is administered post-CW, I did not observe a unilateral decrease in metabolite concentrations during pre-CW starvation. In fact, of the 15 metabolites identified to be significantly ($p \leq 0.01$) different between pre- and post-CW NR larvae, ~27% of these metabolites were higher in pre-CW NR larvae. In whole larvae, this percentage rises to ~30%. OPE, betaine and glycine are significantly higher in starved larvae that arrest *versus* those that progress to pupariation. This contrasts with phenylalanine, tyrosine and OPT, which

are significantly higher in starved larvae that progress to pupariation *versus* those that are arrested. Metabolites like OPE, betaine and glycine may decrease in concentration during progression to pupariation either because their dietary uptake/synthesis decreases or because their catabolism decreases. Measuring metabolite concentrations alone cannot distinguish between these two possibilities but this would be possible using stable isotope labelled metabolites and their precursors to measure rates of flux. Before conducting these labelling studies, it would be interesting to test whether supplementing NR medium with OPE, betaine and/or glycine delays TTP of post-CW NR larvae, which normally progress to pupariation.

6.3 Conversion of OPT to tyrosine is required for timely pupariation

Previous observations in fed larvae showed that OPT and tyrosine increase in the *Drosophila* hemolymph after the L2/L3 moult (Lunan and Mitchell, 1969; Mitchell and Lunan, 1964). A new and striking finding from my polar metabolite comparisons is that this rise in OPT and tyrosine in the hemolymph also occurs in starved L3 larvae that will progress to pupariation but not in those starved larvae that will developmentally arrest. The rise in hemolymph OPT during post-CW starvation that I observe cannot be fuelled by dietary uptake of OPT or tyrosine, thus indicating that OPT is formed/released from internal tissue stores. Interestingly, tyrosine “vacuoles” have been observed to form and disappear in the fat body, between moults, in another fly species: *Calpodes* (McDermid and Locke, 1983). Therefore, the release of stored tyrosine or OPT in *Drosophila* could also occur from the fat body. In fact, protein “granules” have previously been observed to accumulate in the fat body of *Drosophila* during L3 development, although they are thought to contain larval serum proteins (Lsps), which are fairly rich in phenylalanine and tyrosine residues (for the major Lsp, LSP-2: 7.1% phenylalanine and 7.94% tyrosine) (Burmester et al., 1999; Mousseron-Grall et al., 1997). One possibility is that attainment of CW triggers a downstream mechanism to release OPT from fat body vacuoles/granules, delivering it

into the hemolymph, where it is subsequently converted to tyrosine. To begin to test this hypothesis, it would be interesting to measure OPT and tyrosine concentrations via NMR, in fat body tissue dissected from late L3 fed, pre- and post-CW NR larvae.

High levels of tyrosine during the final larval instar of many insects has long been associated with the need for phenolic precursors utilised in cuticle tanning/sclerotization (Bodnaryk, 1970; Chen et al., 1978; Mitchell and Lunan, 1964; Parker et al., 1969). Hence, several compounds found at high concentrations during the final larval instar, such as: OPT in *Drosophila melanogaster*; β-glucosyl-O-tyrosine in *Drosophila busckii*; β-alanyl-L-tyrosine in *Sarcophaga bullata*; and γ-L-glutamyl-L-phenylalanine in *Musca domestica,* have been labelled “tyrosine-storage” molecules - able to rapidly liberate tyrosine via an enzymatic conversion process (Bodnaryk, 1970; Chen et al., 1978; Mitchell and Lunan, 1964; Parker et al., 1969). My findings add to this body of work by showing that OPT/tyrosine are not only important for sclerotization but also for regulating the timing of the larval-to-pupal developmental transition. My genetic analysis of two validated OPT phosphatase enzymes Alp1 and Alp4 (Harper and Armstrong, 1972), shows that they are both required for the correct speed of developmental progression. Moreover, I have shown that Alp1 and Alp4 have different developmental functions, depending upon the nutritional status of the larva. Thus, Alp4 and Alp1 are primarily required for timely pupariation in the feeding and non-feeding stages respectively.

It remains to be observed whether nutritional status differently regulates Alp1 and Alp4 expression. This would provide one possible explanation for their distinct roles. For example, expression of Alp1 could be higher in starved than fed larvae, and *vice versa* for Alp4. This could be tested using a quantitative reverse transcriptase polymerase chain reaction (qRT PCR) on whole fed *versus* NR larvae. I was able to demonstrate the expression of Alp1 in the larval epidermis. Alp1 localisation at the cellular level may be at the plasma membrane due to the presence of a glycosylphosphatidylinositol (GPI) anchor, similar to that of Mammalian

placental alkaline phosphatase (Kozlenkov et al., 2002). This lends support to a hypothesis that membrane-tethered Alp1 on epidermal cells is in direct contact with the hemolymph and so is well placed to convert OPT, released from tissue stores, into hemolymph tyrosine. Alp4 expression has previously been observed in the lower segment of the malpighian tubules (Sözen et al., 1997; M Y Yang et al., 2000). Hemolymph is processed by the malpighian tubules (O'Donnell and Maddrell, 1995). Therefore, Alp4 expression in the lower tubule, an area associated with re-absorption, suggests that it could be involved with tyrosine reclamation from filtered OPT that "escaped" Alp1 action.

This thesis shows that enzymes required for the OPT-to-tyrosine conversion are required for timely development. This finding is highly likely to link with recent work from Ohhara et al., (2015), who observed that a tyramine biosynthetic enzyme (Tdc2) and its receptor (Octβ3R) are required in steroidogenic PG cells to stimulate ecdysone synthesis and thus promote a timely transition from larva-to-pupa. Tyramine is connected to tyrosine metabolism (see Figure 5-3) and I have found that, during L3 progression, Alp1 and Alp4 are required (directly or indirectly) not only for the decrease in the OPT:Tyr ratio but also for the accompanying decrease in whole body tyramine. In double *Alp4*, *Alp1* KD larvae, higher OPT:Tyr and tyramine in the whole body may be indicative of a lower OPT to tyrosine conversion and perhaps also tyramine retention in tissues including the PG. Such retention of tyramine has been previously observed in the PG of arrested larvae that were starved before CW (Ohhara et al., 2015). In future it will be important to test how connected the Ohhara et al. mechanism is with Alp function by examining anti-tyramine staining in the PG of *Alp4i;;Alp1i* larvae. It will also be interesting to see if the developmental delay of *Alp4i;;Alp1i* larvae can be rescued by ecdysone supplementation. Another critical experiment is to follow up the rescue of TTP in *Alp4i;;Alp1i* larvae by dietary tyrosine, by now testing whether such a rescue is blocked when Octβ3R is also inactivated in the PG. This key experiment is complex and will require combined use of GAL4/UAS and another orthologous gene-expression channel such as that involving the LexA/LexOp system (Lai and Lee, 2006; Pfeiffer et al., 2010).

From my data and those of Ohhara et al., (2015) a speculative working model, linking tyrosine metabolism to ecdysone biosynthesis, can be built (Figure 6-1). This model explains how free tyrosine is liberated from its OPT storage form by Alp1 and/or Alp4. A surge of tyrosine in the hemolymph during L3 is required for tyramine synthesis and storage in the PG. This stored tyramine is then released from the PG late in L3 to activate the Octβ3R in an autocrine manner to thus stimulate the Halloween genes, necessary for synthesis of the large bust of ecdysone that precedes pupariation. Speculations made in the model on the expression of Alp1, Alp4 and the hydroxylase activity of Hn during fed and starved conditions could be tested via qRT PCR. Whilst the un/delayed release of tyramine from the PG (the “release” arrow in the model) could be tested by anti-tyramine staining of the PG from control and *Alp4i;;Alp1i* larvae at various stages. Ohhara et al., (2015) postulated that a surge in Octβ3R-mediated tyramine signalling in the PG after CW could increase PG cell responsivness to IIS and PTTH neuropeptide signalling, thus helping to drive the large ecdysone pulse that triggers the larval to pupal transition. My findings now suggest that this PG signalling surge could be driven by the increase in OPT release from tissue stores and subsequent Alp-mediated OPT-to-tyrosine conversion. Increased tyrosine release late in L3 would then help to coordinate the timing of developmental progression (providing a tyramine precursor) and with the process of sclerotization (providing phenolic cuticle precursors).

In mammals, the seceretion of the key human development hormone, GnRH, is regulated by monoamines and, during pubertal maturation, a significant increase in the frequency of GnRH pulses is observed (Sisk and Foster, 2004; Swerdloff and Odell, 1975). The moelcular mechanism regulating this developmental increase in GnRH secretion is not yet known and it would be intersting to test if “monoamine-storage” compounds are involved. In a more striking fly-mammal parallel, catecholamine signalling in Leydig cells of the fetal testis occurs via GPCR receptors related to Octβ3R and this stimulates production of the steroid hormone testosterone (Pointis and Latreille, 1987). This suggests

that monoamine signalling may be a conserved feature of the regulation of steriod hormone production in both insects and mammals.

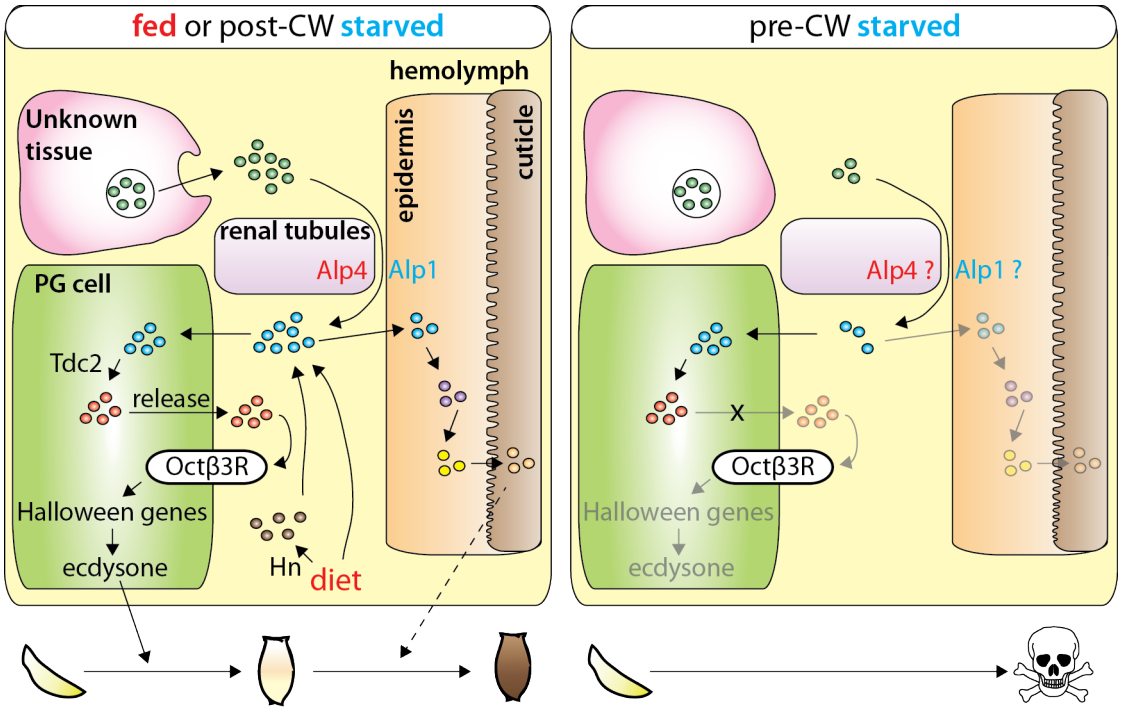
fed or post-CW starved
pre-CW starved
hemolymph
Unknown tissue
epidermis
cuticle
renal tubules
Alp4
Alp1
PG cell
Tdc2
release
Octβ3R
Halloween genes
ecdysone
Hn
diet
Alp4 ?
Alp1 ?
x

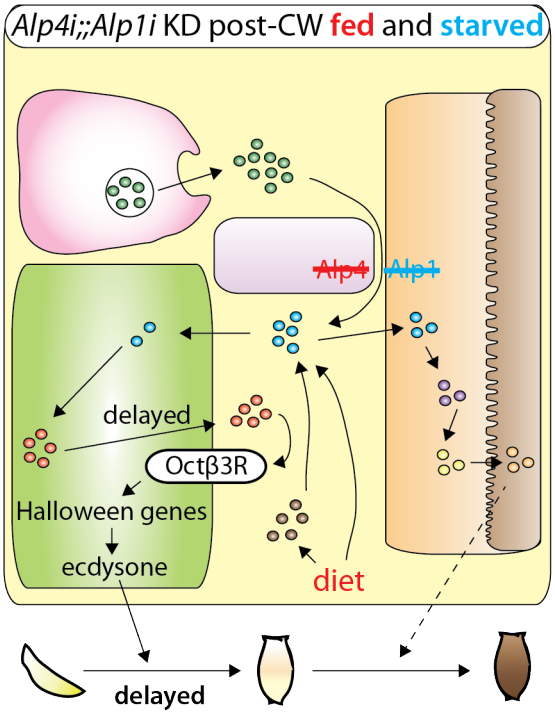
Alp4i;;Alp1i KD post-CW fed and starved
Alp4
Alp1
delayed
Octβ3R
Halloween genes
ecdysone
diet
delayed

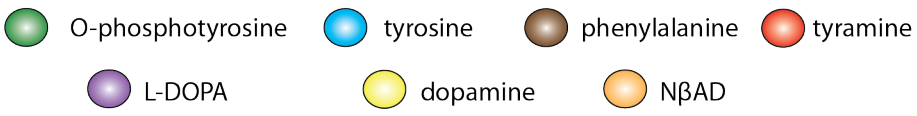
O-phosphotyrosine
tyrosine
phenylalanine
tyramine
L-DOPA
dopamine
NβAD

Figure 6-1: Speculative model for the function of tyrosine in timely developmental progression.

Differential tyrosine generation in normally developing, pre-CW starved and double Alp KD (*Alp4i;;Alp1i*) larvae, may affect developmental progression via the regulation of ecdysone biosynthesis. Red text corresponds to processes active during fed conditions, blue text corresponds to processes active during NR. Transparent sections denote pathways no longer active.

Fed or post-CW starved larvae: Work in this thesis suggests OPT is released into the hemolymph from an unknown tissue source and subsequently converted into tyrosine via Alp1 in the larval epidermis and Alp 4 in the malpighian tubules. Tyrosine is also acquired from the diet and from dietary phenylalanine via Henna (Hn). Tyrosine is subsequently converted within the PG to tyramine via Tdc2. Ohhara et al. 2015 reported how tyramine is secreted from the PG and activates Octβ3R, which regulates Halloween gene expression, enabling generation of sufficient ecdysone for the “puparial ecdysone pulse” and timely development. Tyrosine is also converted into L-DOPA in the epidermis and subsequently into dopamine via Pale and Dopa-decarboxylase respectively. Dopamine is then metabolised through a series of reactions into diphenolic compounds (detailed in Figure 5-1) that are incorporated into the cuticle.

Pre-CW starved larvae: OPT is not efficiently released from the unknown tissue source into the hemolymph. Phenylalanine levels were observed to be below the detection limit but it is not known how starvation affects the expression levels of Alp1 and Alp4. However, Ohhara et al. 2015 reported that tyramine is retained within the PG such that Octβ3R is not activated, the "puparial" ecdysone pulse is not generated and development arrests. In addition, pre-CW starved larvae do not undergo cuticle tanning.

Alp1/4 double KD in fed or post-CW starved larvae: OPT is released into the hemolymph from the unknown tissue source and subsequently converted into tyrosine but at a reduced rate, due to knockdown of the *Alp1* and *Alp4* phosphatases. In turn, this may decrease the synthesis of tyramine and delay its release from the PG, thus resulting in a delayed “puparial" ecdysone pulse and increased TTP, which correlates with a delay but not a complete block in cuticle tanning.

Chapter 7. Appendix

Pipette volume added (µL)	VDTS calculated volume (µL)
4 µL # 1	3.6
4 µL # 2	5.0
4 µL # 3	4.6
10 µL # 1	10.4
10 µL # 2	9.5
10 µL # 3	9.8

Table 5: VDTS calculation of water volumes diluted into 4-Cl-DNBA.

The table displays volumes of water (µL) that were determined by VDTS to have diluted into the 20 µL droplet of 4 mM 4-Cl-DNBA. Each dilution was done in triplicate.

	Average hemolymph volume per larva (nL)	
	Males	**Females**
Pre-CW fed	182 ± 49	312 ± 81
Post-CW fed	292 ± 11	506 ± 83
Continuously fed	364 ± 88	698 ± 100
Pre-CW NR	679 ± 23	627 ± 82
Post-CW NR	456 ± 151	368 ± 1

Table 6: VDTS calculation of hemolymph volumes.

Entries show mean volume of hemolymph released ± 1 standard deciation for two independent experiments of three biological replicates for each condition (n=6). In each condition 10 larvae are "opened" to release hemolymph into a 10 μL drop of 4 mM 4-Cl-DNBA.

	Average homogenate volume per whole larva (μL)	
	Males	**Females**
Pre-CW fed	0.35 ± 0.10	0.33 ± 0.08
Post-CW fed	0.58 ± 0.28	0.58 ± 0.37
Continuously fed	0.77 ± 0.17	1.08 ± 0.14
Pre-CW NR	0.36 ± 0.04	0.34 ± 0.08
Post-CW NR	0.45 ± 0.17	0.33 ± 0.04

Table 7: VDTS calculation of whole larval homogenate volumes.

Entries show mean volume of homogenate recovered ± 1 standard deviation for two independent experiments, each with three biological replicates per condition (n=6). In each condition 10 larvae are homogenised in a 10 μL drop of 25 mM ^{13}C formate.

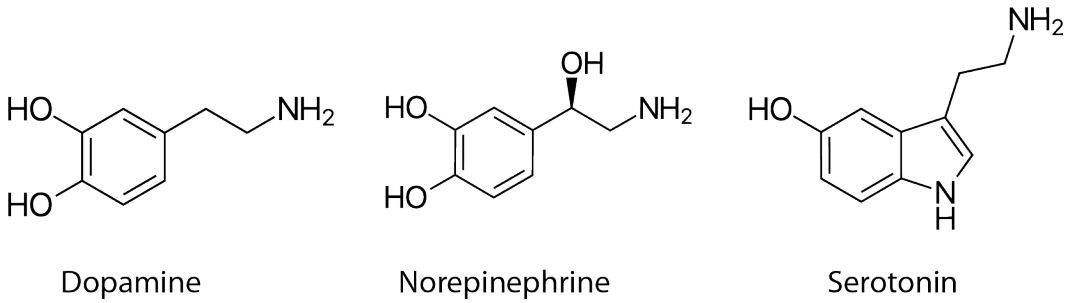

Dopamine Norepinephrine Serotonin

Figure 7-1: Chemical structures of the monoamines that regulate GnRH pulses in the HPG axis.

Reference List

Abdi, H., 2010. Partial least squares regression and projection on latent structure regression (PLS Regression). Wiley Interdiscip. Rev. Comput. Stat. 2, 97–106. doi:10.1002/wics.51

Abdi, H., Williams, L., 2010. Tukey's honestly significant difference (HSD) test. Encycl. Res. Des. Thousand Oaks.

Adamko, D.J., Saude, E., Bear, M., Regush, S., Robinson, J.L., 2016. Urine metabolomic profiling of children with respiratory tract infections in the emergency department: a pilot study. BMC Infect. Dis. 16, 439. doi:10.1186/s12879-016-1709-6

Ahima, R.S., Prabakaran, D., Mantzoros, C., Qu, D., Lowell, B., Maratos-Flier, E., Flier, J.S., 1996. Role of leptin in the neuroendocrine response to fasting. Nature 382, 250–252. doi:10.1038/382250a0

An, P.N. guyen T., Yamaguchi, M., Bamba, T., Fukusaki, E., 2014. Metabolome analysis of Drosophila melanogaster during embryogenesis. PLoS One 9, e99519. doi:10.1371/journal.pone.0099519

Andersen, S.O., 2010. Insect cuticular sclerotization: A review. Insect Biochem. Mol. Biol. 40, 166–178. doi:10.1016/j.ibmb.2009.10.007

Andres, A.J., Thummel, C.S., 1995. The Drosophila 63F early puff contains E63-1, an ecdysone-inducible gene that encodes a novel Ca(2+)-binding protein. Development 121, 2667–79.

Ang, J.E., Revell, V., Mann, A., Mäntele, S., Otway, D.T., Johnston, J.D., Thumser, A.E., Skene, D.J., Raynaud, F., 2012. Identification of human plasma metabolites exhibiting time-of-day variation using an untargeted liquid chromatography-mass spectrometry metabolomic approach. Chronobiol. Int. 29, 868–81. doi:10.3109/07420528.2012.699122

Ashburner, M., Bergman, C.M., 2005. Drosophila melanogaster : A case study of a model genomic sequence and its consequences. Cold Spring Harb. Perspect. Biol. 15, 1661–1667. doi:10.1101/gr.3726705.15

Ashburner, M., Chihara, C., Meltzer, P., Richards, G., 1974. Temporal Control of Puffing Activity in Polytene Chromosomes. Cold Spring Harb. Symp. Quant. Biol. 38, 655–662. doi:10.1101/SQB.1974.038.01.070

Ashburner, M., Richards, G., 1976. Sequential gene activation by ecdysone in polytene chromosomes of Drosophila melanogaster,. Dev. Biol. 54, 241–255. doi:10.1016/0012-1606(76)90302-X

Bakker, K., 1959. Feeding period, growth, and pupation in larvae of Drosophila melanogaster. Entomol. Exp. Appl. 2, 171–186. doi:10.1111/j.1570-7458.1959.tb00432.x

Balcı, M., 2005. Basic ^{1}H- and ^{13}C-NMR spectroscopy. Elsevier.

Baumann, A., Barry, J., Wang, S., Fujiwara, Y., Wilson, T.G., 2010. Paralogous genes involved in juvenile hormone action in Drosophila melanogaster. Genetics 185, 1327–1336. doi:10.1534/genetics.110.116962

Beadle, G., Tatum, E., Clancy, C., 1938. Food level in relation to rate of development and eye pigmentation in Drosophila melanogaster. Biol. Bull.

Beckman, L., Johnson, F.M., 1964. Variations in larval Alkaline Phosphate controlled by Aph alleles in Drosophila Melanogaster. Genetics 49, 829–835.

Bender, M., Imam, F.B., Talbot, W.S., Ganetzky, B., Hogness, D.S., 1997. Drosophila ecdysone receptor mutations reveal functional differences among receptor isoforms. Cell 91, 777–788. doi:10.1016/S0092-8674(00)80466-3

Bligh, E.G., Dyer, W.J., 1959. A rapid method of total lipid extraction and purification. Can. J. Biochem. Physiol. 37, 911–917. doi:10.1139/o59-099

Bodnaryk, R.P., 1970. Biosynthesis of gamma-l-glutamyl-l-phenylalanine by the larva of the housefly Musca domestica. J. Insect Physiol. 16, 919–929.

Brand, A.H., Perrimon, N., 1993. Targeted gene expression as a means of altering cell fates and generating dominant phenotypes. Development 118, 401–15. doi:10.1101/lm.1331809

Burmester, T., Antoniewski, C., Lepesant, J. a., 1999. Ecdysone-regulation of synthesis and processing of Fat Body Protein 1, the larval serum protein receptor of Drosophila melanogaster. Eur. J. Biochem. 262, 49–55.

Callier, V., Shingleton, A.W., Brent, C.S., Ghosh, S.M., Kim, J., Harrison, J.F., 2013. The role of reduced oxygen in the developmental physiology of growth and metamorphosis initiation in Drosophila melanogaster. J. Exp.

Biol. 216, 4334–40. doi:10.1242/jeb.093120

Camacho, D., Fuente, A., Mendes, P., 2005. The origin of correlations in metabolomics data. Metabolomics 1, 53–63. doi:10.1007/s11306-005-1107-3

Cameron, N., 1976. Weight and skinfold variation at menarche and the critical body weight hypothesis. Ann. Hum. Biol. 3, 279–282. doi:10.1080/03014467600001451

Carvalho, M., Sampaio, J.L., Palm, W., Brankatschk, M., Eaton, S., Shevchenko, A., 2012. Effects of diet and development on the Drosophila lipidome. Mol. Syst. Biol. 8, 600. doi:10.1038/msb.2012.29

Casanueva, F.F., Dieguez, C., 1999. Neuroendocrine Regulation and Actions of Leptin. Front. Neuroendocrinol. 20, 317–363. doi:10.1006/frne.1999.0187

Celniker, S.E., Dillon, L.A.L., Gerstein, M.B., Gunsalus, K.C., Henikoff, S., Karpen, G.H., Kellis, M., Lai, E.C., Lieb, J.D., MacAlpine, D.M., Micklem, G., Piano, F., Snyder, M., Stein, L., White, K.P., Waterston, R.H., 2009. Unlocking the secrets of the genome. Nature 459, 927–930. doi:10.1038/459927a

Chávez, V.M., Marqués, G., Delbecque, J.P., Kobayashi, K., Hollingsworth, M., Burr, J., Natzle, J.E., O'Connor, M.B., 2000. The *Drosophila disembodied* gene controls late embryonic morphogenesis and codes for a cytochrome P450 enzyme that regulates embryonic ecdysone levels. Development 127, 4115–4126.

Chen, C., Jack, J., Garofalo, R.S., 1996. The Drosophila insulin receptor is required for normal growth. Endocrinology 137, 846–856. doi:10.1210/endo.137.3.8603594

Chen, P.S., Mitchell, H.K., Neuweg, M., 1978. Tyrosine glucoside in Drosophila busckii. Insect Biochem. 8, 279–286. doi:10.1016/0020-1790(78)90038-0

Cheng, L.Y., Bailey, A.P., Leevers, S.J., Ragan, T.J., Driscoll, P.C., Gould, A.P., 2011. Anaplastic lymphoma kinase spares organ growth during nutrient restriction in Drosophila. Cell 146, 435–47.

Cheung, C.C., Thornton, J.E., Kuijper, J.L., Weigle, D.S., Clifton, D.K., Steiner, R.A., 1997. Leptin Is a Metabolic Gate for the Onset of Puberty in the

Female Rat. Endocrinology 138, 855–858. doi:10.1210/endo.138.2.5054

Church, R.B., Robertson, F.W., 1966. A biochemical study of the growth of Drosophila melanogaster. J. Exp. Zool. 162, 337–352.

Colombani, J., Bianchini, L., Layalle, S., Pondeville, E., Dauphin-Villemant, C., Antoniewski, C., Carré, C., Noselli, S., Léopold, P., 2005. Antagonistic actions of ecdysone and insulins determine final size in Drosophila. Science 310, 667–70. doi:10.1126/science.1119432

Currie, C., Ahluwalia, N., Godeau, E., Gadhainn, S.N., Due, P., Currie, D.B., 2009. The health behaviour in school-aged children: WHO collaborative cross-national (HBSC) study: Origins, concept, history and development 1982-2008. Int. J. Public Health 54. doi:10.1007/s00038-009-5404-x

Daimon, T., Kozaki, T., Niwa, R., Kobayashi, I., Furuta, K., Namiki, T., Uchino, K., Banno, Y., Katsuma, S., Tamura, T., Mita, K., Sezutsu, H., Nakayama, M., Itoyama, K., Shimada, T., Shinoda, T., 2012. Precocious Metamorphosis in the Juvenile Hormone–Deficient Mutant of the Silkworm, Bombyx mori. PLoS Genet. 8, e1002486. doi:10.1371/journal.pgen.1002486

De Moed, G.H., Kruitwagen, C.L.J.J., De Jong, G., Scharloo, W., 1999. Critical weight for the induction of pupariation in Drosophila melanogaster: genetic and environmental variation. J. Evol. Biol. 12, 852–858. doi:10.1046/j.1420-9101.1999.00103.x

De Reggi, M.L., Hirin, M.H., Delaage, M.A., 1975. Radioimmunoassay of ecdysone. An application to Drosophila larvae and pupae. Biochem. Biophys. Res. Commun. 66, 1307–1315.

Di Cara, F., King-Jones, K., 2013. How Clocks and Hormones Act in Concert to Control the Timing of Insect Development. pp. 1–36. doi:10.1016/B978-0-12-396968-2.00001-4

Dieterle, F., Ross, A., Schlotterbeck, G., Senn, H., 2006. Probabilistic quotient normalization as robust method to account for dilution of complex biological mixtures. Application in 1H NMR metabonomics. Anal. Chem. 78, 4281–90. doi:10.1021/ac051632c

Dietzl, G., Chen, D., Schnorrer, F., Su, K.-C., Barinova, Y., Fellner, M., Gasser,

B., Kinsey, K., Oppel, S., Scheiblauer, S., Couto, A., Marra, V., Keleman, K., Dickson, B.J., 2007. A genome-wide transgenic RNAi library for conditional gene inactivation in Drosophila. Nature 448, 151–6. doi:10.1038/nature05954

Edgar, B.A., 2006. How flies get their size: genetics meets physiology. Nat. Rev. Genet. 7, 907–916. doi:10.1038/nrg1989

Edgar, B.A., 1999. From small flies come big discoveries about size control. Nat. Cell Biol. 1, E191-3. doi:10.1038/70217

Fan, T.W.-M., Lane, A.N., 2016. Applications of NMR spectroscopy to systems biochemistry. Prog. Nucl. Magn. Reson. Spectrosc. 92–93, 18–53. doi:10.1016/j.pnmrs.2016.01.005

Fernández-Fernández, R., Navarro, V.M., Barreiro, M.L., Vigo, E.M., Tovar, S., Sirotkin, A. V., Casanueva, F.F., Aguilar, E., Dieguez, C., Pinilla, L., Tena-Sempere, M., 2005. Effects of Chronic Hyperghrelinemia on Puberty Onset and Pregnancy Outcome in the Rat. Endocrinology 146, 3018–3025. doi:10.1210/en.2004-1622

Flockhart, I., Booker, M., Kiger, A., Boutros, M., Armknecht, S., Ramadan, N., Richardson, K., Xu, A., Perrimon, N., Mathey-Prevot, B., 2006. FlyRNAi: the Drosophila RNAi screening center database. Nucleic Acids Res. 34, D489-94. doi:10.1093/nar/gkj114

Frisch, R.., Revelle, R., Cook, S., 1973. Components of Weight at Menarche and the Initiation of the Adolescent Growth Spurt in Girls : Estimated Total Water , Lean Body Weight and Fat. Hum. Biol. 45, 469–483.

Frisch, R.E., 1981. Nutrition, fatness, puberty, and fertility. Compr. Ther. 7, 15–23.

Frisch, R.E., 1972. Weight at menarche: similarity for well-nourished and undernourished girls at differing ages, and evidence for historical constancy. Pediatrics 50.

Frisch, R.E., McArthur, J.W., 1974. Menstrual Cycles: Fatness as a Determinant of Minimum Weight for Height Necessary for Their Maintenance or Onset. Science (80-.). 185, 949–951. doi:10.1126/science.185.4155.949

Frisch, R.E., Revelle, R., 1971. Height and weight at menarche and a

hypothesis of menarche. Arch. Dis. Child. 46, 695–701.

Frisch, R.E., Revelle, R., 1970. Height and weight at menarche and a hypothesis of critical body weights and adolescent events. Science (80-.). 169, 397–9. doi:10.1126/science.169.3943.397

Froguel, P., Clément, K., Vaisse, C., Lahlou, N., Cabrol, S., Pelloux, V., Cassuto, D., Gourmelen, M., Dina, C., Chambaz, J., Lacorte, J.-M., Basdevant, A., Bougnères, P., Lebouc, Y., Guy-Grand, B., 1998. A mutation in the human leptin receptor gene causes obesity and pituitary dysfunction. Nature 392, 398–401. doi:10.1038/32911

Fuchs, S., Bundy, J.G., Davies, S.K., Viney, J.M., Swire, J.S., Leroi, A.M., 2010. A metabolic signature of long life in Caenorhabditis elegans. BMC Biol. 8, 14. doi:10.1186/1741-7007-8-14

Galko, M.J., Krasnow, M.A., 2004. Cellular and Genetic Analysis of Wound Healing in Drosophila Larvae. PLoS Biol. 2, e239. doi:10.1371/journal.pbio.0020239

Ghosh, S.M., Testa, N.D., Shingleton, A.W., 2013. Temperature-size rule is mediated by thermal plasticity of critical size in Drosophila melanogaster. Zookeys 298. doi:10.1098/rspb.2013.0174

Gibbens, Y.Y., Warren, J.T., Gilbert, L.I., O'Connor, M.B., 2011. Neuroendocrine regulation of Drosophila metamorphosis requires TGFbeta/Activin signaling. Development 138, 2693–703. doi:10.1242/dev.063412

Gilbert, L.I., 2004. Halloween genes encode P450 enzymes that mediate steroid hormone biosynthesis in Drosophila melanogaster. Mol. Cell. Endocrinol. 215, 1–10. doi:10.1016/j.mce.2003.11.003

Gilbert, L.I., Rybczynski, R., Warren, J.T., 2002. Control and biochemical nature of the ecdysteroidogenic pathway. Annu. Rev. Entomol. 47, 883–916.

Gogna, N., Singh, V.J., Sheeba, V., Dorai, K., 2015. NMR-based investigation of the Drosophila melanogaster metabolome under the influence of daily cycles of light and temperature. Mol. Biosyst. 11, 3305–3315. doi:10.1039/c5mb00386e

Gowda, G.A.N., Raftery, D., 2017. Recent Advances in NMR-Based

Metabolomics. Anal. Chem. 89, 490–510. doi:10.1021/acs.analchem.6b04420

Grumbach, M., Grave, G., Mayer, F., 1974. Control of the Onset of Puberty. John Wiley Sons 1.

Grumbach, M.M., 1978. The Central Nervous System and the Onset of Puberty, in: Human Growth. Springer US, Boston, MA, pp. 215–238. doi:10.1007/978-1-4684-2622-9_8

Gunther, U., Ludwig, C., Ruterjans, H., 2000. NMRLAB-Advanced NMR data processing in matlab. J. Magn. Reson. 145, 201–8. doi:10.1006/jmre.2000.2071

Harper, R.A., Armstrong, F.B., 1973. Alkaline phosphatase of Drosophila melanogaster. II. Biochemical comparison among four allelic forms. Biochem. Genet. 10, 29–38. doi:10.1007/BF00485746

Harper, R.A., Armstrong, F.B., 1972. Alkaline phosphatase of Drosophila melanogaster. I. Partial purification and characterization. Biochem. Genet. 6, 75–82. doi:10.1007/BF00485968

Heinrichsen, E.T., Zhang, H., Robinson, J.E., Ngo, J., Diop, S., Bodmer, R., Joiner, W.J., Metallo, C.M., Haddad, G.G., 2014. Metabolic and transcriptional response to a high-fat diet in Drosophila melanogaster. Mol. Metab. 3, 42–54. doi:10.1016/j.molmet.2013.10.003

Hill, J.W., Elmquist, J.K., Elias, C.F., 2008. Hypothalamic pathways linking energy balance and reproduction. Am. J. Physiol. Endocrinol. Metab. 294, E827–E832. doi:10.1152/ajpendo.00670.2007

Hu, X., Cherbas, L., Cherbas, P., 2003. Transcription Activation by the Ecdysone Receptor (EcR/USP): Identification of Activation Functions. Mol. Endocrinol. 17, 716–731. doi:10.1210/me.2002-0287

Kanehisa, M., Bundy, J.G., Davies, S.K., Viney, J.M., Swire, J.S., Leroi, A.M., Katayama, T., Araki, M., Hirakawa, M., Tokimatsu, T., Yamanishi, Y., Gallup, D., Ilkayeva, O., Wenner, B., Yancy, W., Eisenson, H., Musante, G., Surwit, R., Millington, D., Butler, M., Svetkey, L., Paton, N., Lilley, K., Kell, D., Oliver, S., 2000. KEGG: Kyoto Encyclopedia of Genes and Genomes. Nucleic Acids Res. 28, 27–30. doi:10.1093/nar/28.1.27

Kapoor, A.K., Kapoor, S., 1986. The effects of high altitude on age at menarche and menopause. Int. J. Biometeorol. 30, 21–26. doi:10.1007/BF02192054

Karim, F.D., Thummel, C.S., 1991. Ecdysone coordinates the timing and amounts of E74A and E74B transcription in Drosophila. Genes Dev. 5, 1067–1079. doi:10.1101/gad.5.6.1067

Karlson, P., Sekeris, C.E., 1962. N-Acetyl-dopamine as Sclerotizing Agent of the Insect Cuticle. Nature 195, 183–184. doi:10.1038/195183a0

Keeler, J., 2010. Understanding NMR spectroscopy. Wiley.

Kelch, R.P., Kaplan, S.L., Ghumbach, M.M., 1973. Suppression of urinary and plasma follicle-stimulating hormone by exogenous estrogens in prepubertal and pubertal children. J. Clin. Invest. 52, 1122–8. doi:10.1172/JCI107278

Kemsley, E.K., 1996. Discriminant analysis of high-dimensional data: a comparison of principal components analysis and partial least squares data reduction methods. Chemom. Intell. Lab. Syst. 33, 47–61. doi:10.1016/0169-7439(95)00090-9

Kennedy, G.C., Mitra, J., 1963. Body weight and food intake as initiating factors for puberty in the rat. J. Physiol. 166, 408–418. doi:10.1113/jphysiol.1963.sp007112

Kershaw, E.E., Flier, J.S., 2004. Adipose Tissue as an Endocrine Organ. J. Clin. Endocrinol. Metab. 89, 2548–2556. doi:10.1210/jc.2004-0395

Koelle, M.R., Talbot, W.S., Segraves, W.A., Bender, M.T., Cherbas, P., Hogness, D.S., 1991. The *Drosophila EcR* gene encodes an ecdysone receptor, a new member of the steroid receptor superfamily. Cell 67, 59–77. doi:10.1016/0092-8674(91)90572-G

Koyama, T., Rodrigues, M.A., Athanasiadis, A., Shingleton, A.W., Mirth, C.K., 2014. Nutritional control of body size through FoxO-Ultraspiracle mediated ecdysone biosynthesis. Elife 3, e03091. doi:10.7554/eLife.03091

Kozlenkov, A., Manes, T., Hoylaerts, M.F., Mill??n, J.L., 2002. Function assignment to conserved residues in mammalian alkaline phosphatases. J. Biol. Chem. 277, 22992–22999. doi:10.1074/jbc.M202298200

Lai, S.-L., Lee, T., 2006. Genetic mosaic with dual binary transcriptional systems in Drosophila. Nat. Neurosci. 9, 703–709. doi:10.1038/nn1681

Lee, T., Luo, L., 1999. Mosaic Analysis with a Repressible Cell Marker for Studies of Gene Function in Neuronal Morphogenesis. Neuron 22, 451–461. doi:10.1016/S0896-6273(00)80701-1

Lehmann, M., 1996. Drosophila Sgs genes: Stage and tissue specificity of hormone responsiveness. BioEssays 18, 47–54. doi:10.1002/bies.950180110

Ludwig, C., Günther, U.L., 2011. MetaboLab - advanced NMR data processing and analysis for metabolomics.

Lunan, K.D., Mitchell, H.K., 1969. The metabolism of tyrosine-O-phosphate in Drosophila. Arch. Biochem. Biophys. 132, 450–456. doi:10.1016/0003-9861(69)90388-9

Markley, J.L., Brüschweiler, R., Edison, A.S., Eghbalnia, H.R., Powers, R., Raftery, D., Wishart, D.S., 2017. The future of NMR-based metabolomics. Curr. Opin. Biotechnol. 43, 34–40. doi:10.1016/j.copbio.2016.08.001

Marygold, S.J., 2015. Alkaline phosphatase genes in D. melanogaster.

McBrayer, Z., Ono, H., Shimell, M., Parvy, J.P., Beckstead, R.B., Warren, J.T., Thummel, C.S., Dauphin-Villemant, C., Gilbert, L.I., O'Connor, M.B., 2007. Prothoracicotropic Hormone Regulates Developmental Timing and Body Size in Drosophila. Dev. Cell 13, 857–871. doi:10.1016/j.devcel.2007.11.003

McDermid, H., Locke, M., 1983. Tyrosine storage vacuoles in insect fat body. Tissue Cell 15, 137–158. doi:10.1016/0040-8166(83)90039-3

Mercier, P., Lewis, M.J., Chang, D., Baker, D., Wishart, D.S., 2011. Towards automatic metabolomic profiling of high-resolution one-dimensional proton NMR spectra. J. Biomol. NMR 49, 307–23. doi:10.1007/s10858-011-9480-x

Minami, Y., Kasukawa, T., Kakazu, Y., Iigo, M., Sugimoto, M., Ikeda, S., Yasui, A., van der Horst, G.T.J., Soga, T., Ueda, H.R., 2009. Measurement of internal body time by blood metabolomics. Proc. Natl. Acad. Sci. U. S. A. 106, 9890–5. doi:10.1073/pnas.0900617106

Mirth, C., Riddiford, L., 2007. Size assessment and growth control: how adult size is determined in insects. Bioessays.

Mirth, C., Truman, J.W., Riddiford, L.M., 2005. The role of the prothoracic gland

in determining critical weight for metamorphosis in Drosophila melanogaster. Curr. Biol. 15, 1796–807. doi:10.1016/j.cub.2005.09.017

Mirth, C.K., Shingleton, A.W., 2012. Integrating Body and Organ Size in Drosophila: Recent Advances and Outstanding Problems. Front. Endocrinol. (Lausanne). 3, 49. doi:10.3389/fendo.2012.00049

Mitchell, H.K., Lunan, K.D., 1964. Tyrosine-O-phosphate in Drosophila. Arch. Biochem. Biophys. 106, 219–222. doi:10.1016/0003-9861(64)90179-1

Mizoguchi, A., Oka, T., Kataoka, H., Nagasawa, H., Suzuki, A., Ishizaki, H., 1990. Immunohistochemical Localization of Prothoracicotropic Hormone-Producing Neurosecretory Cells in the Brain of Bombyx mori. Dev. Growth Differ. 32, 591–598. doi:10.1111/j.1440-169X.1990.00591.x

Mou, X., Duncan, D.M., Baehrecke, E.H., Duncan, I., 2012. Control of target gene specificity during metamorphosis by the steroid response gene E93. Proc. Natl. Acad. Sci. U. S. A. 109, 2949–54. doi:10.1073/pnas.1117559109

Mousseron-Grall, S., Kejzlarova-Lepesant, J., Burmester, T., Chihara, C., Barray, M., Delain, E., Pictet, R., Lepesant, J. a, 1997. Sequence, structure and evolution of the ecdysone-inducible Lsp-2 gene of Drosophila melanogaster. Eur J Biochem 245, 191–198. doi:10.1111/j.1432-1033.1997.00191.x

Nagana Gowda, G.A., Raftery, D., 2015. Can NMR solve some significant challenges in metabolomics? J. Magn. Reson. 260, 144–60. doi:10.1016/j.jmr.2015.07.014

Nijhout, H.F., 1975. A Threshold Size For Metamorphosis In The Tobacoo Hornworm, Manduca Sexta (L.). Biol. Bull. 149, 214–225. doi:10.2307/1540491

Nijhout, H.F., Williams, C.M., 1974. Control of moulting and metamorphosis in the Tobacco Hornworm, Manduca Sexta (L.): Cessation of Juvenile hormone secretion as a trigger for pupation. J. Exp. Biol 6, 493–501.

Nimrod, A., Ryan, K.J., 1975. Aromatization of Androgens by Human Abdominal and Breast Fat Tissue. J. Clin. Endocrinol. Metab. 40, 367–372. doi:10.1210/jcem-40-3-367

Niwa, R., Namiki, T., Ito, K., Shimada-Niwa, Y., Kiuchi, M., Kawaoka, S., Kayukawa, T., Banno, Y., Fujimoto, Y., Shigenobu, S., Kobayashi, S., Shimada, T., Katsuma, S., Shinoda, T., 2010. Non-molting glossy/shroud encodes a short-chain dehydrogenase/reductase that functions in the "Black Box" of the ecdysteroid biosynthesis pathway. Development 137, 1991–9. doi:10.1242/dev.045641

Nüsslein-Volhard, C., Wieschaus, E., 1980. Mutations affecting segment number and polarity in Drosophila. Nature 287, 795–801. doi:10.1038/287795a0

O'Donnell, M.J., Maddrell, S.H., 1995. Fluid reabsorption and ion transport by the lower Malpighian tubules of adult female Drosophila. J. Exp. Biol. 198, 1647–1653.

Ober, C., Loisel, D.A., Gilad, Y., 2008. Sex-specific genetic architecture of human disease. Nat. Rev. Genet. 9, 911–922. doi:10.1038/nrg2415

Ohhara, Y., Shimada-Niwa, Y., Niwa, R., Kayashima, Y., Hayashi, Y., Akagi, K., Ueda, H., Yamakawa-Kobayashi, K., Kobayashi, S., 2015. Autocrine regulation of ecdysone synthesis by β3-octopamine receptor in the prothoracic gland is essential for Drosophila metamorphosis. Proc. Natl. Acad. Sci. U. S. A. 112, 1452–1457. doi:10.1073/pnas.1414966112

Osler, D.C., Crawford, J.D., 1973. Examination of the hypothesis of a critical weight at menarche in ambulatory and bedridden mentally retarded girls. Pediatrics 51.

Ou, Q., King-Jones, K., 2013. What goes up must come down: transcription factors have their say in making ecdysone pulses. Curr. Top. Dev. Biol. 103, 35–71. doi:10.1016/B978-0-12-385979-2.00002-2

Ou, Q., Magico, A., King-Jones, K., Berreur-Bonnenfant, J., Belinski-Deutsch, S., 2011. Nuclear Receptor DHR4 Controls the Timing of Steroid Hormone Pulses During Drosophila Development. PLoS Biol. 9, e1001160. doi:10.1371/journal.pbio.1001160

Padmanabha, D., Baker, K.D., 2014. Drosophila gains traction as a repurposed tool to investigate metabolism. Trends Endocrinol. Metab.

Parent, A.-S., Teilmann, G., Juul, A., Skakkebaek, N.E., Toppari, J.,

Bourguignon, J.-P., 2003. The Timing of Normal Puberty and the Age Limits of Sexual Precocity: Variations around the World, Secular Trends, and Changes after Migration. Endocr. Rev. 24, 668–693. doi:10.1210/er.2002-0019

Parker, S.B., Levenbook, B.L., Bodnaryk, R.P., Spande, T.F., 1969. β-alanyl-L-tyrosine. Chemical synthesis, properties and occurrence in larvae of the fleshfly Sarcophaga bullata Parker 50, 837–841.

Partridge, L., Alic, N., Bjedov, I., Piper, M.D.W., 2011. Ageing in Drosophila: the role of the insulin/Igf and TOR signalling network. Exp. Gerontol. 46, 376–81. doi:10.1016/j.exger.2010.09.003

Petryk, A., Warren, J.T., Marqués, G., Jarcho, M.P., Gilbert, L.I., Kahler, J., Parvy, J.-P., Li, Y., Dauphin-Villemant, C., O'Connor, M.B., 2003. Shade is the Drosophila P450 enzyme that mediates the hydroxylation of ecdysone to the steroid insect molting hormone 20-hydroxyecdysone. Proc. Natl. Acad. Sci. U. S. A. 100, 13773–8. doi:10.1073/pnas.2336088100

Pfeiffer, B.D., Ngo, T.T.B., Hibbard, K.L., Murphy, C., Jenett, A., Truman, J.W., Rubin, G.M., 2010. Refinement of tools for targeted gene expression in Drosophila. Genetics 186, 735–755. doi:10.1534/genetics.110.119917

Plant, T.M., 2015. The hypothalamo-pituitary-gonadal axis. J. Endocrinol. 226, T41-54. doi:10.1530/JOE-15-0113

Pointis, G., Latreille, M., 1987. Catecholamine-induced stimulation of testosterone production by Leydig cells from fetal mouse testis. J. Reprod. Fertil.

Prabhu, S.S., Robertson, F.W., 1963. The ecological genetics of growth in Drosophila VI. The genetic correlation between the duration of the larval period and body size in relation to larval diet. Genet. Res. 4, 74–92. doi:10.1017/S0016672300000902

Ragan, T.J., Bailey, A.P., Gould, A.P., Driscoll, P.C., 2013. Volume determination with two standards allows absolute quantification and improved chemometric analysis of metabolites by NMR from submicroliter samples. Anal. Chem. 85, 12046–12054. doi:10.1021/ac403111s

Ragan, T.J., Bailey, A.P., Gould, A.P., Driscoll, P.C., 2013. Supp_info_ Volume

determination with two standards allows absolute quantification and improved chemometric analysis of metabolites by NMR from submicroliter samples. Anal. Chem. 85, 12046–54. doi:10.1021/ac403111s

Rakoff, A.E., 1967. Menstrual disorders of the Adolescent. Ann. N. Y. Acad. Sci. 142, 801–806. doi:10.1111/j.1749-6632.1967.tb14693.x

Rattle, H., 1995. An NMR primer for life scientists. Partnership Press.

Rewitz, K.F., Yamanaka, N., Gilbert, L.I., O'Connor, M.B., 2009. The insect neuropeptide PTTH activates receptor tyrosine kinase torso to initiate metamorphosis. Science 326, 1403–5. doi:10.1126/science.1176450

Rewitz, K.F., Yamanaka, N., O'Connor, M.B., 2013. Chapter One – Developmental Checkpoints and Feedback Circuits Time Insect Maturation, in: Current Topics in Developmental Biology. pp. 1–33. doi:10.1016/B978-0-12-385979-2.00001-0

Riddiford, L.M., Truman, J.W., 1993. Hormone Receptors and the Regulation of Insect Metamorphosis. Am. Zool. 33, 340–347.

Roa, J., García-Galiano, D., Castellano, J.M., Gaytan, F., Pinilla, L., 2010. Metabolic control of puberty onset: New players, new mechanisms. Mol. Cell. Endocrinol. 324, 87–94. doi:10.1016/j.mce.2009.12.018

Ryder, E., Blows, F., Ashburner, M., Bautista-Llacer, R., Coulson, D., Drummond, J., Webster, J., Gubb, D., Gunton, N., Johnson, G., O'Kane, C.J., Huen, D., Sharma, P., Asztalos, Z., Baisch, H., Schulze, J., Kube, M., Kittlaus, K., Reuter, G., Maroy, P., Szidonya, J., Rasmuson-Lestander, A., Ekström, K., Dickson, B., Hugentobler, C., Stocker, H., Hafen, E., Lepesant, J.A., Pflugfelder, G., Heisenberg, M., Mechler, B., Serras, F., Corominas, M., Schneuwly, S., Preat, T., Roote, J., Russell, S., 2004. The DrosDel collection: a set of P-element insertions for generating custom chromosomal aberrations in Drosophila melanogaster. Genetics 167, 797–813. doi:10.1534/genetics.104.026658

Sarup, P., Pedersen, S.M.M., Nielsen, N.C., Malmendal, A., Loeschcke, V., 2012. The metabolic profile of long-lived Drosophila melanogaster. PLoS One 7, e47461. doi:10.1371/journal.pone.0047461

Savorani, F., Tomasi, G., Engelsen, S.B., 2010. icoshift: A versatile tool for the

rapid alignment of 1D NMR spectra. J. Magn. Reson. 202, 190–202. doi:10.1016/j.jmr.2009.11.012

Schneiderman, H., Young, W.J., Childs, B., 1966. Patterns of alkaline phosphatase in developing Drosophila. Science (80-.). 151, 461–3. ST–Patterns of alkaline phosphatase in d.

Scott, E.C., Johnston, F.E., 1982. Critical Fat, Menarche, and the Maintenance of Menstrual Cycles. J. Adolesc. Heal. Care 2, 249–260. doi:10.1001/archpedi.1975.02120380011003

Shen, X., Liu, H., Xiang, H., Qin, X., Du, G., Tian, J., 2016. Combining biochemical with 1 H NMR-based metabolomics approach unravels the antidiabetic activity of genipin and its possible mechanism. J. Pharm. Biomed. Anal. 129, 80–89. doi:10.1016/j.jpba.2016.06.041

Sisk, C.L., Foster, D.L., 2004. The neural basis of puberty and adolescence. Nat. Neurosci. 7, 1040–1047. doi:10.1038/nn1326

Smith, J.T., 2013. Sex Steroid Regulation of Kisspeptin Circuits. Springer New York, pp. 275–295. doi:10.1007/978-1-4614-6199-9_13

Smolinska, A., Blanchet, L., Buydens, L.M.C., Wijmenga, S.S., 2012. NMR and pattern recognition methods in metabolomics: from data acquisition to biomarker discovery: a review. Anal. Chim. Acta 750, 82–97. doi:10.1016/j.aca.2012.05.049

Sokolowski, M.B., 2001. Drosophila : Genetics Meets Behaviour 2.

Soriano-Guillén, L., Barrios, V., Chowen, J.A., Sánchez, I., Vila, S., Quero, J., Argente, J., 2004. Ghrelin levels from fetal life through early adulthood: relationship with endocrine and metabolic and anthropometric measures. J. Pediatr. 144, 30–35. doi:10.1016/j.jpeds.2003.08.050

Sözen, M.A., Armstrong, J.D., Yang, M., Kaiser, K., Dow, J.A., 1997. Functional domains are specified to single-cell resolution in a Drosophila epithelium. Proc. Natl. Acad. Sci. U. S. A. 94, 5207–12. doi:10.1073/pnas.94.10.5207

St Johnston, D., 2002. The art and design of genetic screens: Drosophila melanogaster. Nat. Rev. Genet. 3, 176–88. doi:10.1038/nrg751

Stieper, B.C., Kupershtok, M., Driscoll, M. V, Shingleton, A.W., 2008. Imaginal discs regulate developmental timing in Drosophila melanogaster. Dev. Biol.

321, 18–26. doi:10.1016/j.ydbio.2008.05.556

Strobel, A., Issad, T., Camoin, L., Ozata, M., Strosberg, A.D., 1998. A leptin missense mutation associated with hypogonadism and morbid obesity. Nat. Genet. 18, 213–215. doi:10.1038/ng0398-213

Sugumaran, M., Giglio, L. (Burgio), Kundzicz, H., Saul, S., Semensi, V., 1992. Studies on the enzymes involved in puparial cuticle sclerotization in Drosophila melanogaster. Arch. Insect Biochem. Physiol. 19, 271–283. doi:10.1002/arch.940190406

Swerdloff, R.S., Odell, W.D., 1975. Hormonal mechanisms in the onset of puberty. Postgrad. Med. J. 51, 200–8.

Szuperak, M., Pachnis, P., Froldi, F., Costas, O., Fernando, T., Gould, A.P., Cheng, L.Y., n.d. Histidine deprivation selectively inhibts the growth of Myc-dependent neural tumours in Drosophila.

Talbot, W.S., Swyryd, E.A., Hogness, D.S., 1993. Drosophila tissues with different metamorphic responses to ecdysone express different ecdysone receptor isoforms. Cell 73, 1323–1337. doi:10.1016/0092-8674(93)90359-X

Tena-Sempere, M., 2007. Ghrelin and Reproduction: Ghrelin as Novel Regulator of the Gonadotropic Axis, in: Vitamins and Hormones. pp. 285–300. doi:10.1016/S0083-6729(06)77012-1

Tennessen, J.M., Bertagnolli, N.M., Evans, J., Sieber, M.H., Cox, J., Thummel, C.S., 2014. Coordinated metabolic transitions during Drosophila embryogenesis and the onset of aerobic glycolysis. G3 (Bethesda). 4, 839–50. doi:10.1534/g3.114.010652

Tennessen, J.M., Thummel, C.S., 2011. Coordinating growth and maturation - insights from Drosophila. Curr. Biol. 21, R750-7. doi:10.1016/j.cub.2011.06.033

Trussell, J., 1980. Statistical Flaws in Evidence for the Frisch Hypothesis that Fatness Triggers Menarche. Hum. Biol. 52, 711–720.

Ulrich, E.L., Akutsu, H., Doreleijers, J.F., Harano, Y., Ioannidis, Y.E., Lin, J., Livny, M., Mading, S., Maziuk, D., Miller, Z., Nakatani, E., Schulte, C.F., Tolmie, D.E., Kent Wenger, R., Yao, H., Markley, J.L., 2008. BioMagResBank. Nucleic Acids Res. 36, 402–408.

doi:10.1093/nar/gkm957

van den Berg, R.A., Hoefsloot, H.C.J., Westerhuis, J.A., Smilde, A.K., van der Werf, M.J., 2006. Centering, scaling, and transformations: improving the biological information content of metabolomics data. BMC Genomics 7, 142. doi:10.1186/1471-2164-7-142

Warren, J.T., Petryk, A., Marques, G., Jarcho, M., Parvy, J.-P., Dauphin-Villemant, C., O'Connor, M.B., Gilbert, L.I., 2002. Molecular and biochemical characterization of two P450 enzymes in the ecdysteroidogenic pathway of Drosophila melanogaster. Proc. Natl. Acad. Sci. U. S. A. 99, 11043–8. doi:10.1073/pnas.162375799

Warren, J.T., Petryk, A., Marqués, G., Parvy, J.-P., Shinoda, T., Itoyama, K., Kobayashi, J., Jarcho, M., Li, Y., O'Connor, M.B., Dauphin-Villemant, C., Gilbert, L.I., 2004. Phantom encodes the 25-hydroxylase of Drosophila melanogaster and Bombyx mori: a P450 enzyme critical in ecdysone biosynthesis. Insect Biochem. Mol. Biol. 34, 991–1010. doi:10.1016/j.ibmb.2004.06.009

Warren, J.T., Yerushalmi, Y., Shimell, M.J., O'Connor, M.B., Restifo, L.L., Gilbert, L.I., 2006. Discrete pulses of molting hormone, 20-hydroxyecdysone, during late larval development of Drosophila melanogaster: correlations with changes in gene activity. Dev. Dyn. 235, 315–26. doi:10.1002/dvdy.20626

Weber, M., Hellriegel, C., Rueck, A., Wuethrich, J., Jenks, P., 2014. Using high-performance 1H NMR (HP-qNMR??) for the certification of organic reference materials under accreditation guidelines-Describing the overall process with focus on homogeneity and stability assessment. J. Pharm. Biomed. Anal. 93, 102–110. doi:10.1016/j.jpba.2013.09.007

Wei, F., Furihata, K., Miyakawa, T., Tanokura, M., 2014. A pilot study of NMR-based sensory prediction of roasted coffee bean extracts. Food Chem. 152, 363–369. doi:10.1016/j.foodchem.2013.11.161

Weljie, A.M., Newton, J., Mercier, P., Carlson, E., Slupsky, C.M., 2006. Targeted profiling: quantitative analysis of 1H NMR metabolomics data. Anal. Chem. 78, 4430–4442. doi:10.1021/ac060209g

Wijeyesekera, A., Selman, C., Barton, R.H., Holmes, E., Nicholson, J.K., Withers, D.J., 2012. Metabotyping of long-lived mice using 1H NMR spectroscopy. J. Proteome Res. 11, 2224–35. doi:10.1021/pr2010154

Wishart, D.S., Tzur, D., Knox, C., Eisner, R., Guo, A.C., Young, N., Cheng, D., Jewell, K., Arndt, D., Sawhney, S., Fung, C., Nikolai, L., Lewis, M., Coutouly, M.A., Forsythe, I., Tang, P., Shrivastava, S., Jeroncic, K., Stothard, P., Amegbey, G., Block, D., Hau, D.D., Wagner, J., Miniaci, J., Clements, M., Gebremedhin, M., Guo, N., Zhang, Y., Duggan, G.E., MacInnis, G.D., Weljie, A.M., Dowlatabadi, R., Bamforth, F., Clive, D., Greiner, R., Li, L., Marrie, T., Sykes, B.D., Vogel, H.J., Querengesser, L., 2007. HMDB: The human metabolome database. Nucleic Acids Res. 35, 521–526. doi:10.1093/nar/gkl923

Wold, S., Esbensen, K., Geladi, P., 1987. Principal component analysis. Chemom. Intell. Lab. Syst. 2, 37–52. doi:10.1016/0169-7439(87)80084-9

Worley, B., Halouska, S., Powers, R., 2013. Utilities for quantifying separation in PCA/PLS-DA scores plots. Anal. Biochem. 433, 102–4. doi:10.1016/j.ab.2012.10.011

Worley, B., Powers, R., 2013. Multivariate Analysis in Metabolomics. Curr. Biol. 1, 92–107.

Yang, M.Y., Wang, Z., MacPherson, M., Dow, J.A., Kaiser, K., 2000. A novel Drosophila alkaline phosphatase specific to the ellipsoid body of the adult brain and the lower Malpighian (renal) tubule. Genetics 154, 285–97.

Yang, M.Y., Wang, Z., MacPherson, M., Dow, J.A.T., Kaiser, K., 2000. A Novel Drosophila Alkaline Phosphatase Specific to the Ellipsoid Body of the Adult Brain and the Lower Malpighian (Renal) Tubule. Genetics 154, 285–297.

Yao, T.-P., Forman, B.M., Jiang, Z., Cherbas, L., Chen, J.-D., McKeown, M., Cherbas, P., Evans, R.M., 1993. Functional ecdysone receptor is the product of EcR and Ultraspiracle genes. Nature 366, 476–479.

Yao, T.P., Segraves, W.A., Oro, A.E., McKeown, M., Evans, R.M., Clark, K.E., Natzle, J.E., O'Connor, M.B., 1992. Drosophila ultraspiracle modulates ecdysone receptor function via heterodimer formation. Cell 71, 63–72. doi:10.1016/0022-1910(83)90089-6

Yoshiyama, T., Namiki, T., Mita, K., Kataoka, H., Niwa, R., 2006. Neverland is an evolutionally conserved Rieske-domain protein that is essential for ecdysone synthesis and insect growth. Development 133, 2565–74. doi:10.1242/dev.02428

Zhang, X., Zhu, X., Wang, C., Zhang, H., Cai, Z., Zhang, X., Zhu, X., Wang, C., Zhang, H., Cai, Z., 2016. Non-targeted and targeted metabolomics approaches to diagnosing lung cancer and predicting patient prognosis. Oncotarget 7, 63437–63448. doi:10.18632/oncotarget.11521

Zhang, Y., Proenca, R., Maffei, M., Barone, M., Leopold, L., Friedman, J.M., 1994. Positional cloning of the mouse obese gene and its human homologue. Nature 372, 425–432. doi:10.1038/372425a0

Zhao, Q., Spradling, A.C., Mattei, B., An, H.J., Weinstock, G.M., Holt, R.A., Zheng, L., Harris, M., Ke, Z., Zaveri, J.S., Reinert, K., Ferraz, C., Morris, J., Doup, L.E., Davies, P., Scherer, S.E., Adams, M.D., Pittman, G.S., Kulp, D., Andrews-Pfannkoch, C., Butler, H., Pfeiffer, B.D., Blazej, R.G., Chandra, I., Zhang, G., Howland, T.J., Gabrielian, A.E., Cherry, J.M., Shen, H., Wortman, J.R., Williams, S.M., Dietz, S.M., Gabor, G.L., Busam, D.A., Dahlke, C., Palazzolo, M., Sutton, G.G., Ferriera, S., Worley, K.C., Gu, Z., Yang, S., Nelson, K.A., Pablos, B. de, Levitsky, A.A., Borkova, D., Agbayani, A., Kalush, F., Liang, Y., Yandell, M.D., Nelson, C.R., Lai, Z., Celniker, S.E., Evans, C.A., Nixon, K., Fosler, C., Zhan, M., Brokstein, P., Baxter, E.G., Kimmel, B.E., Murphy, B., Muzny, D.M., Zhou, X., Zhong, W., Turner, R., Brandon, R.C., Nelson, D.L., Kennison, J.A., Weissenbach, J., Wassarman, D.A., Puri, V., Wang, Z.Y., Yeh, R.F., Cawley, S., Reese, M.G., Beeson, K.Y., Liu, X., Lasko, P., Gelbart, W.M., Fleischmann, W., Kodira, C.D., Tector, C., Kraft, C., Hernandez, J.R., Delcher, A., Champe, M., Dugan-Rocha, S., Li, Z., Siden-Kiamos, I., Ketchum, K.A., Nelson, D.R., Bhandari, D., McPherson, D., Cadieu, E., Glodek, A., Dodson, K., Richards, S., Baxendale, J., Zhu, X., Stapleton, M., Brottier, P., Zhang, Q., Mount, S.M., Lewis, S.E., Center, A., Moy, M., Doyle, C., Harvey, D., Bouck, J., Wei, M.H., Skupski, M.P., Chen, L.X., Dunn, P., Milshina, N. V., Glasser, K., Karpen, G.H., Berman, B.P., Pollard, J., Gibbs, R.A., Henderson, S.N.,

Davenport, L.B., Baldwin, D., Ye, J., Ibegwam, C., Venter, J.C., Gocayne, J.D., Burtis, K.C., Deng, Z., Benos, P. V., Jalali, M., Dunkov, B.C., Downes, M., WoodageT, Rogers, Y.H., Scheeler, F., Nusskern, D.R., Smith, T., Amanatides, P.G., Guan, P., Zhong, F.N., Moshrefi, A., Basu, A., Strong, R., Ashburner, M., Saunders, R.D., Houck, J., Lei, Y., Pacleb, J.M., Yao, Q.A., Simpson, M., Remington, K., McIntosh, T.C., Mobarry, C., Pan, S., Spier, E., Hoskins, R.A., Myers, E.W., Helt, G., Smith, H.O., Wang, X., Galle, R.F., Zhu, S., Svirskas, R., Shue, B.C., Mays, A.D., Abril, J.F., Merkulov, G., Gong, F., Murphy, L., Lin, X., Heiman, T.J., Durbin, K.J., Garg, N.S., George, R.A., Li, J., Wu, D., Hostin, D., Wan, K.H., Evangelista, C.C., Venter, E., Dew, I., Bolshakov, S., Harris, N.L., Ballew, R.M., Wang, A.H., Houston, K.A., Rubin, G.M., Botchan, M.R., Sun, E., Zheng, X.H., Bayraktaroglu, L., Li, P.W., Kravitz, S., Gorrell, J.H., Beasley, E.M., McLeod, M.P., 2000. The genome sequence of Drosophila melanogaster. Science (80-.). 287, 2185—2195. doi:10.1126/science.287.5461.2185